NASA TECHNICAL MEMORANDUM

NASA TM X-1174

NASA TM X-1174

AERODYNAMIC ABORT-SEPARATION CHARACTERISTICS OF A PARALLEL-STAGED REUSABLE LAUNCH VEHICLE FROM MACH 0.60 TO 1.20

by John P. Decker

Langley Research Center
Langley Station, Hampton, Va.

NATIONAL AERONAUTICS AND SPACE ADMINISTRATION - WASHINGTON, D. C. - NOVEMBER 1965

NASA TM X-1174

AERODYNAMIC ABORT-SEPARATION CHARACTERISTICS OF A PARALLEL-STAGED REUSABLE LAUNCH VEHICLE FROM MACH 0.60 TO 1.20

By John P. Decker

Langley Research Center
Langley Station, Hampton, Va.

NATIONAL AERONAUTICS AND SPACE ADMINISTRATION

AERODYNAMIC ABORT-SEPARATION CHARACTERISTICS OF A PARALLEL-STAGED REUSABLE LAUNCH VEHICLE FROM MACH 0.60 TO 1.20*

By John P. Decker
Langley Research Center

SUMMARY

A wind-tunnel investigation of the abort-separation characteristics was made of a conceptual design of a parallel-staged reusable launch vehicle system. The launch vehicle consisted of a winged reusable first stage, a winged reusable second stage, and a third-stage winged reusable spacecraft with an expendable space-maneuvering propulsion package. Various upper-stage configurations were separated from the upper surface of the first stage. The first- and upper-stage configurations were separately mounted on six-component balances and for this investigation were maintained essentially parallel to each other and at the same longitudinal position. The wind-tunnel investigation was conducted at Mach numbers from 0.60 to 1.20, at angles of attack from approximately -5° to 17°, and for spacing distances based upon the equivalent base diameter of the first-stage fuselage of 0.25 to 1.45.

The results show that, for the first stage, abort separation at the Mach numbers of this investigation generally incurred significant changes in both the lift-curve slope and the longitudinal stability. For the upper-stage configurations, abort separation generally incurred extremely large decreases in both the lift-curve slope and the longitudinal stability. At angles of attack as small as 2°, the upper-stage configurations with the second-stage wing on became extremely unstable. The changes in the lift and pitching-moment characteristics of both the first- and upper-stage configurations were dependent on Mach number, upper-stage configuration, spacing, and angle of attack. The magnitude of these changes could present potentially hazardous stability and control problems for both the first and upper stages during an abort-separation maneuver, especially if separation occurred at high dynamic pressures.

INTRODUCTION

During the past several years some interest has been shown in reusable launch vehicle systems. Many of the systems have consisted of two or more vehicle stages having fixed wings or lifting-body shapes and mounted parallel

*Title, Unclassified.

to each other. Because of this interest in parallel-arranged stages for reusable launch vehicle systems, the Langley Research Center is conducting investigations to ascertain the aerodynamic characteristics at conditions representative of launch, recovery, stage separation, and abort separation. References 1 to 4 present longitudinal and lateral aerodynamic results at Mach numbers from 0.6 to 6.0 for one concept of a parallel-staged horizontal-take-off horizontal-landing reusable launch vehicle system. Reference 5 presents results for the same vehicle at Mach numbers from 3.00 to 6.00 which simulate stage- and abort-separation conditions.

The purpose of the present paper is to extend the range of data for simulated abort conditions to the transonic and subsonic ranges. The results obtained are employed to examine the physical phenomena associated with one mode of separation. The present investigation was limited, as was reference 5, to the conditions that both major components (the first-stage configuration and the upper-stage configuration) remain essentially parallel to each other and at the same longitudinal position. These limitations were imposed in order to reduce the number of variables for the initial abort-separation investigation. Other modes of separation such as variable incidence and/or longitudinal displacement were not considered herein.

Tests were conducted on a 1/75-scale model of the launch vehicle (refs. 1 to 5) in the Langley 8-foot transonic pressure tunnel at Mach numbers from 0.60 to 1.20 and at angles of attack from approximately -5° to 17°. The two major components were individually mounted to measure forces and moments for spacing distances based upon the equivalent base diameter of the first-stage fuselage of 0.25 to 1.45. The average test Reynolds numbers per foot (per meter) varied from approximately 3.16×10^6 (0.96×10^6) at a Mach number of 0.60 to 4.22×10^6 (1.29×10^6) at a Mach number of 1.20.

SYMBOLS

The aerodynamic characteristics for the first- and upper-stage configurations have been referred to the stability axes. The moment reference center for both the first- and upper-stage configurations was 12.47 inches (31.67 cm) forward of the base in the stage-separation plane (fig. 1(b)). The aerodynamic coefficients for the first stage are based on the geometry of the first-stage wing, whereas the aerodynamic coefficients for the upper stages are based on the geometry of the second-stage wing. The physical quantities defined in this paper are given in both the U.S. Customary System of Units and the International System of Units (SI). Factors relating the two systems are given in reference 6.

C_L lift coefficient, $\frac{\text{Lift}}{qS}$

C_D drag coefficient, $\frac{\text{Drag}}{qS}$

C_m pitching-moment coefficient, $\frac{\text{Pitching moment}}{qS\bar{c}}$

c local chord, ft (m)

$\bar{c}$ reference mean aerodynamic chord based on reference wing area, 1.222 ft (0.3725 m) for first-stage configuration and 0.707 ft (0.2156 m) for upper-stage configurations

d equivalent base diameter of first-stage fuselage, 0.320 ft (0.0975 m)

h spacing between flat upper surface of first stage and flat lower surface of second stage (see fig. 1(b))

M free-stream Mach number

q free-stream dynamic pressure, $\frac{\text{lb}}{\text{sq ft}}$ $\left(\frac{\text{N}}{\text{m}^2}\right)$

R Reynolds number, ft^{-1} (m^{-1})

S reference wing area, 1.222 sq ft (0.1135 m^2) for first-stage configuration and 0.522 sq ft (0.0485 m^2) for upper-stage configurations

x_{cp} location of center of pressure forward of base of first- or upper-stage configuration

α angle of attack (referred to stage-separation plane), deg

h/d nondimensional spacing, based upon equivalent base diameter of first-stage fuselage

$\frac{x_{cp}}{d}$ nondimensional location of center of pressure, based upon equivalent base diameter of first-stage fuselage

ΔC_L incremental change in lift coefficient due to interference, $(C_L)_{h/d} - (C_L)_{h/d=\infty}$

ΔC_m incremental change in pitching-moment coefficient due to interference, $(C_m)_{h/d} - (C_m)_{h/d=\infty}$

$\Delta \frac{x_{cp}}{d}$ incremental change in center-of-pressure location due to interference, $\left(\frac{x_{cp}}{d}\right)_{h/d} - \left(\frac{x_{cp}}{d}\right)_{h/d=\infty}$

Subscripts:

I	first-stage configuration
II	upper-stage configurations

Component designations:

B	second-stage fuselage
W	second-stage wing
F	second-stage vertical fins
M	maneuver propulsion package
S	spacecraft and adapter fairing
S'	forebody fairing

DESCRIPTION OF MODEL

The complete launch vehicle, which was identical to the model in references 1 and 2, and its components are shown in figure 1. The launch vehicle consisted of a winged reusable first stage with a canard, a winged reusable second stage, and a third-stage winged reusable spacecraft with an expendable space-maneuvering propulsion package. The two upper stages were arranged in tandem, and this combination was placed parallel to the first stage. Figure 1(b) shows the relative positions of the first-stage reusable booster and the upper stages for the present investigation. Model dimensions are presented in table I, and photographs showing the first-stage reusable booster separated from various upper-stage configurations are shown in figure 2.

First-Stage Reusable Booster

The first-stage reusable booster consisted of a semicylindrical fuselage with an ogival forebody, a delta canard, and a delta wing with trapezoidal vertical fins mounted outboard on nacelles (fig. 1(c)). The wing had a leading-edge sweep of 70° and was a symmetrical wedge to the 40-percent-chord station with a constant maximum thickness of 0.050c rearward to the 85-percent-chord station. A wedge or boattail on the lower surface of the wing extended from the 85-percent-chord station to the wing trailing edge. (See fig. 1(d).) The wing was flat on the upper surface rearward of the 40-percent-chord station to allow mating with the second-stage wing. The wing was set at an incidence angle of 0°. The requirement of a flat upper surface resulted in a wing dihedral angle of about $3\frac{1}{2}^\circ$. The exposed area of the canard was approximately 7 percent of the total area of the first-stage wing.

The vertical fins were located at two-thirds of the wing semispan. The total fin area, which was equally distributed above and below the wing, was approximately 15 percent of the total wing area. The vertical fins had a panel aspect ratio of 1.15 and a taper ratio of 0.5. The nacelles were cylindrical with a parabolic nose and were considered to house the flyback engines. The nacelles formed the juncture between the first-stage wing and vertical fins.

Second-Stage Reusable Booster

The second-stage reusable booster consisted of a cylindrical fuselage and a trapezoidal wing with two outboard-mounted vertical fins located at two-thirds of the wing semispan. The fuselage incorporated a side fairing which extended vertically from the center line of the second-stage fuselage to the upper surface of the first-stage fuselage. The wing thickness was chosen to achieve a total profile thickness of 0.065c (based on the chord of the first-stage wing) when the first- and second-stage wings were mated. The forward 0.40c of the upper surface of the second-stage wing formed a coplanar surface with the first-stage wing. A portion of the leading edge was removed from the second-stage wing to form a constant leading-edge radius identical to that of the first-stage wing. The purpose of this arrangement was to fair the wings together to reduce the interference during launch. The second-stage vertical fins were almost identical to the first-stage vertical fins, but only the upper element was employed.

Orbital Stage

The spacecraft was a wing-body configuration with wing-tip-mounted vertical fins (fig. 1(e)). The spacecraft wing was unsymmetrical with the camber on the lower surface of the wing, and the span (including vertical fins) was approximately equal to the width of the first-stage fuselage. A pad to support the spacecraft on the launch vehicle was removed for this investigation. (See fig. 1(b).)

The maneuver propulsion package was an expendable rocket booster designed as a short cylinder with the same diameter as the second-stage fuselage and incorporating the same type of side fairing as the second-stage fuselage. When the model was tested without the maneuver propulsion package, the spacecraft was moved rearward to connect directly with the second-stage fuselage. This configuration was considered to meet the requirements for a type of mission in which no appreciable in-orbit maneuvering capability is needed.

A forebody fairing was tested in place of the spacecraft and adapter fairing, for which case the configuration was considered to place a ballistic payload into orbit.

APPARATUS AND TESTS

The present investigation was conducted in the Langley 8-foot transonic pressure tunnel at Mach numbers from 0.60 to 1.20, at angles of attack from approximately -5° to 17°, and for spacing distances based upon the equivalent base diameter of the first-stage fuselage of 0.25 to 1.45. The variation with Mach number of the average test Reynolds numbers is shown in figure 3.

Separate sting supports were provided for the first- and upper-stage configurations, with the relative movement between the configurations being provided in the vertical plane by the support system to which the stings were attached. While the spacing distance was varied, the first- and upper-stage configurations remained essentially parallel, with bases alined, throughout the angle-of-attack range. (See fig. 1(b).) Static aerodynamic force and moment data were simultaneously obtained for the first- and upper-stage configurations by use of individual internal six-component strain-gage balances. No composite configurations, that is, configurations with the first stage and upper stages connected, were tested in the present investigation; data for composite configurations are shown in reference 2.

Boundary-layer transition was fixed on the models with an 0.1-inch-wide (0.25-cm) strip of No. 80 carborundum grains located at the 5-percent station on all surfaces. The angle-of-attack data for the first- and upper-stage configurations were corrected for balance and sting deflections under load. The drag coefficients of the first- and upper-stage configurations were corrected to correspond to the free-stream static pressures on the base areas of the respective fuselages.

Figure 4 shows that the deviation in angle of attack of the upper stages in relation to the first stage at all test Mach numbers became progressively larger as the test angle of attack was increased or decreased from 0°. This deviation was caused by the difference in forces and moments on the separate balance-sting combinations for the first- and upper-stage configurations.

PRESENTATION OF RESULTS

The longitudinal aerodynamic characteristics of the first-stage and upper-stage configurations in the presence of each other are shown in figures 5 to 16; some of the results are summarized in figures 17 to 22. The various upper-stage configurations are identified by letter symbols. (See symbol list for component designations.) An outline of the contents of the data figures is as follows:

DISCUSSION

The results obtained during the present investigation have been divided, insofar as practicable, into two principal parts - the aerodynamic characteristics of the first-stage configurations in the presence of the upper-stage

configurations and the aerodynamic characteristics of the upper-stage configurations in the presence of the first-stage configurations. Because only a limited amount of data was obtained for a first-stage configuration other than the complete first stage and because of the complexity of the aerodynamic phenomena resulting from the present design concept, the discussion is limited to the salient effects of the mutual interferences between the complete first stage and the various upper-stage configurations. Furthermore, since safe and practicable separation of the major components is considered of paramount interest, the principal focus is directed toward stability and control implications.

First-Stage Characteristics

The basic aerodynamic data for the first stage (figs. 5 to 9) show that the proximity of the several upper-stage configurations produced marked changes in the basic longitudinal aerodynamic coefficients. The aerodynamic characteristics of the first stage in the presence of upper-stage configurations have been compared with the interference-free aerodynamic characteristics (ref. 2), and it can be seen that the region of significant influence of the upper-stage configurations on the first stage generally extends beyond the maximum values of the test spacing h/d.

Lift.- The interference during abort separation between the first stage and the upper-stage configurations with the second-stage wing off (figs. 6 and 8) had little effect on either C_L or lift-curve slope throughout the angle-of-attack and Mach number ranges of this investigation. However, the interference between the first stage and the upper-stage configurations with the second-stage wing on (figs. 5, 7, and 9) resulted in significant changes in lift-curve slope from interference-free values. The overall changes in C_L for the first stage in the presence of the second-stage wing-on configurations at high angles of attack resulted in corresponding angle-of-attack increments as large as 3°.

Figure 17 shows lift-coefficient increment (ΔC_L) as a function of vehicle spacing at angles of attack of 0° and 6°. The data at $\alpha = 0^\circ$ are representative of the data at angles of attack between 4° and -4°, and the data at $\alpha = 6^\circ$ are representative of the data at angles of attack greater than 4°. The figure indicates that the lift-coefficient increments are dependent on upper-stage configuration, Mach number, spacing, and angle of attack. At subsonic speeds and at $\alpha = 0^\circ$, removal of the second-stage wing did not appreciably change the magnitude of the lift-coefficient increments. However, at supersonic speeds and at $\alpha = 0^\circ$, removal of the wing had a significant effect on the magnitude of these increments. At $\alpha = 0^\circ$ (fig. 17(a)), the lift-coefficient increment for the complete first stage in the presence of the upper-stage configuration with the second-stage wing on reached a maximum at the smallest test spacing $(h/d = 0.25)$. As h/d was increased, $(\Delta C_L)_I$ appeared to gradually approach the interference-free value $\left((\Delta C_L)_I = 0\right)$. At $\alpha = 6^\circ$ (fig. 17(b)) for the same vehicle combination, the lift-coefficient increment reached a maximum at the larger test spacings, but it was not clear at what spacings the interference-free value would be reached.

Longitudinal stability.- The basic data for the first stage in the presence of the upper-stage configurations with the second-stage wing off (figs. 6 and 8) show that the longitudinal stability (slope of the pitching-moment curves, negative for positive stability) did not change appreciably with spacing. However, the interference between these major components resulted in negative displacement of the pitching-moment curves. The data for the first stage in the presence of second-stage wing-on configurations (figs. 5, 7, and 9) show that the longitudinal stability increased significantly at angles of attack greater than 4° and at the smaller values of h/d. The observed increases in stability together with increases in C_L at angles of attack greater than about 4° for the first stage in the presence of the wing-on configurations may be analogous to the flow phenomena associated with a slotted flap on a wing, where the slots channel high energy air in such a manner as to delay flow separation on the wing and increase the wing loading. The presence of the second-stage wing is believed to have delayed flow separation on the first-stage wing and increased the wing loading rearward of the moment reference center; consequently, both the lift and longitudinal stability of the first stage increased.

Comparison of the subsonic Mach number data for the forward spacecraft position in figure 5(b) with that in figure 6(b) and of the subsonic Mach number data for the rearward spacecraft position in figure 7(b) with that in figure 8(b) shows that the magnitude and shape of the pitching-moment curves in the range of α from 4° to -4° were nearly the same whether a second-stage wing-on configuration or a second-stage wing-off configuration was used. Similar results are shown for the lift curves. (See figs. 5(a), 6(a), 7(a), and 8(a).) Furthermore, comparison of the subsonic Mach number data in figure 5(b) with that in figure 7(b) or of the subsonic Mach number data in figure 6(b) with that in figure 8(b) shows that moving the spacecraft closer to the moment reference center (moving the spacecraft rearward 1.25d) had little effect on the longitudinal stability of the first stage in the range of α from 4° to -4°. These results could be anticipated at the subsonic speeds, since the exposed area of the second-stage wing is only approximately 25 percent of the projected area of the first stage, and the projected area of the spacecraft and adapter fairing is only 12 percent of the projected area of the first stage.

Examination of schlieren photographs, typical examples of which are shown in figures 23 and 24, indicates that the first-order interference effects on the pitching-moment and lift characteristics for the first stage at small angles of attack (in the range of α from 4° to -4°) and at Mach numbers greater than 1.00 were caused by the impingement of the shock waves from the second-stage wing and the spacecraft on the first stage, and that only secondary effects were incurred by subsequent reflections. The affected area and its location would be directly proportional to the spacing h/d and inversely proportional to the tangent of the effective shock-wave angle of the disturbance caused by the upper-stage configuration. Therefore, the differences in the pitching-moment and lift characteristics of the first stage at Mach numbers greater than 1.00 caused by changing the upper-stage configurations (see figs. 5 to 9) in the range of α from 4° to -4° could be anticipated, since the affected areas and locations would change with the different upper-stage configurations. For example, removal of the second-stage wing would remove area affected by the impingement of the shock wave from the wing and therefore increase the lift on the

first stage and produce a nose-down pitching moment since the affected area would be rearward of the moment reference center. This result can be seen by comparison of second-stage wing-on data with second-stage wing-off data in figures 5 and 6, respectively, or in figures 7 and 8, respectively.

The combined interference effects of normal-force and pitching-moment coefficients on the complete first stage in the presence of two upper-stage configurations have been indicated in figure 19 by showing the change in center of pressure with spacing at $\alpha = 6^\circ$ and in figure 20 by showing the variation in center of pressure with angle of attack for different values of h/d. Both positive and negative increments in center-of-pressure location as large as 1.0 are shown in figure 19 for the first stage in the presence of the wing-on configuration, whereas only negative increments as large as 0.5 are shown for the first stage in the presence of the wing-off configuration. The values of $\left(\Delta \frac{x_{cp}}{d}\right)_I$ are shown to vary appreciably with spacing for the wing-on configuration, whereas the values are nearly constant with spacing for the wing-off configuration.

Upper-Stage Characteristics

The basic aerodynamic data for the several upper-stage configurations (figs. 11 to 15) show that the proximity of the first stage produced large changes in the basic longitudinal aerodynamic coefficients. The results have been compared with the interference-free aerodynamic data superimposed on the figures.

Lift.- The interference effects on upper-stage configurations caused by the presence of the first stage (figs. 11 to 15) during abort separation produced large decreases in lift-curve slope at all test Mach numbers. At the smaller spacing distances in the angle-of-attack range from about -4° to 3°, C_L is shown to remain approximately constant, whereas at angles greater than 3° and at the smaller spacings, C_L is shown to decrease to zero and then to negative values. (See fig. 11, for example.)

The incremental changes in C_L at angles of attack of 0° and 6° for upper-stage configurations with the second-stage wing on and off are shown in figure 18. The lift-coefficient increments for the upper-stage configurations are dependent on Mach number, upper-stage configuration, spacing, and angle of attack. At $\alpha = 0^\circ$ the lift-coefficient increment for the second-stage wing-on configuration in the presence of the complete first stage reached a maximum at the smallest test spacing. As h/d was increased, $(\Delta C_L)_{II}$ apparently approached the interference-free value $\left((\Delta C_L)_{II} = 0\right)$. The lift-coefficient increments shown at $\alpha = 6^\circ$ for the wing-on configuration are considerably larger than those shown at $\alpha = 0^\circ$.

Longitudinal stability.- The basic data for the upper-stage configurations with the second-stage wing off (figs. 12 and 14) show that the presence of the first stage increased the longitudinal stability (slope of the pitching-moment

curves, negative for positive stability) in the angle-of-attack range from about -4° to 5°. At higher angles of attack, the pitching-moment curves for these configurations became nonlinear at the smaller values of h/d. The data for the upper-stage configurations with the second-stage wing on (figs. 11, 13, and 15) show that the presence of the first stage considerably reduced the longitudinal stability in the angle-of-attack range from -4° to about 2°. At angles of attack of 2° and higher, the upper-stage configurations with the second-stage wing on became extremely unstable, with the slope of the pitching-moment curves approaching infinity at the smaller values of h/d. The data indicate that the upper-stage longitudinal stability is dependent on Mach number, upper-stage configuration, spacing, and angle of attack.

In contrast to the results for the first stage, comparison of the data in figures 11 and 12 or in figures 13 and 14 shows that at all Mach numbers the magnitude and shape of the pitching-moment curves were significantly different for the wing-on and wing-off configurations. Similar results are shown for the lift curves.

Examination of the schlieren photographs in figures 23 and 24 indicates that the observed changes in lift and pitching-moment characteristics for the upper-stage configurations at Mach numbers greater than 1.00 and at small angles of attack (in the range of α from 4° to -4°) were probably caused by the first reflection of the disturbances generated by the upper-stage configuration coupled with the primary disturbances from the first stage. At angles of attack larger than about 4° and at all Mach numbers, the data in figure 11, for example, indicate some form of progressive blanketing which is illustrated by the decrease in lift-curve slope to zero and then to negative values at almost all spacing distances. This blanketing effect is probably caused by the upper-stage configuration being in the first-stage wake or downwash field, which causes a reduction in the effective angle of attack of the upper-stage configuration together with a reduction in the energy of the flow (low local dynamic pressures) from free-stream conditions.

The combined interference effects of normal-force and pitching-moment coefficients for second-stage wing-on and wing-off configurations in the presence of the first stage have been shown in figures 21 and 22 in a representation identical to that presented in figures 19 and 20 for the first stage in the presence of the upper-stage configurations. Figure 21 shows that positive increments in center-of-pressure location as large as 4.0 occurred at $\alpha = 6^\circ$ for both the wing-on and wing-off configurations. For either the wing-on or wing-off configuration, the values of $\left(\Delta \frac{x_{cp}}{d}\right)_{II}$ are shown in figure 21 to reach a maximum at the smallest test spacing and then rapidly approach the interference-free value.

CONCLUDING REMARKS

An investigation has been conducted in the Langley 8-foot transonic pressure tunnel to ascertain some of the low-speed abort-separation aerodynamic

characteristics of a parallel-staged reusable launch vehicle. The launch vehicle consisted of a winged reusable first stage, a winged reusable second stage, and a third-stage winged reusable spacecraft with an expendable space-maneuvering propulsion package. Various upper-stage configurations were separated from the upper surface of the first stage. The first- and upper-stage configurations were separately mounted on six-component balances and were maintained essentially parallel to each other and at the same longitudinal position. The wind-tunnel investigation was conducted at Mach numbers from 0.60 to 1.20, at angles of attack from approximately -5° to 17°, and for spacing distances based upon the equivalent base diameter of the first-stage fuselage of 0.25 to 1.45.

For the first stage, abort separation over the Mach number range of this investigation generally incurred significant changes in the lift-curve slope and the longitudinal stability. These changes were found to vary rapidly with spacing and were also dependent on Mach number, upper-stage configuration, and angle of attack.

For the upper-stage configurations, abort separation generally incurred extremely large decreases in both the lift-curve slope and the longitudinal stability. At angles of attack as small as 2°, the upper-stage configurations with the second-stage wing on became extremely unstable. The changes in lift and pitching-moment characteristics were found to vary rapidly with spacing and were also dependent on Mach number, upper-stage configuration, and angle of attack.

The present results indicate that potentially hazardous stability and control problems can be expected for both the first and upper stages during a low-speed abort-separation maneuver, especially if separation occurs at high dynamic pressures. The conclusion should not be inferred, at this time, that separation of parallel stages at significant dynamic pressures is completely impracticable, since the present investigation has examined only one method of separation. A full assessment of the feasibility of separating parallel stages would require, in addition to measured static aerodynamic data, inclusion of both the dynamic and aeroelastic characteristics of each major component during separation.

Langley Research Center,
National Aeronautics and Space Administration,
Langley Station, Hampton, Va., August 16, 1965.

REFERENCES

1. Decker, John P.; and Clark, Larry R.: Static Aerodynamic Characteristics of a Model of a Horizontal-Take-Off Reusable Launch Vehicle at Mach Numbers 1.60, 2.16, and 2.86. NASA TM X-1097, 1965.

2. Clark, Larry R.; and Pierpont, P. Kenneth: Transonic Characteristics of a Hydrogen-Fueled Multistage Horizontal-Take-Off Reusable Launch Vehicle. NASA TM X-1008, 1964.

3. Clark, Larry R.; and Decker, John P.: Longitudinal Aerodynamic Characteristics of a Model of a Horizontal-Take-Off Reusable Launch Vehicle at Mach Numbers From 3 to 6. NASA TM X-1030, 1964.

4. Norris, John D.; and Decker, John P.: Lateral Aerodynamic Characteristics of a Conceptual Horizontal-Take-Off Reusable Launch Vehicle From Mach 3 to 6. NASA TM X-1148, 1965.

5. Decker, John P.; and Pierpont, P. Kenneth: Aerodynamic Separation Characteristics of Conceptual Parallel-Staged Reusable Launch Vehicle at Mach 3 to 6. NASA TM X-1051, 1965.

6. Mechtly, E. A.: The International System of Units - Physical Constants and Conversion Factors. NASA SP-7012, 1964.

TABLE I.- GEOMETRIC DESIGN CHARACTERISTICS OF MODEL

First-stage reusable booster:		
Fuselage -		
Length	39.600 in.	100.584 cm
Equivalent base diameter	3.839 in.	9.751 cm
Maximum height	3.203 in.	8.136 cm
Nose radius	0.160 in.	0.406 cm
Base area	11.567 in^2	74.626 cm^2
Wing -		
Total area	176.000 in^2	1135.482 cm^2
Exposed area	95.70 in^2	617.418 cm^2
Span	16.000 in.	40.640 cm
Root chord	22.000 in.	55.880 cm
Tip chord	0 in.	0 cm
Maximum thickness, percent chord	5	
Leading-edge sweep angle, deg	70	
Leading-edge radius	0.040 in.	0.102 cm
Mean aerodynamic chord	14.667 in.	37.254 cm
Moment reference center, percent mean aerodynamic chord	15	
Moment reference center	12.47 in.	31.674 cm
Vertical fins -		
Area of each fin (exposed)	6.400 in^2	41.290 cm^2
Height (exposed)	1.920 in.	4.877 cm
Root chord	4.440 in.	11.278 cm
Tip chord	2.220 in.	5.639 cm
Leading-edge sweep angle, deg	60	
Trailing-edge sweep angle, deg	29.921	
Leading-edge radius	0.040 in.	0.102 cm
Wing nacelles -		
Length	6.637 in.	16.858 cm
Maximum diameter	0.960 in.	2.438 cm
Fineness ratio	6.914	
Nose radius	0.160 in.	0.406 cm
Canard -		
Total area	35.568 in^2	229.471 cm^2
Exposed area	12.440 in^2	80.258 cm^2
Span	7.200 in.	18.288 cm
Root chord	9.880 in.	25.095 cm
Tip chord	0 in.	0 cm
Maximum thickness, percent chord	5	
Leading-edge sweep angle, deg	70	
Leading-edge radius	0.040 in.	0.102 cm

TABLE I.- GEOMETRIC DESIGN CHARACTERISTICS OF MODEL - Continued

Second-stage reusable booster:		
Fuselage -		
Length	16.000 in.	40.640 cm
Equivalent base diameter	2.276 in.	5.781 cm
Base area	4.067 in^2	26.239 cm^2
Wing -		
Total area	75.200 in^2	485.160 cm^2
Exposed area	51.700 in^2	333.548 cm^2
Span	9.600 in.	24.384 cm
Root chord	11.780 in.	29.921 cm
Tip chord	3.852 in.	9.784 cm
Maximum thickness, percent chord	2.800	
Leading-edge sweep angle, deg	58.75	
Leading-edge radius	0.040 in.	0.102 cm
Mean aerodynamic chord	8.49 in.	21.565 cm
Moment reference center	12.47 in.	31.674 cm
Vertical fins -		
Area of each fin (exposed)	6.321 in^2	40.781 cm^2
Height	2.082 in.	5.288 cm
Root chord	4.300 in.	10.922 cm
Tip chord	2.220 in.	5.639 cm
Leading-edge sweep angle	60	
Trailing-edge sweep angle, deg	29.921	
Leading-edge radius	0.040 in.	0.102 cm
Orbital stage:		
Fuselage -		
Length, including interstage	10.080 in.	25.603 cm
Diameter	1.120 in.	2.845 cm
Interstage base diameter	2.134 in.	5.420 cm
Interstage taper, included angle, deg	35.2	
Length of nose cone	1.428 in.	3.627 cm
Nose-cone included angle, deg	35	
Nose radius	0.160 in.	0.406 cm
Wing -		
Total area	23.685 in^2	152.806 cm^2
Exposed area (top surface)	14.852 in^2	95.819 cm^2
Exposed area (bottom surface)	8.510 in^2	54.903 cm^2
Span	4.177 in.	10.610 cm
Root chord	8.827 in.	22.421 cm
Tip chord	2.648 in.	6.726 cm
Maximum thickness, percent chord	5	
Leading-edge sweep angle, deg	72.5	
Leading-edge radius	0.040 in.	0.102 cm
Wing nose radius	0.160 in.	0.406 cm

TABLE I.- GEOMETRIC DESIGN CHARACTERISTICS OF MODEL - Concluded

Vertical fins -		
Area	2.405 in^2	15.516 cm^2
Height	1.430 in.	3.632 cm
Root chord	2.648 in.	6.726 cm
Tip chord	0.800 in.	2.032 cm
Maximum thickness, percent chord	5	
Leading-edge sweep angle, deg	55	
Leading-edge radius	0.048 in.	0.122 cm
Lateral inclination angle, deg	3	
Pad -		
Length	10.080 in.	25.603 cm
Maximum width	2.134 in.	5.420 cm
Nose radius	0.160 in.	0.406 cm
Wedge included angle, deg	72.5	
Maneuver propulsion package -		
Length	4.800 in.	12.192 cm
Diameter	2.134 in.	5.420 cm

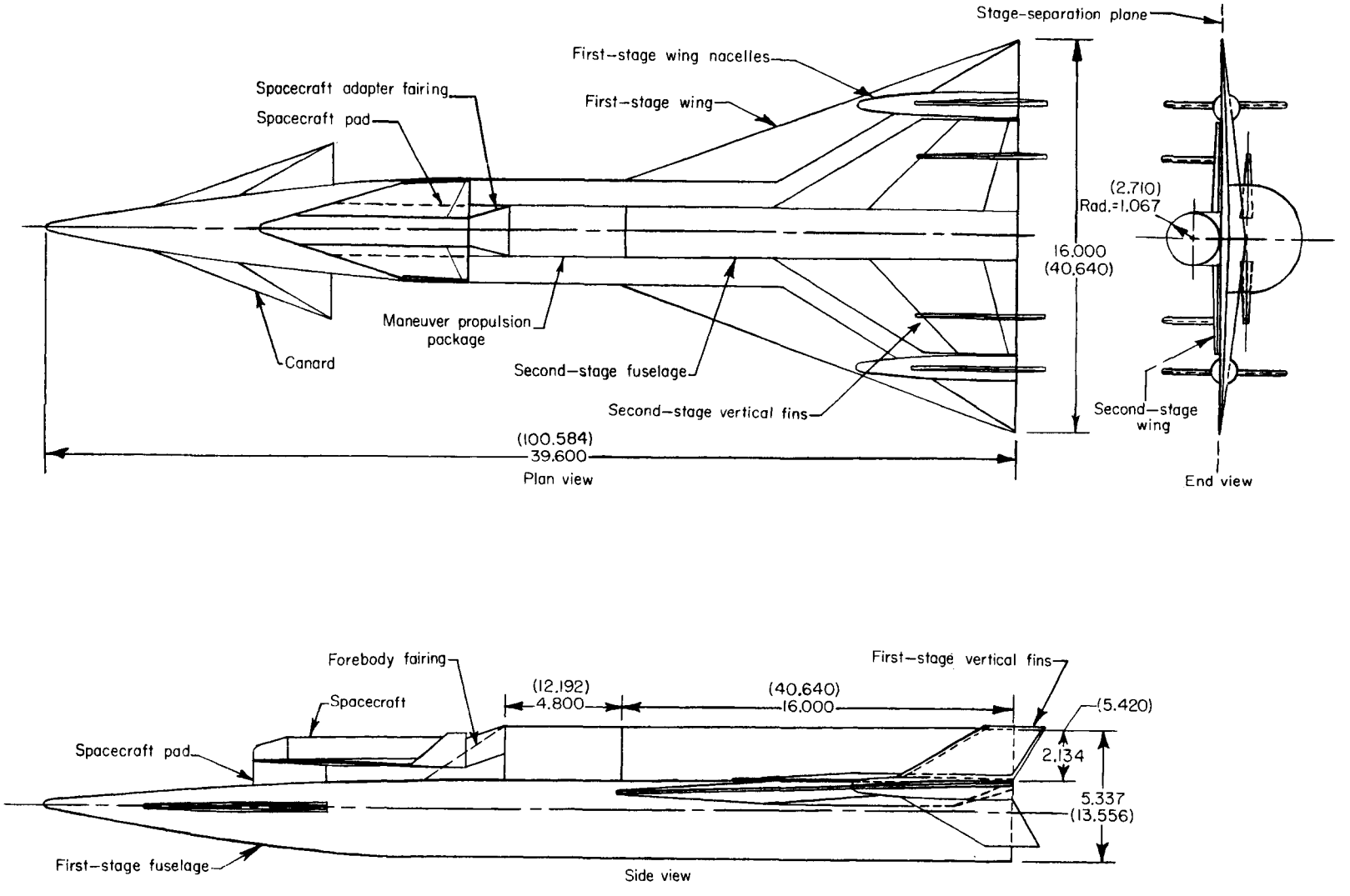

(a) General arrangement of the launch vehicle prior to separation.

Figure 1.- Arrangement and geometric details of a three-stage horizontal-take-off reusable booster system. Dimensions are given in inches and parenthetically in centimeters.

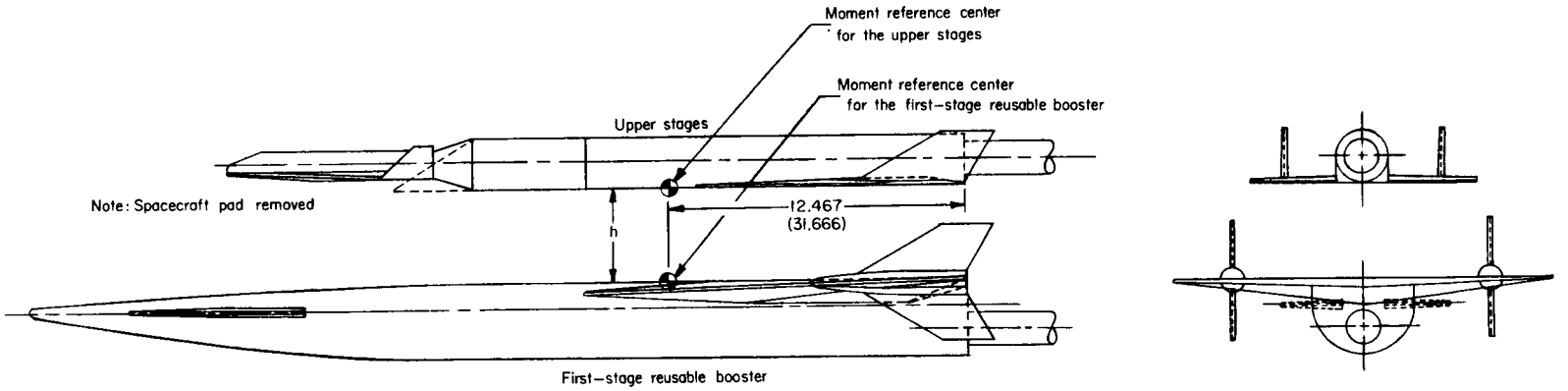

(b) General arrangement of the first-stage reusable booster and the upper stages during abort-separation investigation.

Figure 1.- Continued.

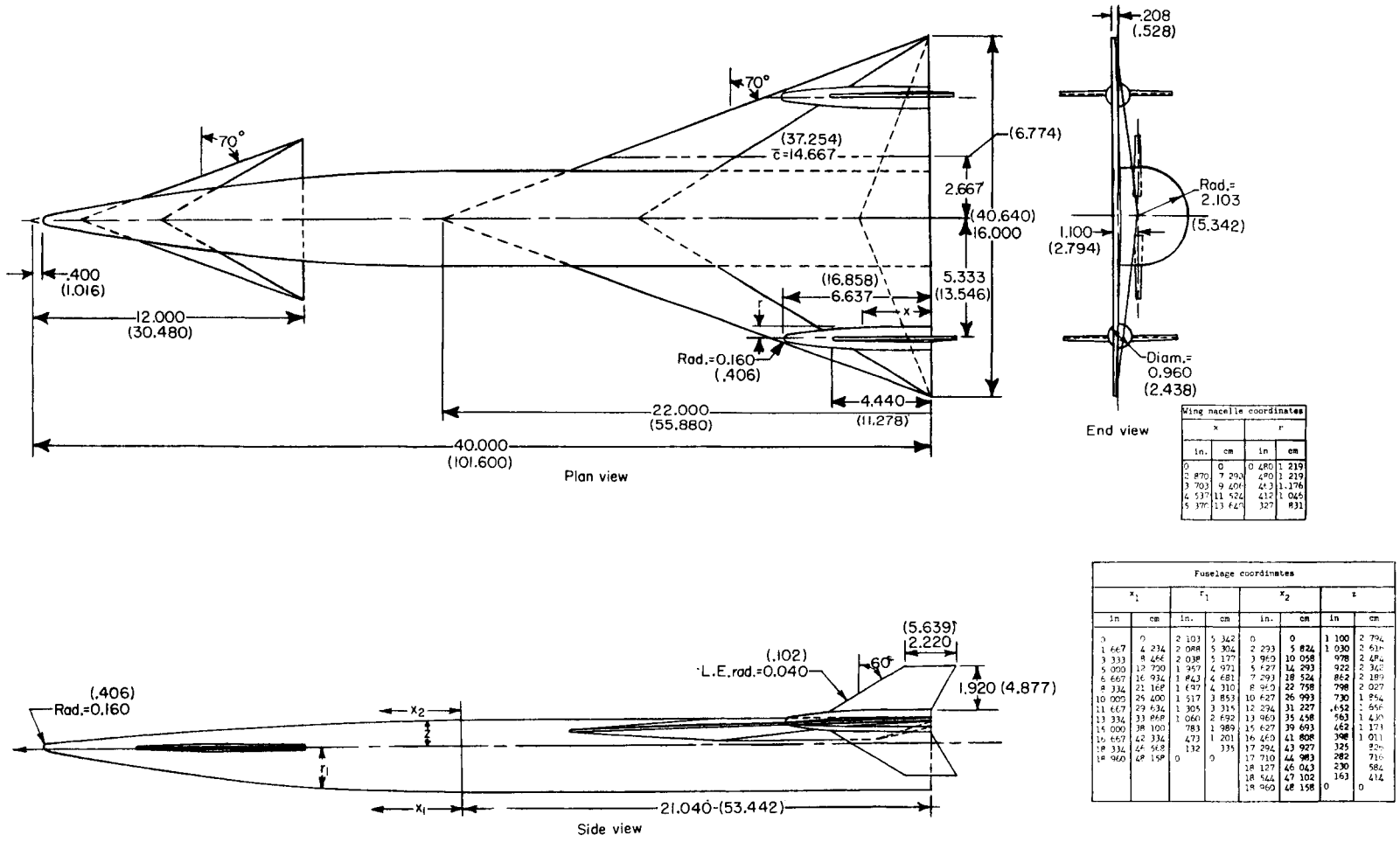

Wing nacelle coordinates

x		r	
in.	cm	in	cm
0	0	0.480	1.219
2.870	7.290	480	1.219
3.703	9.404	443	1.176
4.537	11.524	412	1.046
5.371	13.645	327	831

Fuselage coordinates

x_1		r_1		x_2		r	
in	cm	in.	cm	in.	cm	in	cm
0	0	2.103	5.342	0	0	1.100	2.794
1.667	4.234	2.088	5.304	2.293	5.824	1.030	2.616
3.333	8.466	2.038	5.177	3.960	10.058	978	2.484
5.000	12.700	1.957	4.971	5.627	14.293	922	2.342
6.667	16.934	1.843	4.681	7.293	18.524	862	2.189
8.334	21.168	1.697	4.310	8.960	22.758	798	2.027
10.000	25.400	1.517	3.853	10.627	26.993	730	1.854
11.667	29.634	1.305	3.315	12.294	31.227	.652	1.656
13.334	33.868	1.060	2.692	13.960	35.458	563	1.430
15.000	38.100	.783	1.989	15.627	39.693	462	1.171
16.667	42.334	.473	1.201	16.460	41.808	398	1.011
18.334	46.568	.132	.335	17.294	43.927	325	.826
18.960	48.158	0	0	17.710	44.983	282	.716
				18.127	46.043	230	.584
				18.544	47.102	163	.414
				18.960	48.158	0	0

(c) Details of first-stage reusable booster.

Figure 1.- Continued.

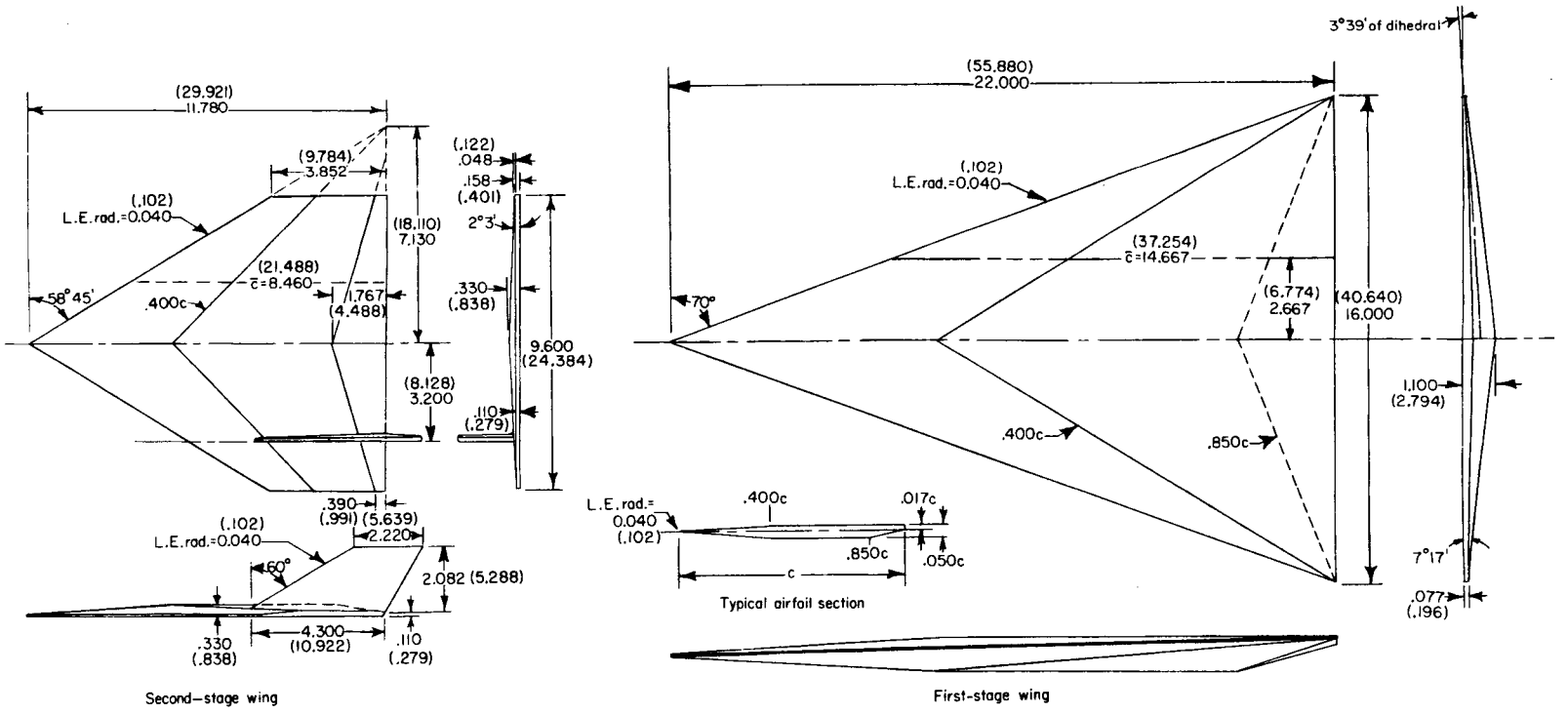

(d) Details of first- and second-stage wings.

Figure 1.- Continued.

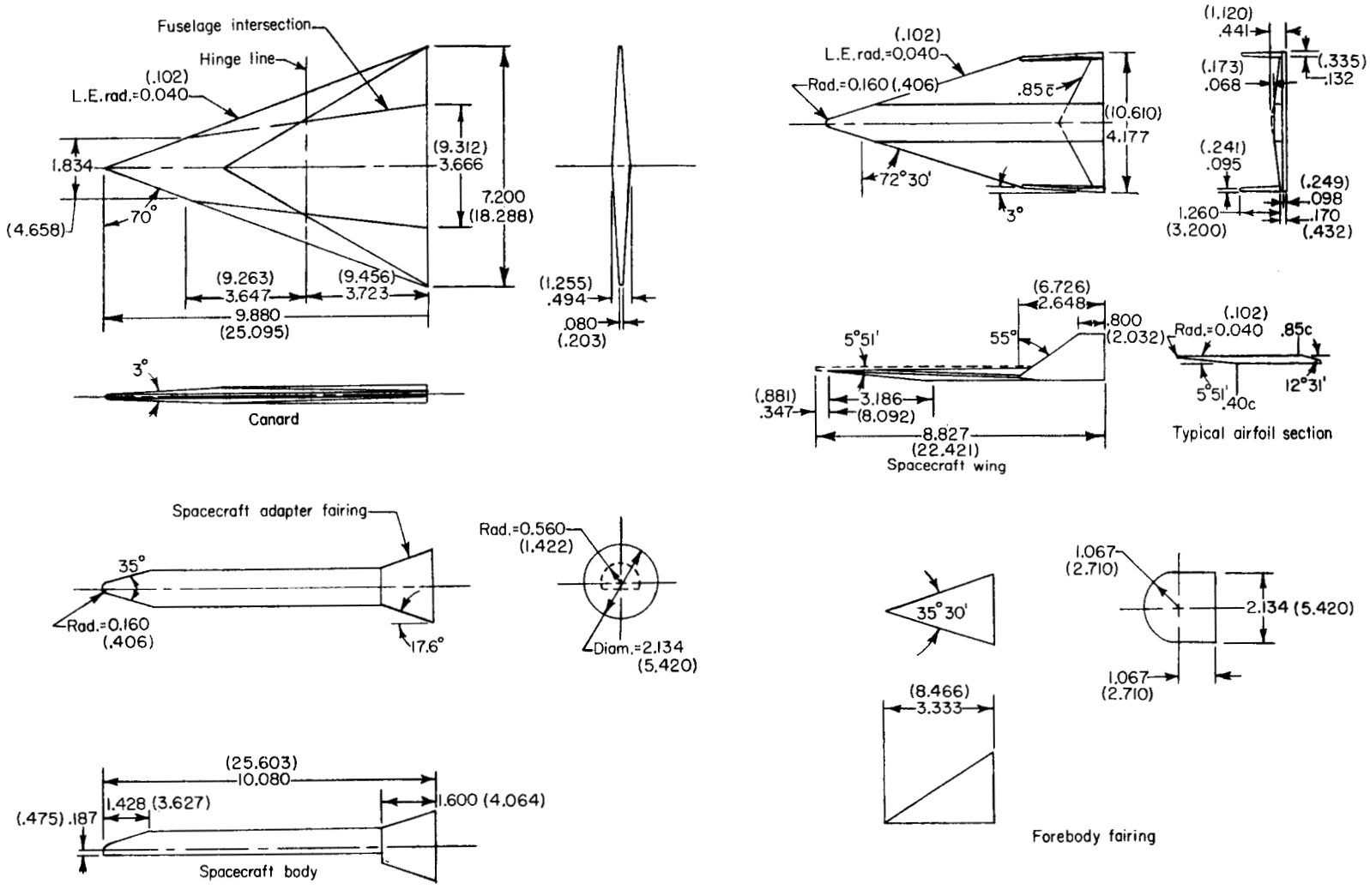

(e) Details of canard, spacecraft, and forebody fairing.

Figure 1.- Concluded.

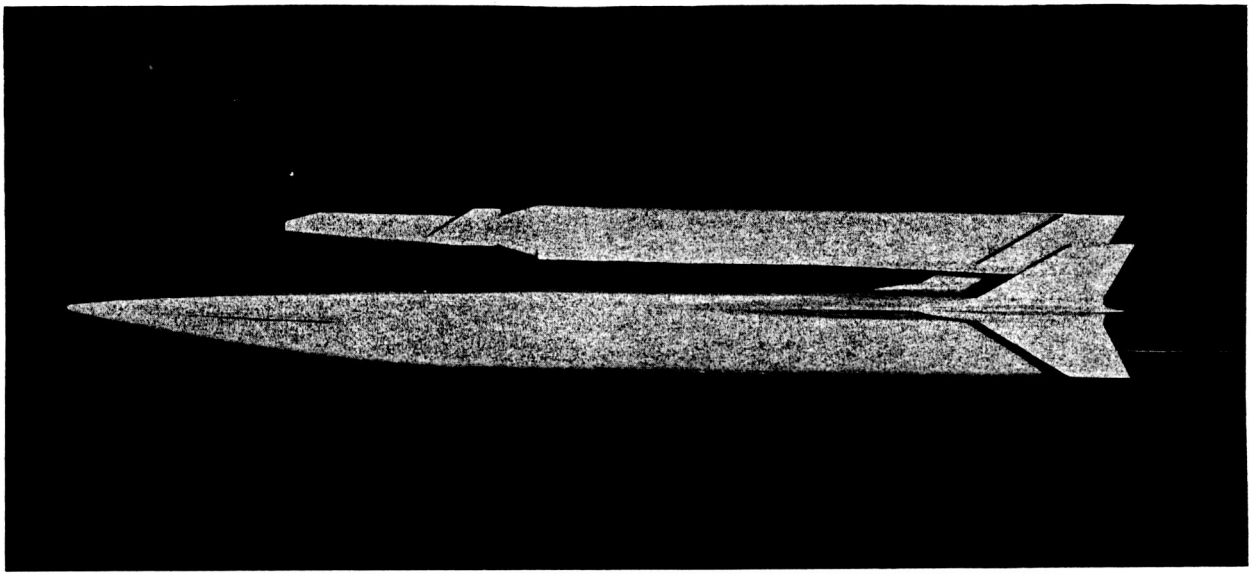

(a) Complete upper-stage configuration; h/d = 0.25. L-64-3209

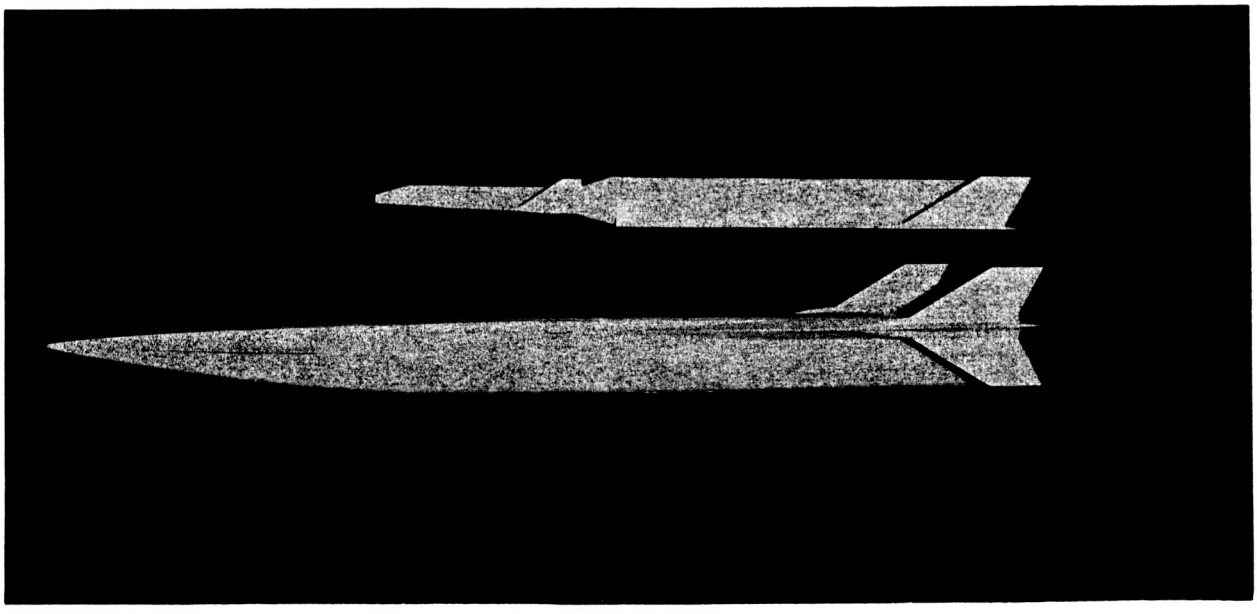

L-64-3219

(b) Upper-stage configuration without the maneuver propulsion package; h/d = 1.00.

Figure 2.- Photographs of various upper-stage configurations separated from the complete first stage.

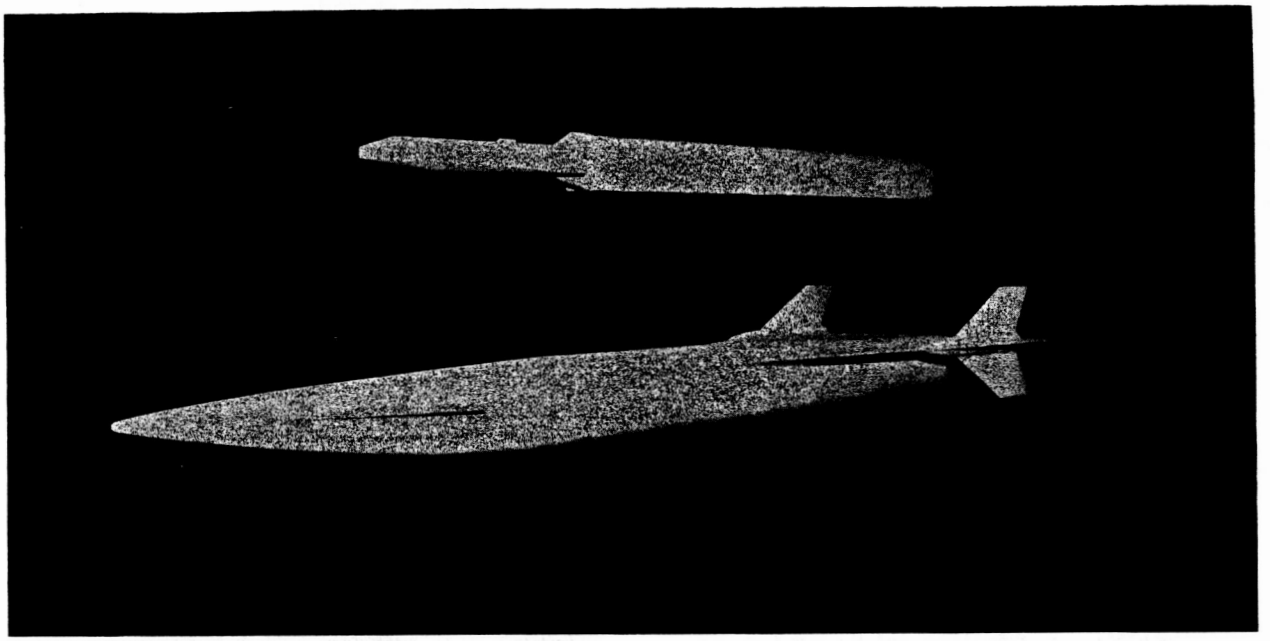

(c) Upper-stage configuration without the second-stage wing; h/d = 1.50. L-64-3225

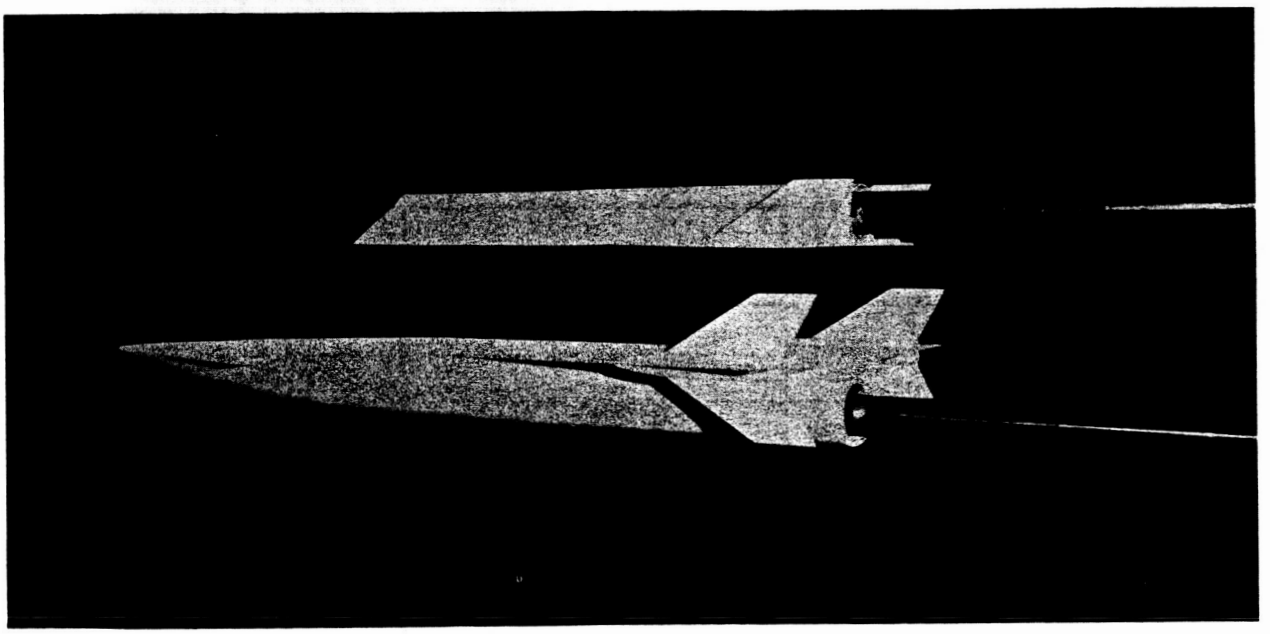

L-64-3211

(d) Upper-stage configuration with the spacecraft and adapter fairing replaced with a forebody fairing; h/d = 1.00.

Figure 2.- Concluded.

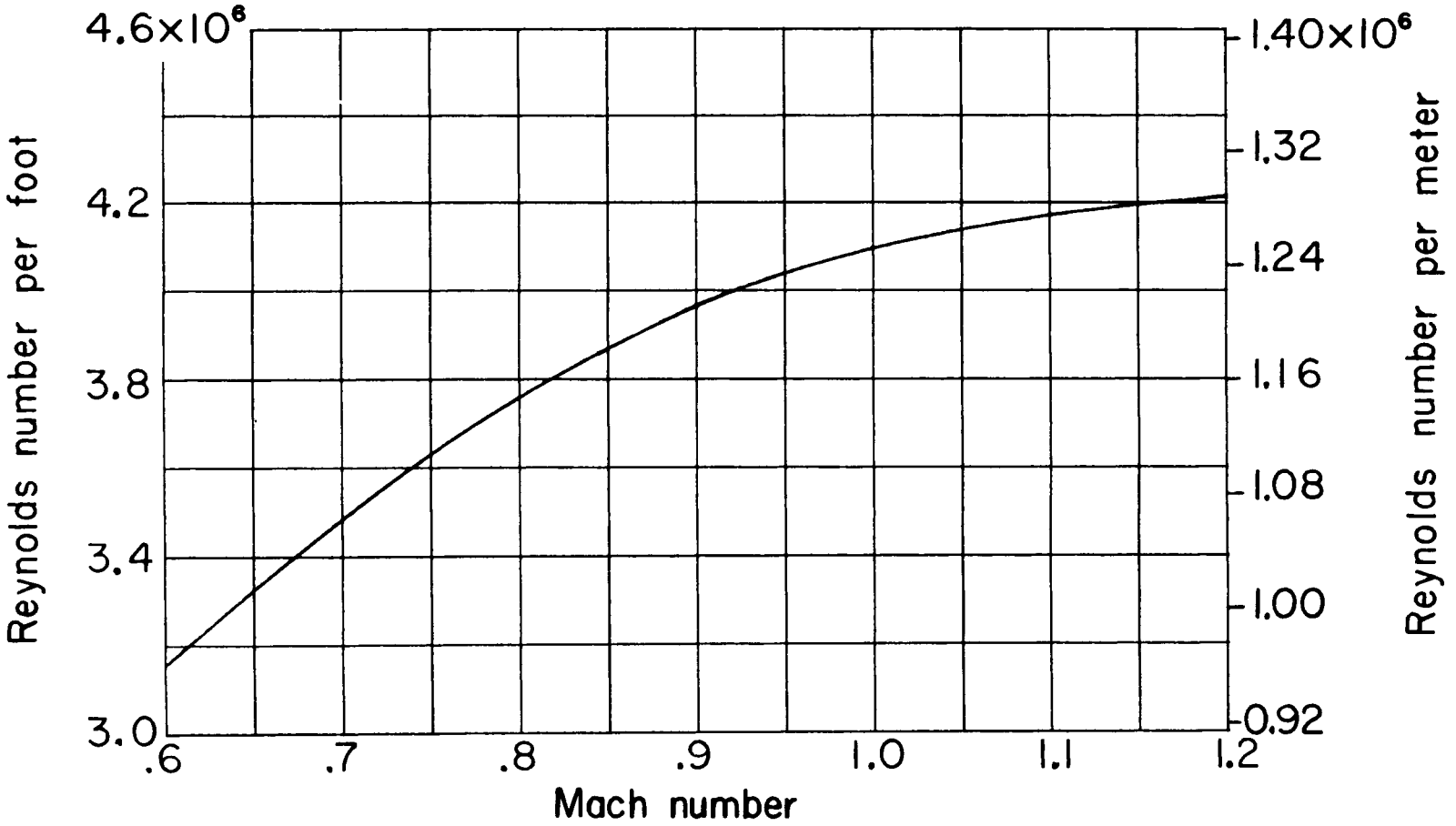

Figure 3.- Variation with Mach number of the average test Reynolds numbers.

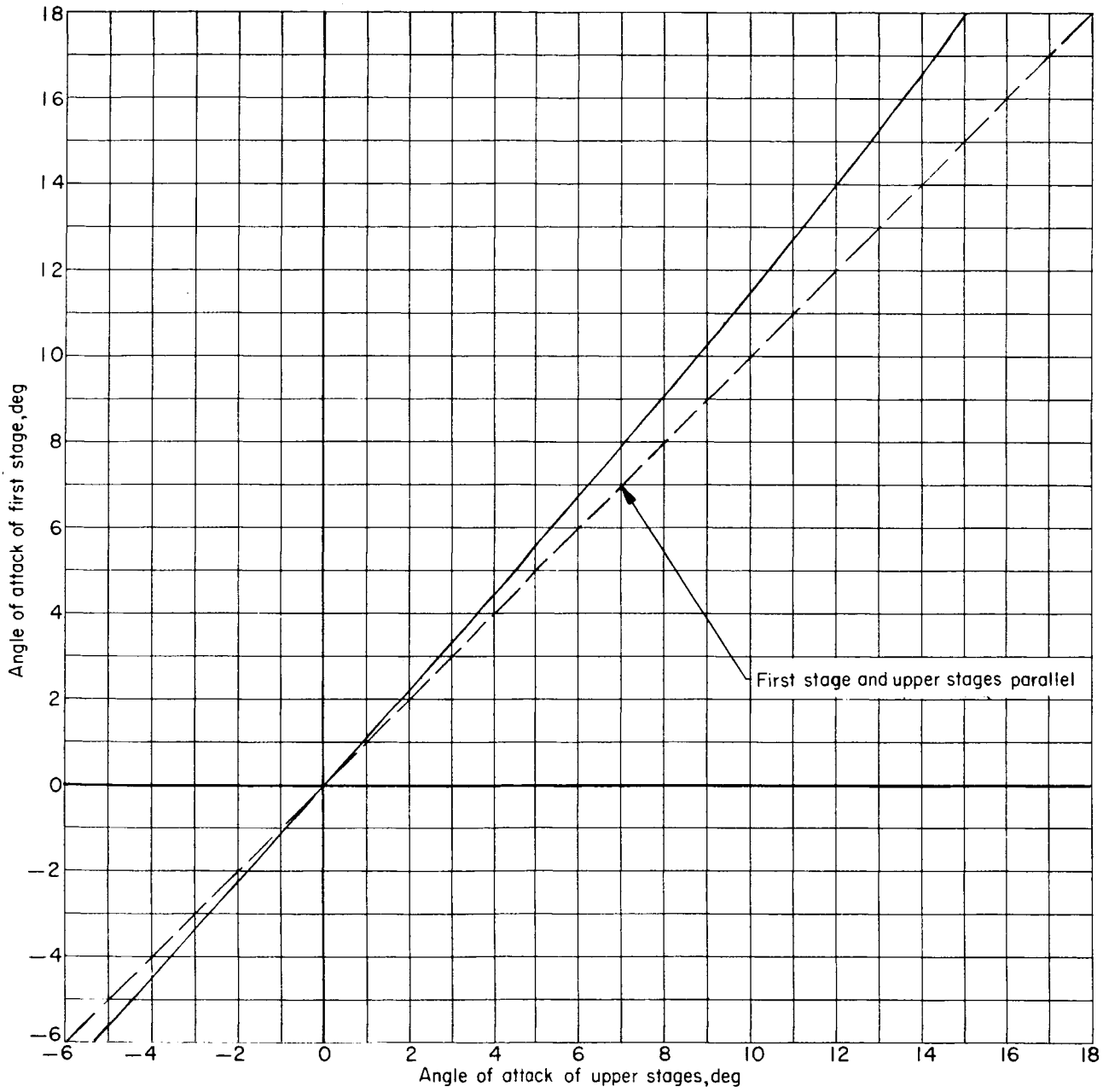

Figure 4.- Typical angle-of-attack deviation at all test Mach numbers, due to balance and sting deflection under load, between the first-stage reusable booster and the upper stages.

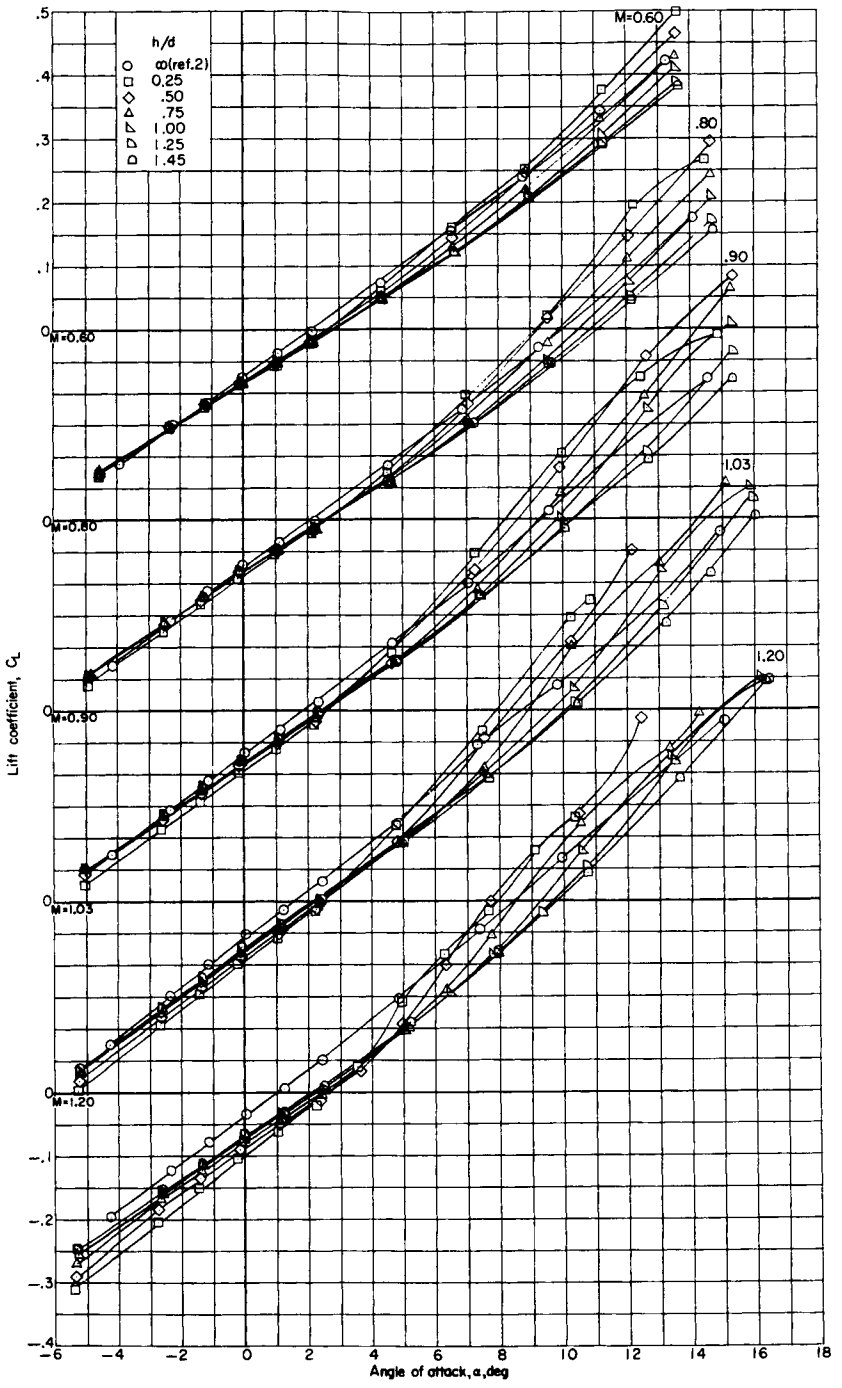

(a) Variation of lift coefficient with angle of attack.

Figure 5.- Longitudinal aerodynamic characteristics of the complete first stage in presence of BWFMS.

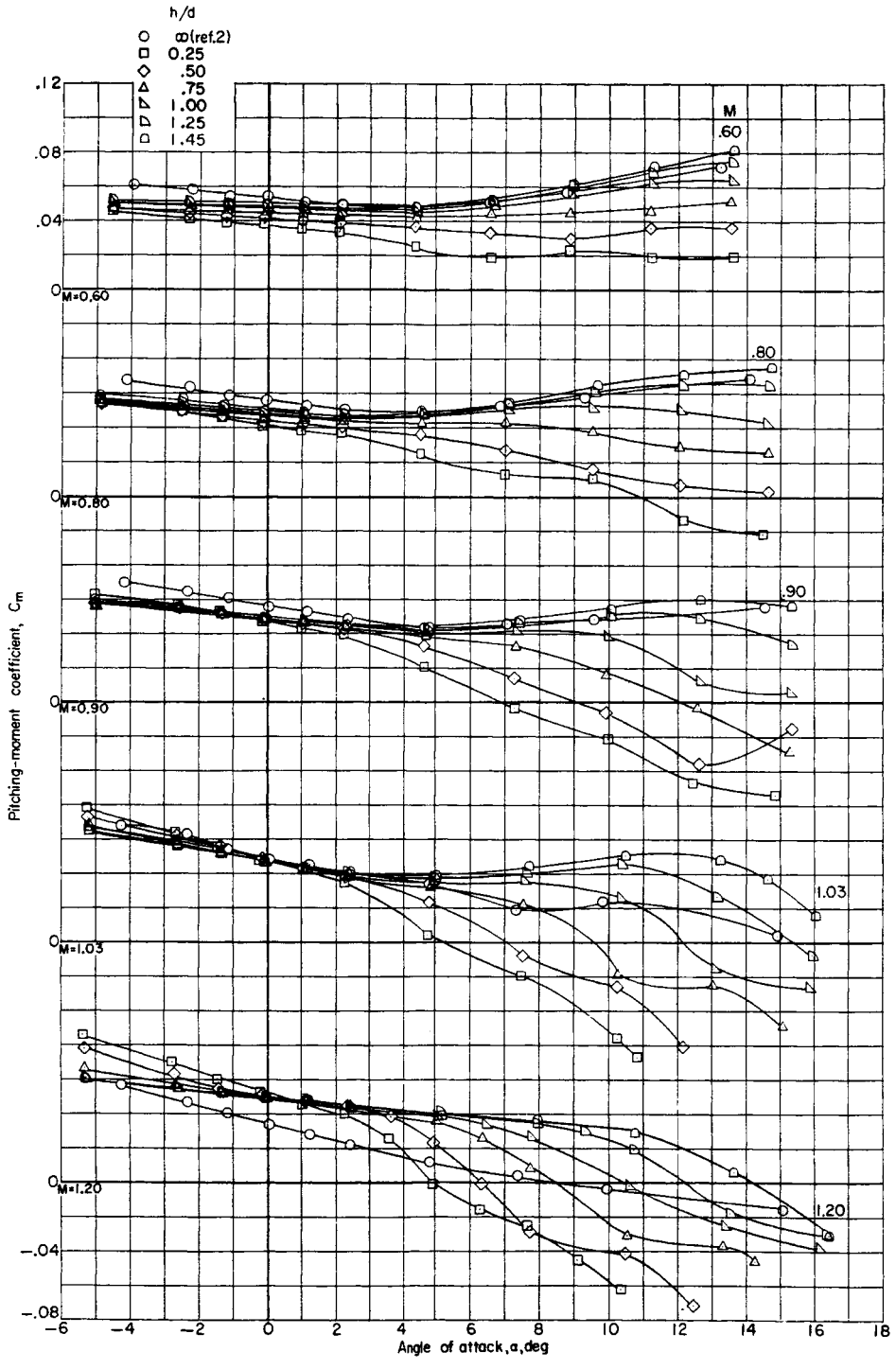

(b) Variation of pitching-moment coefficient with angle of attack.

Figure 5.- Continued.

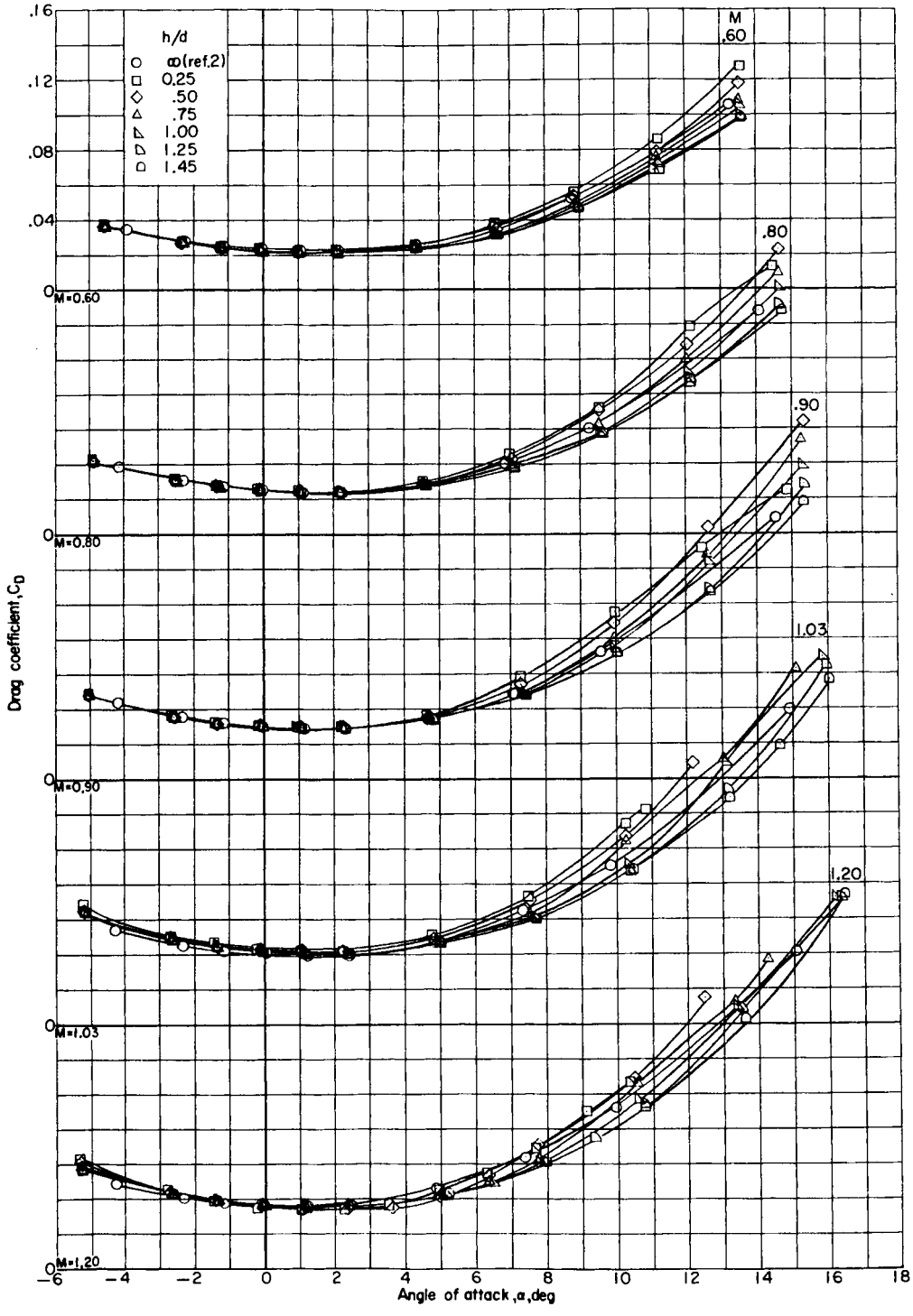

(c) Variation of drag coefficient with angle of attack.

Figure 5.- Concluded.

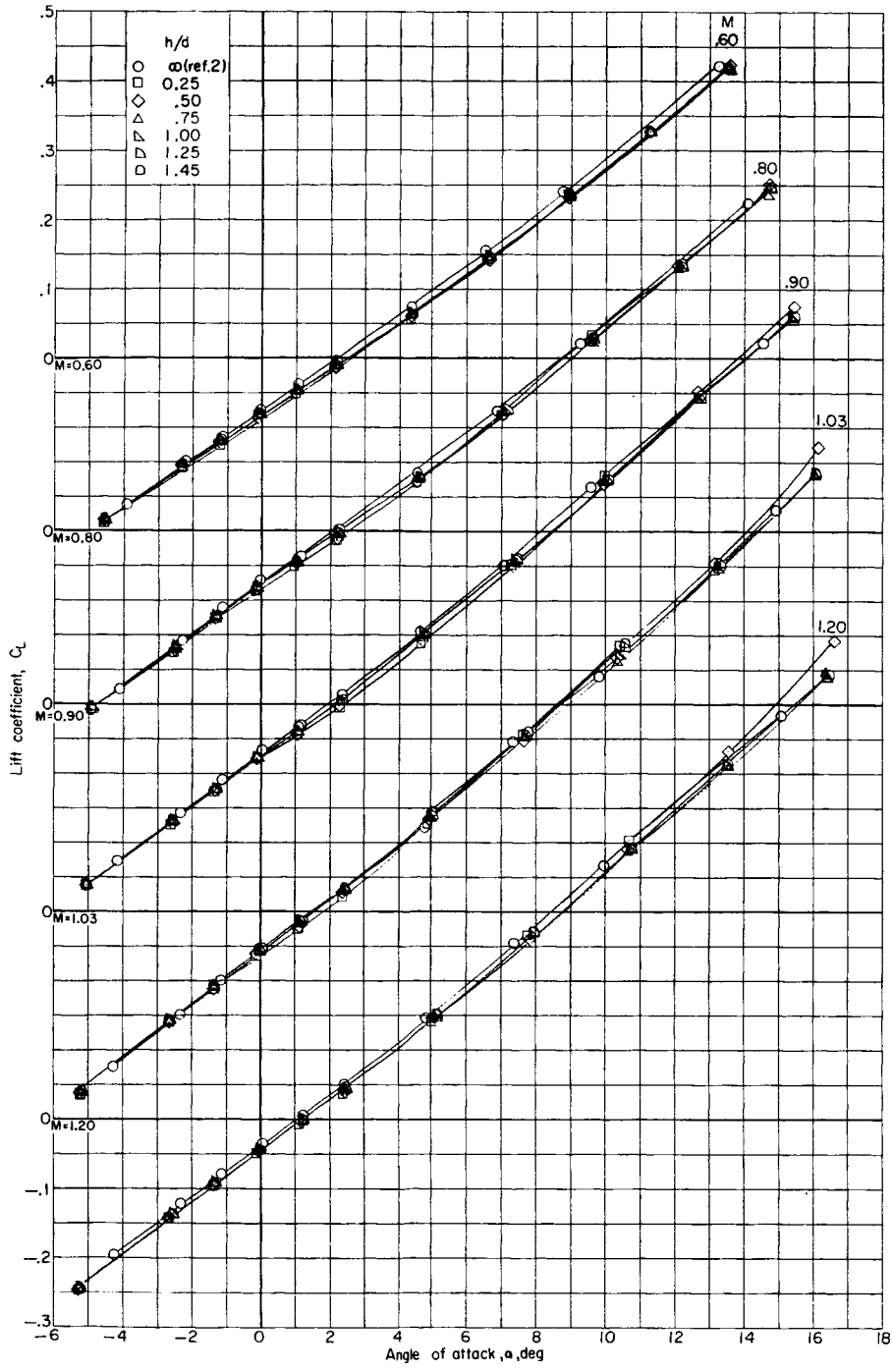

(a) Variation of lift coefficient with angle of attack.

Figure 6.- Longitudinal aerodynamic characteristics of the complete first stage in presence of BMS.

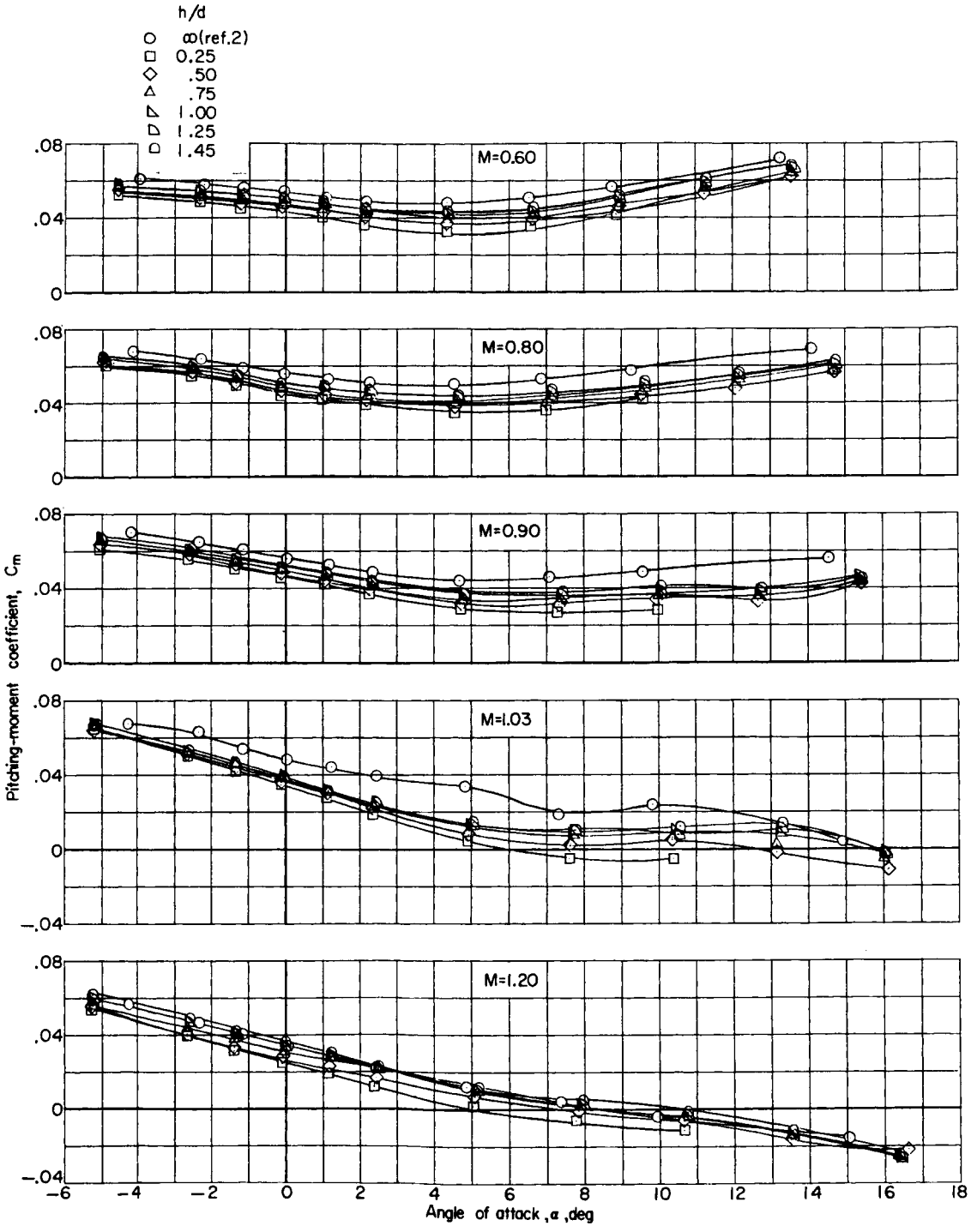

(b) Variation of pitching-moment coefficient with angle of attack.

Figure 6.- Continued.

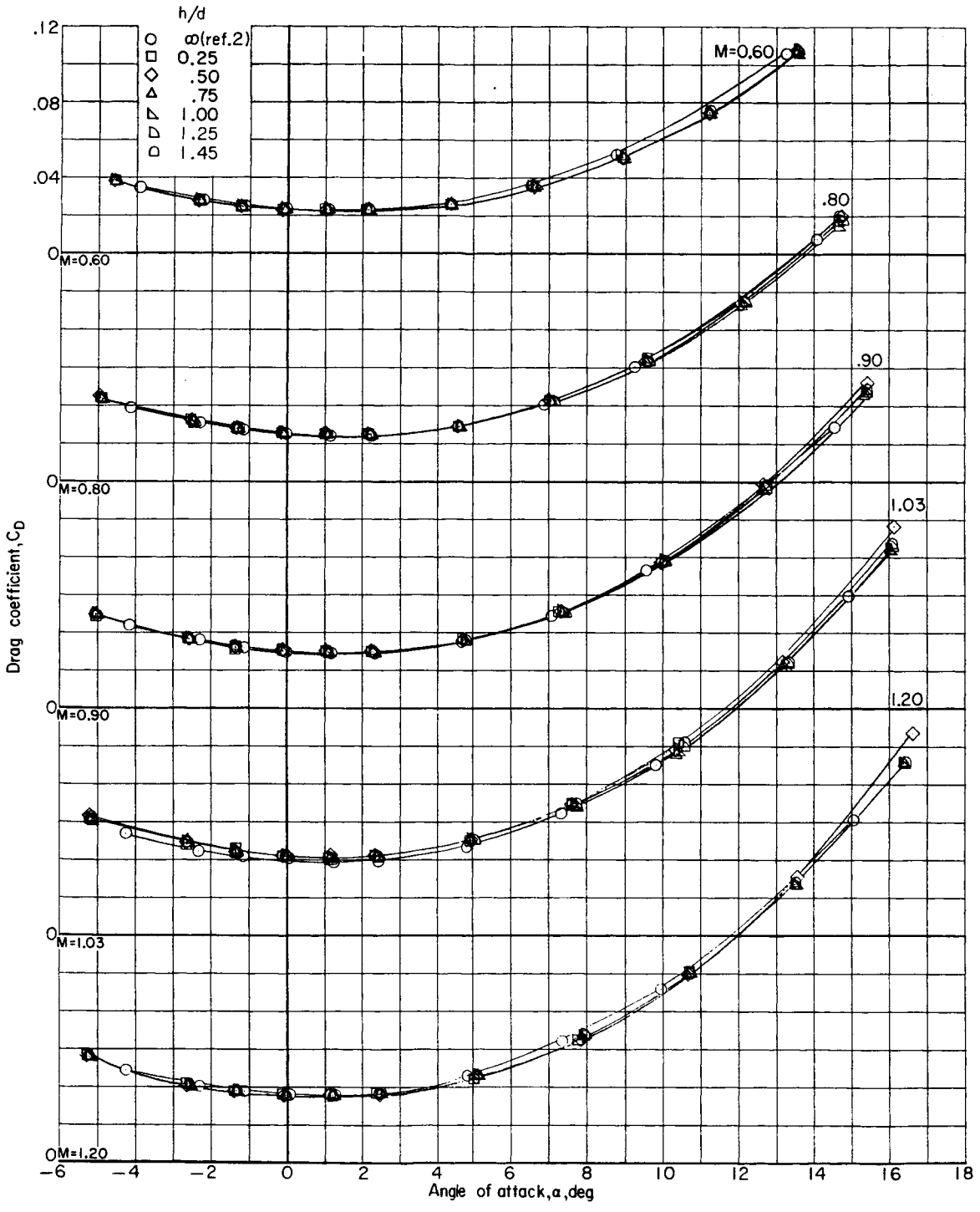

(c) Variation of drag coefficient with angle of attack.

Figure 6.- Concluded.

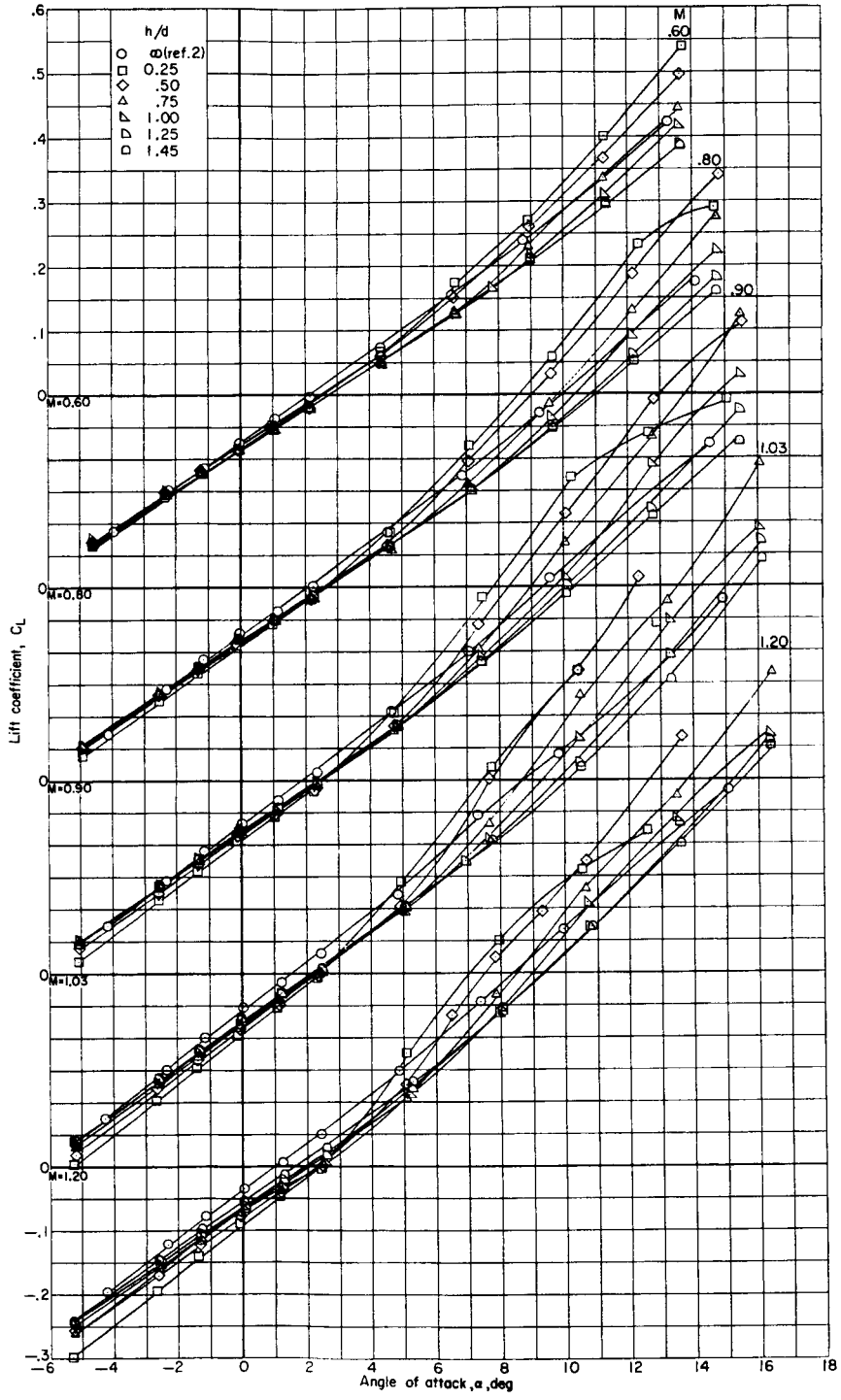

(a) Variation of lift coefficient with angle of attack.

Figure 7.- Longitudinal aerodynamic characteristics of the complete first stage in presence of BWFS.

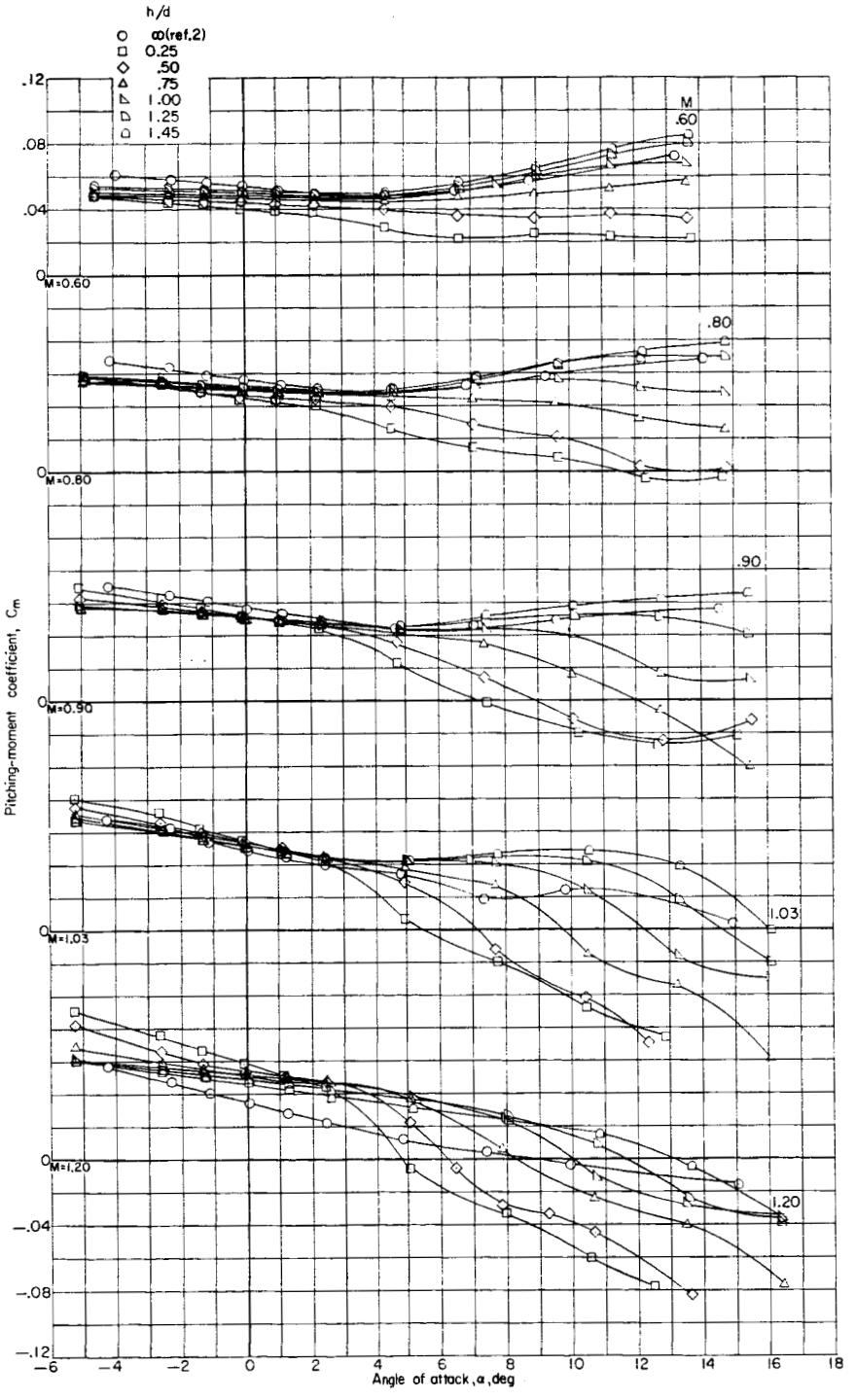

(b) Variation of pitching-moment coefficient with angle of attack.

Figure 7.- Continued.

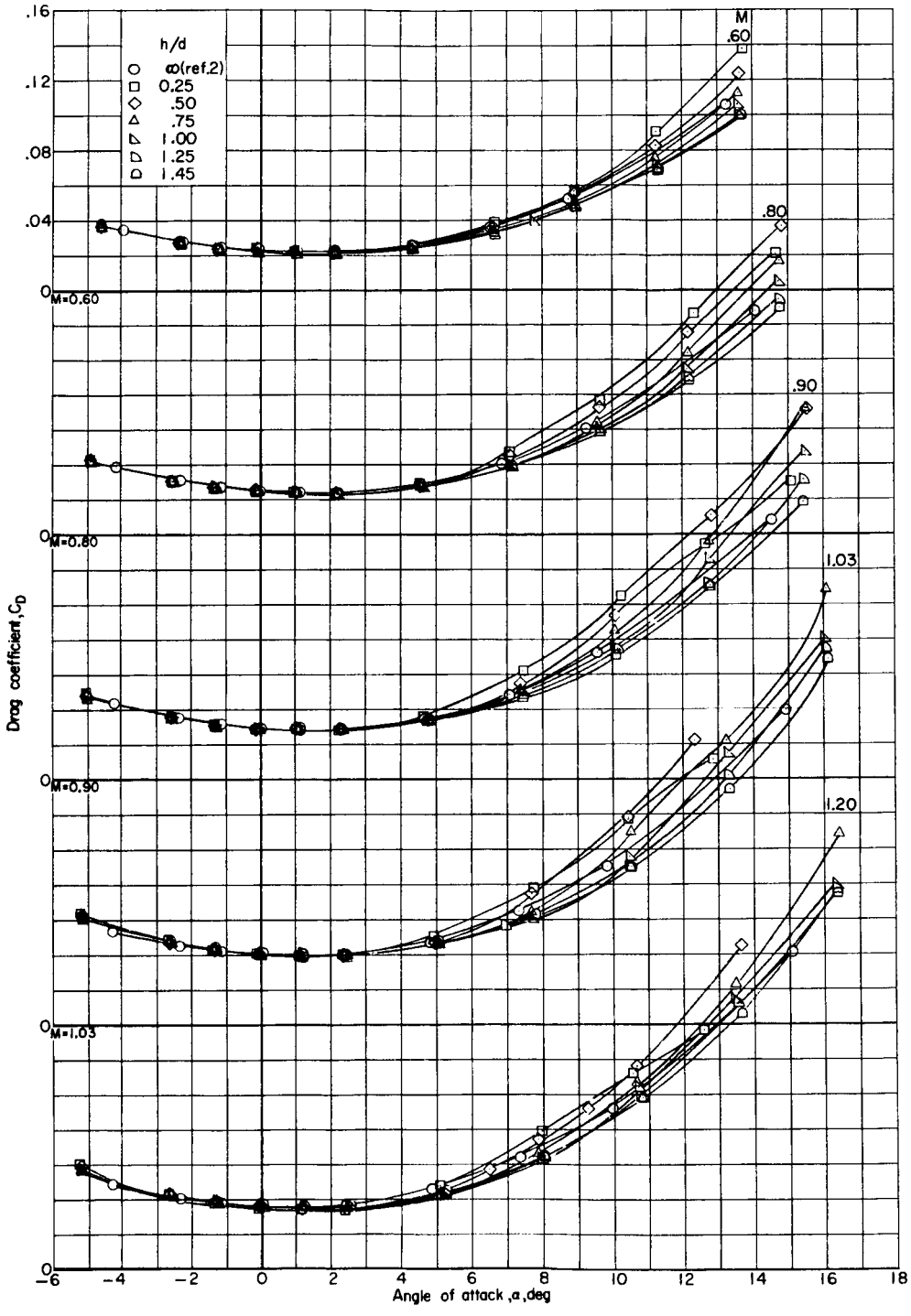

(c) Variation of drag coefficient with angle of attack.

Figure 7.- Concluded.

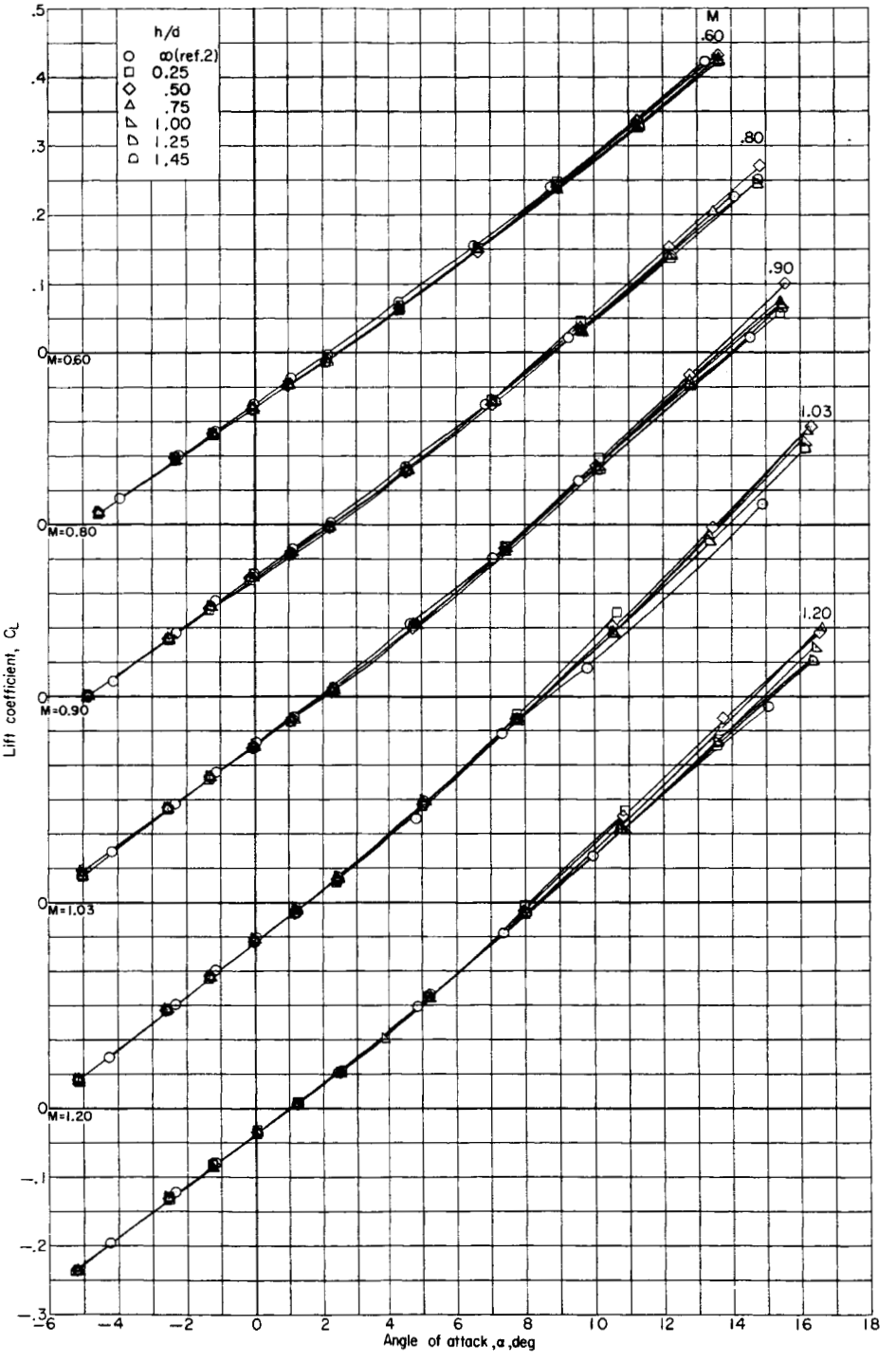

(a) Variation of lift coefficient with angle of attack.

Figure 8.- Longitudinal aerodynamic characteristics of the complete first stage in presence of BS.

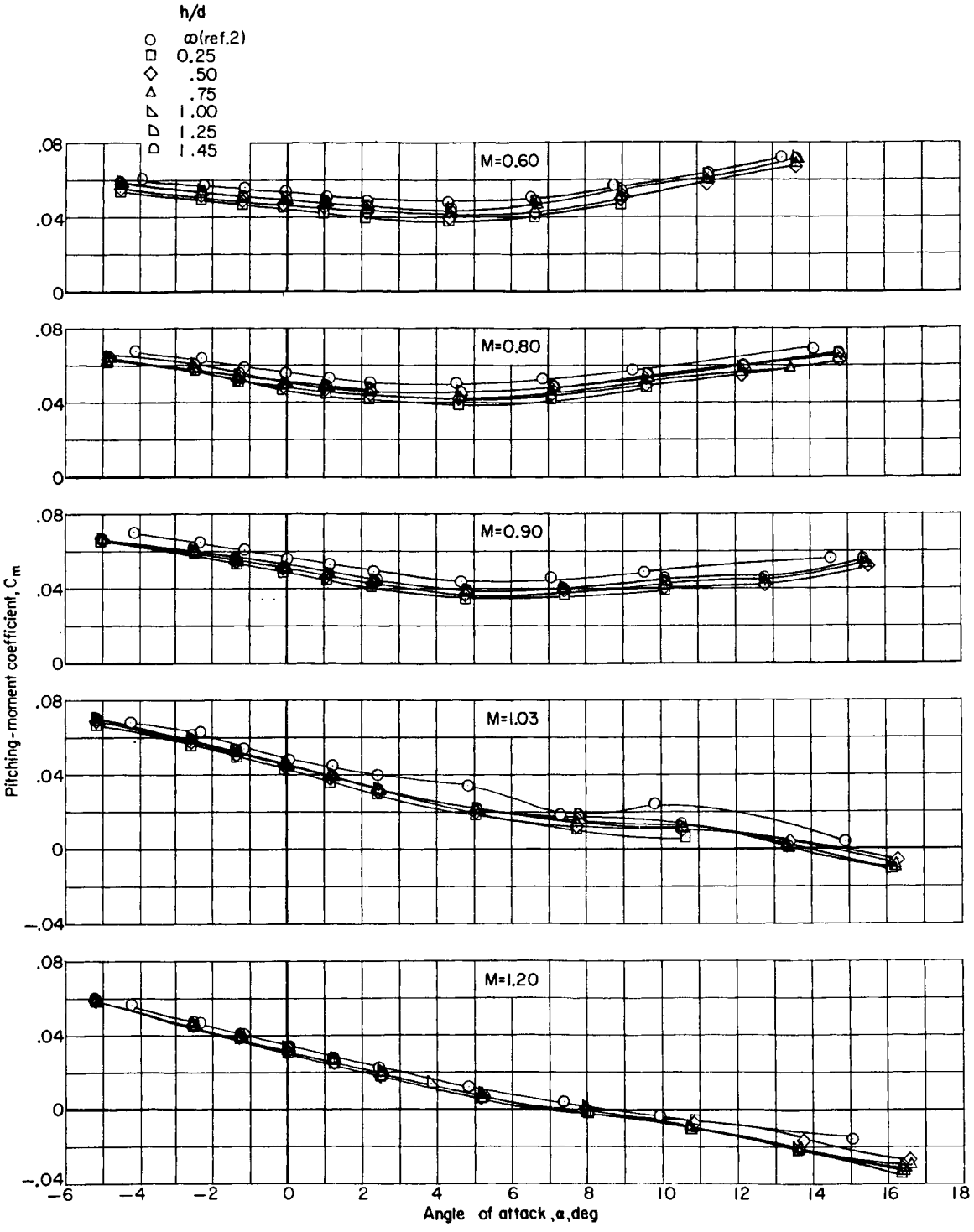

(b) Variation of pitching-moment coefficient with angle of attack.

Figure 8.- Continued.

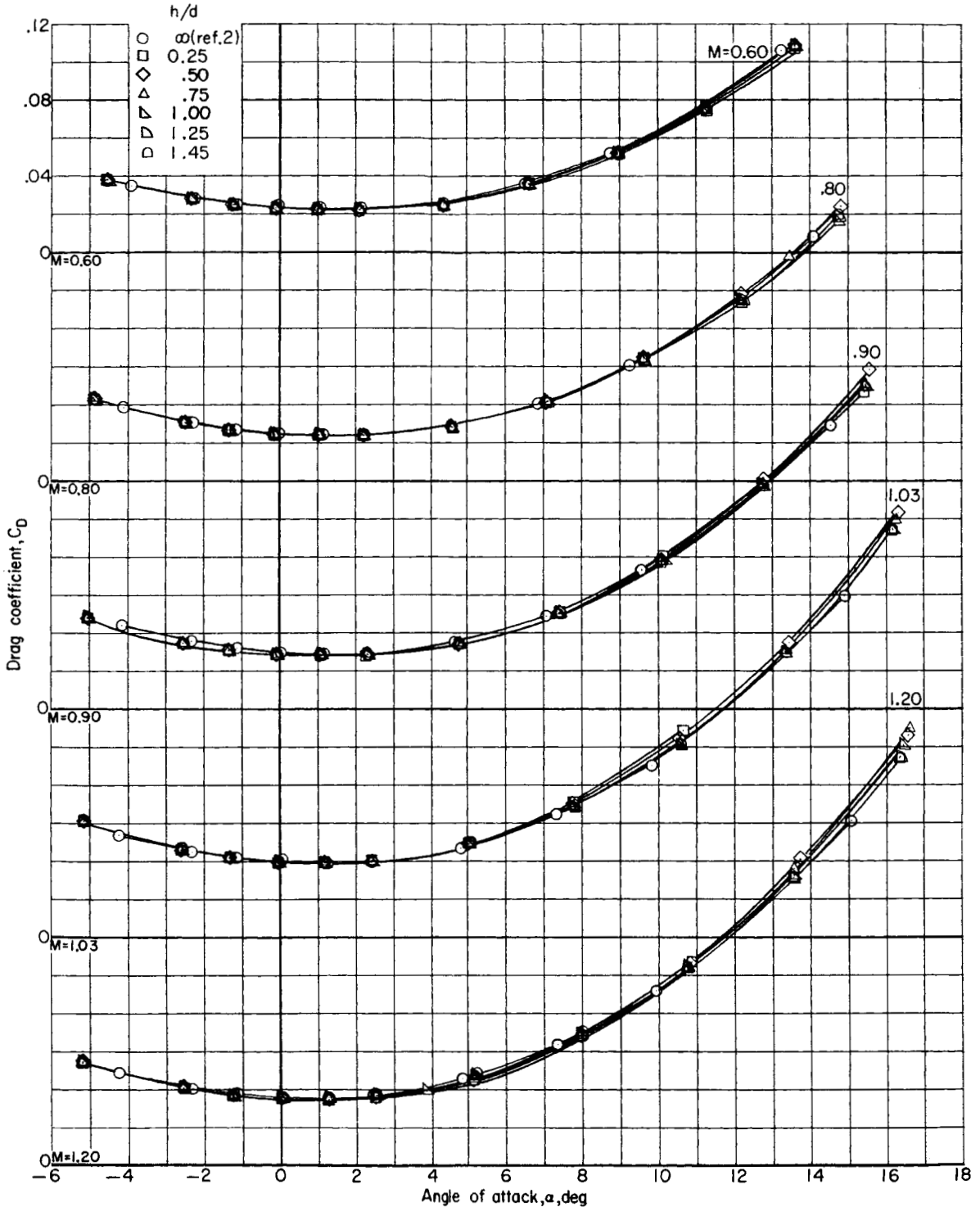

(c) Variation of drag coefficient with angle of attack.

Figure 8.- Concluded.

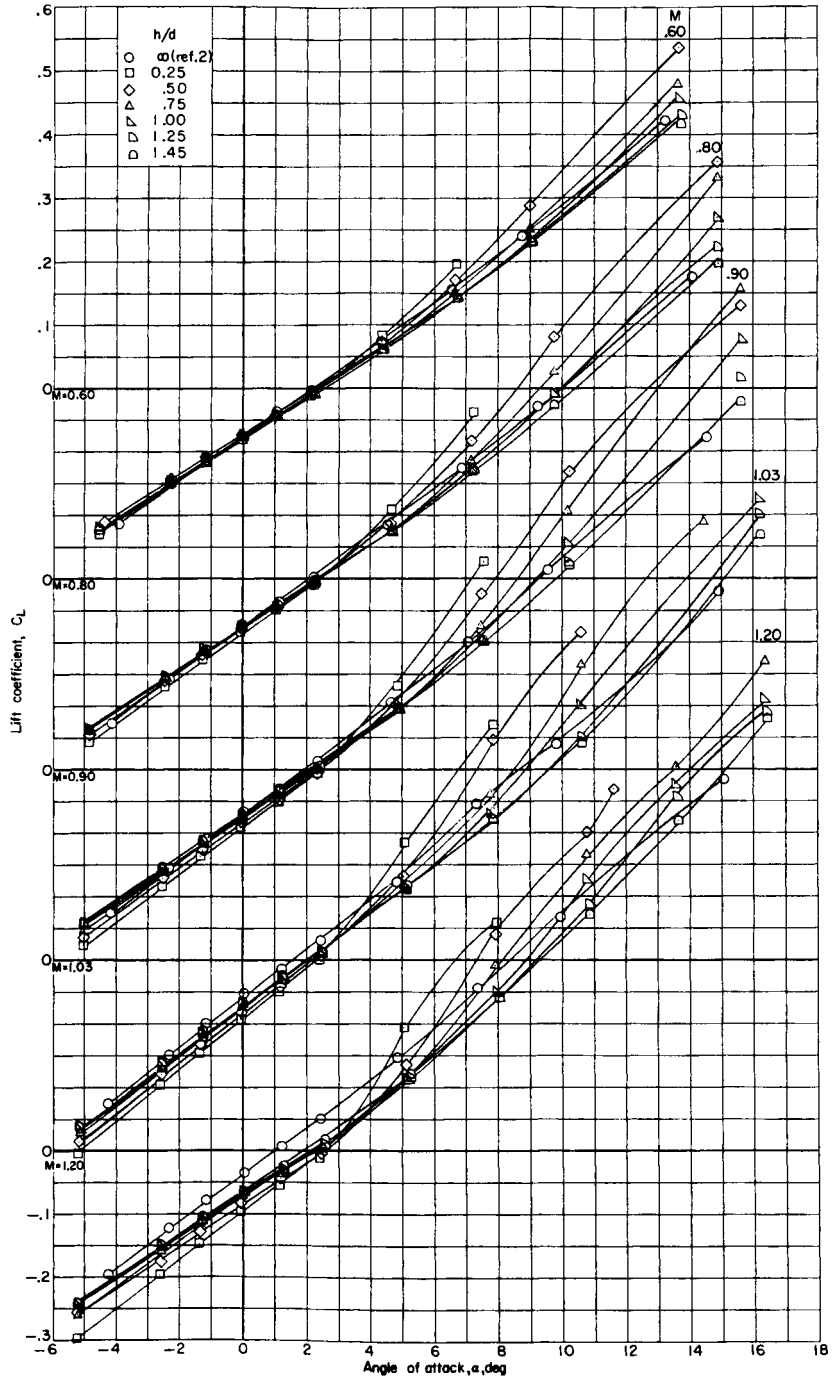

(a) Variation of lift coefficient with angle of attack.

Figure 9.- Longitudinal aerodynamic characteristics of the complete first stage in presence of BWFMS'.

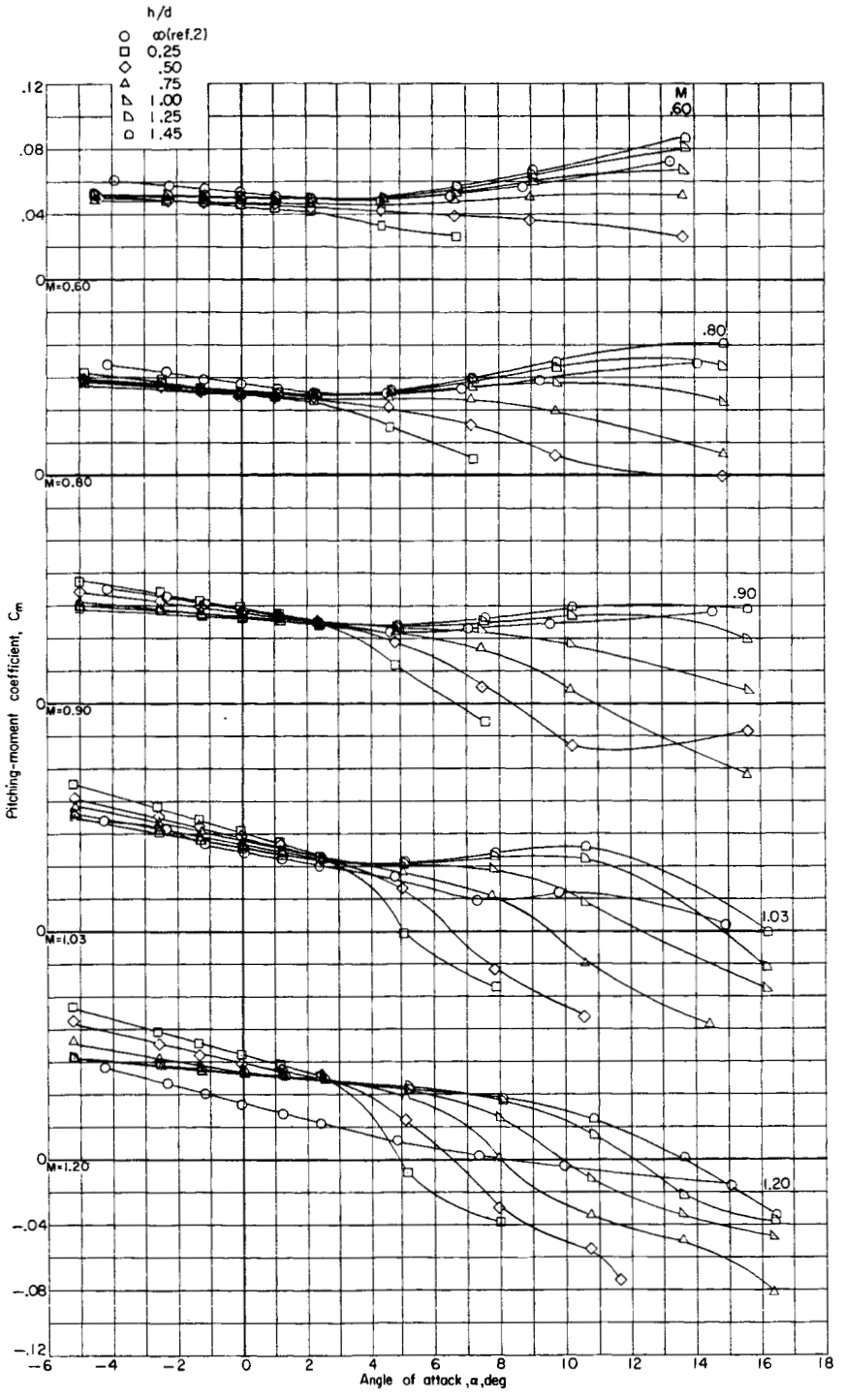

(b) Variation of pitching-moment coefficient with angle of attack.

Figure 9.- Continued.

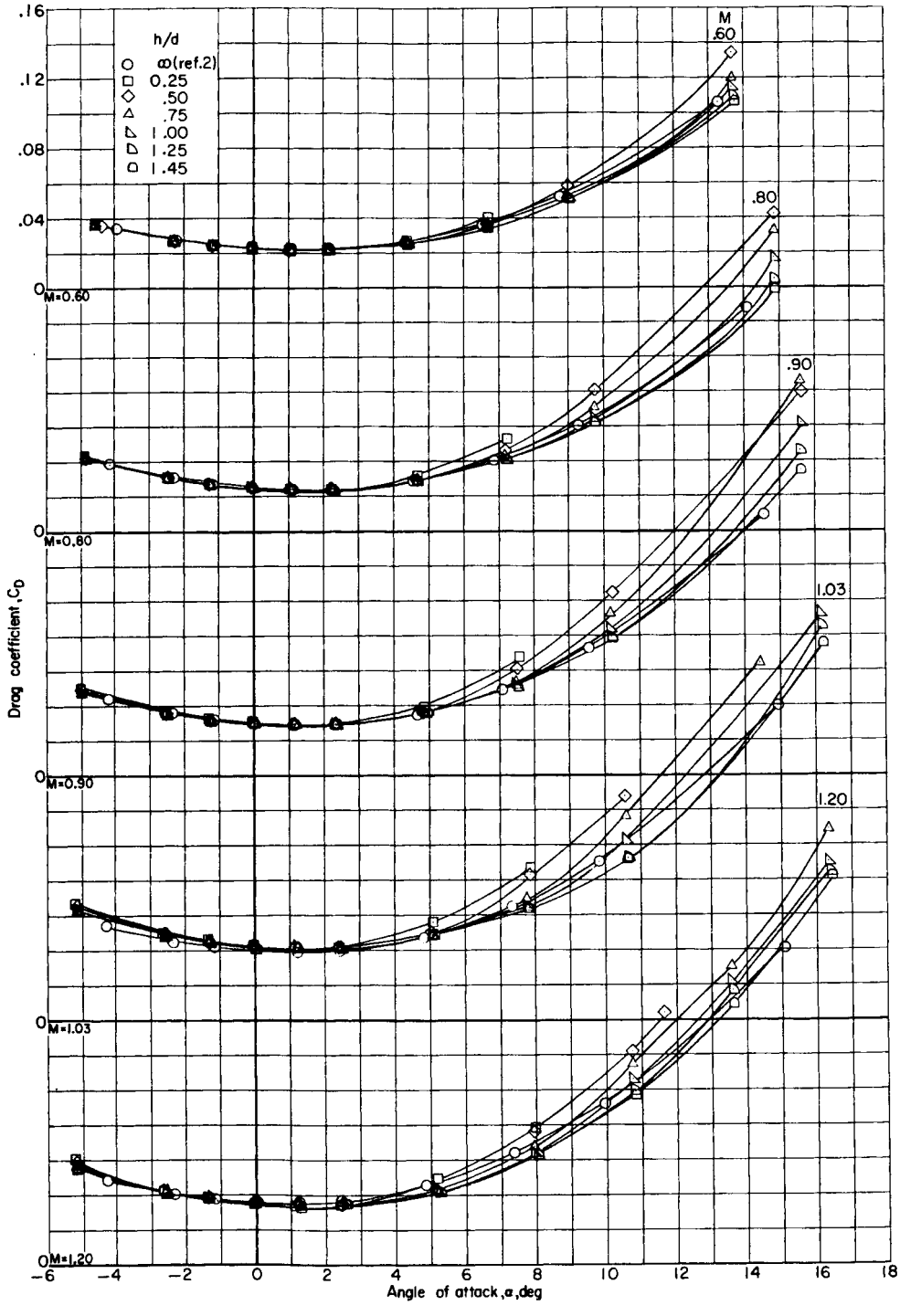

(c) Variation of drag coefficient with angle of attack.

Figure 9.- Concluded.

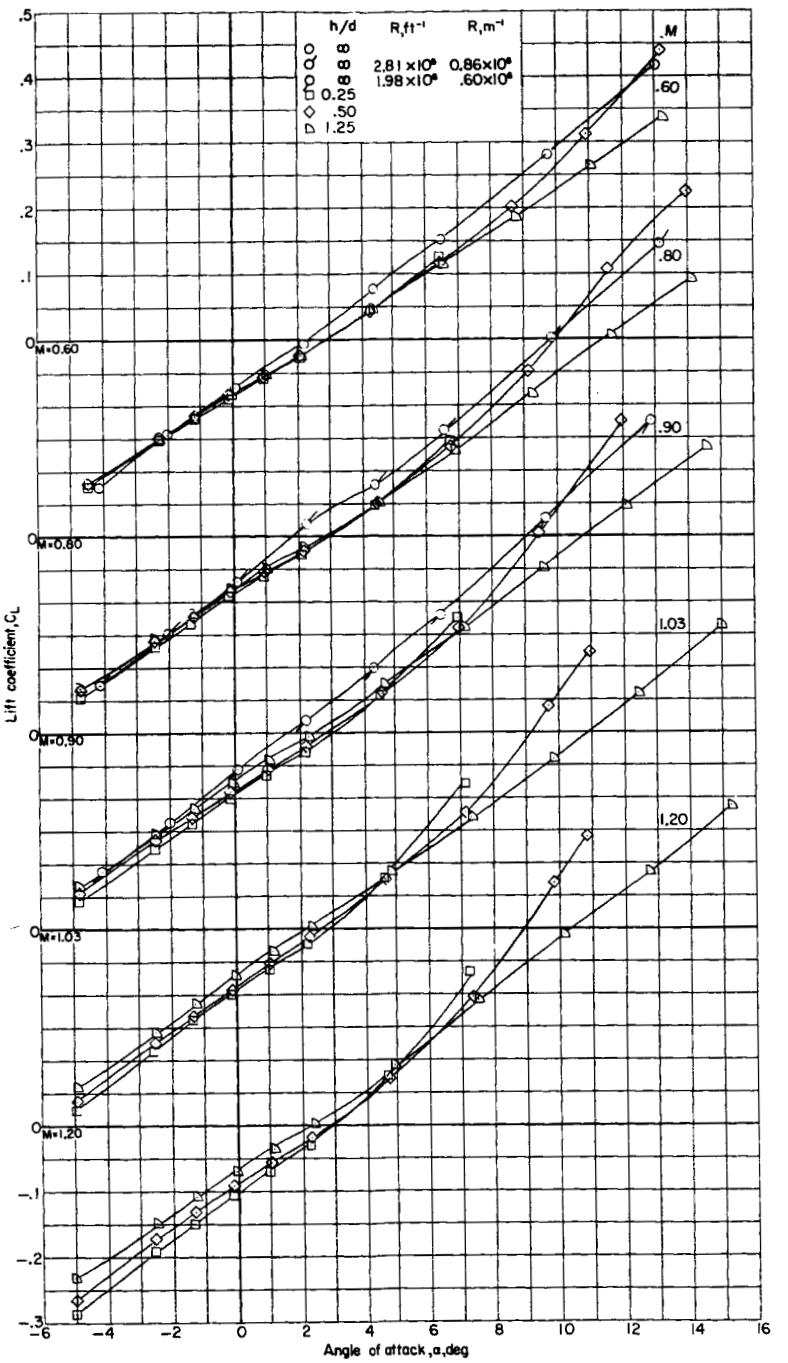

(a) Variation of lift coefficient with angle of attack.

Figure 10.- Longitudinal aerodynamic characteristics of the first stage without the canard in presence of BWFMS.

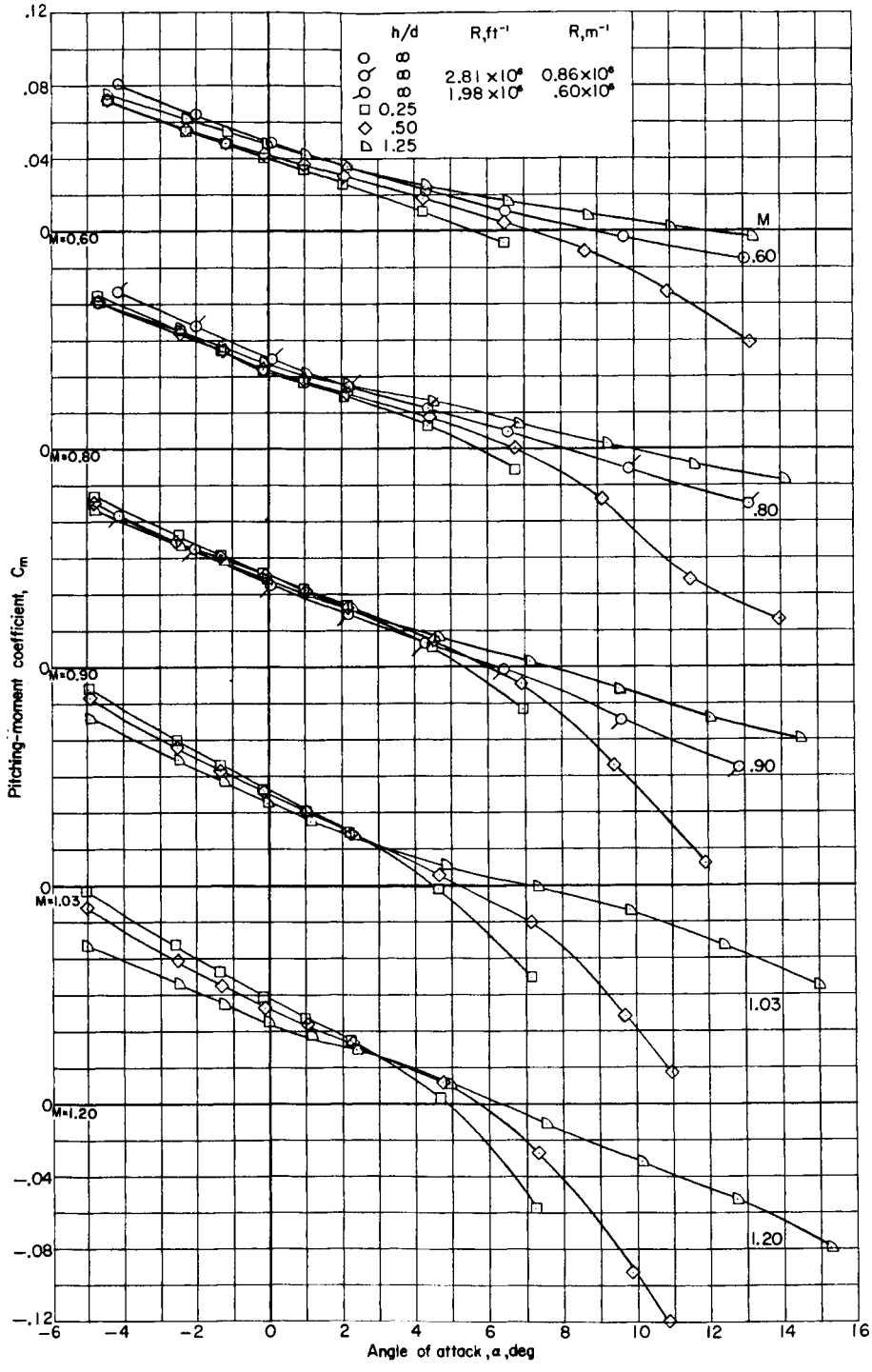

(b) Variation of pitching-moment coefficient with angle of attack.

Figure 10.- Continued.

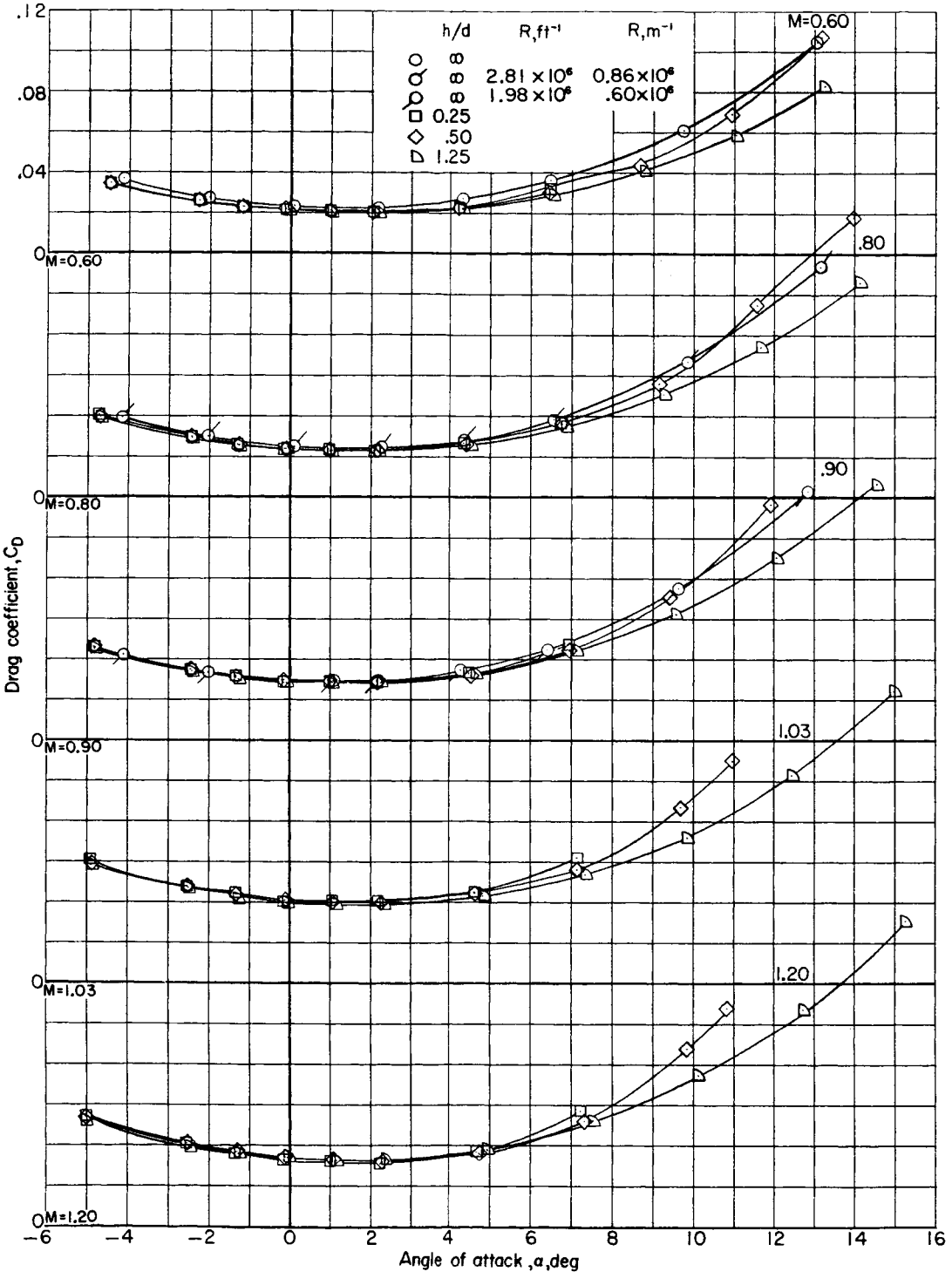

(c) Variation of drag coefficient with angle of attack.

Figure 10.- Concluded.

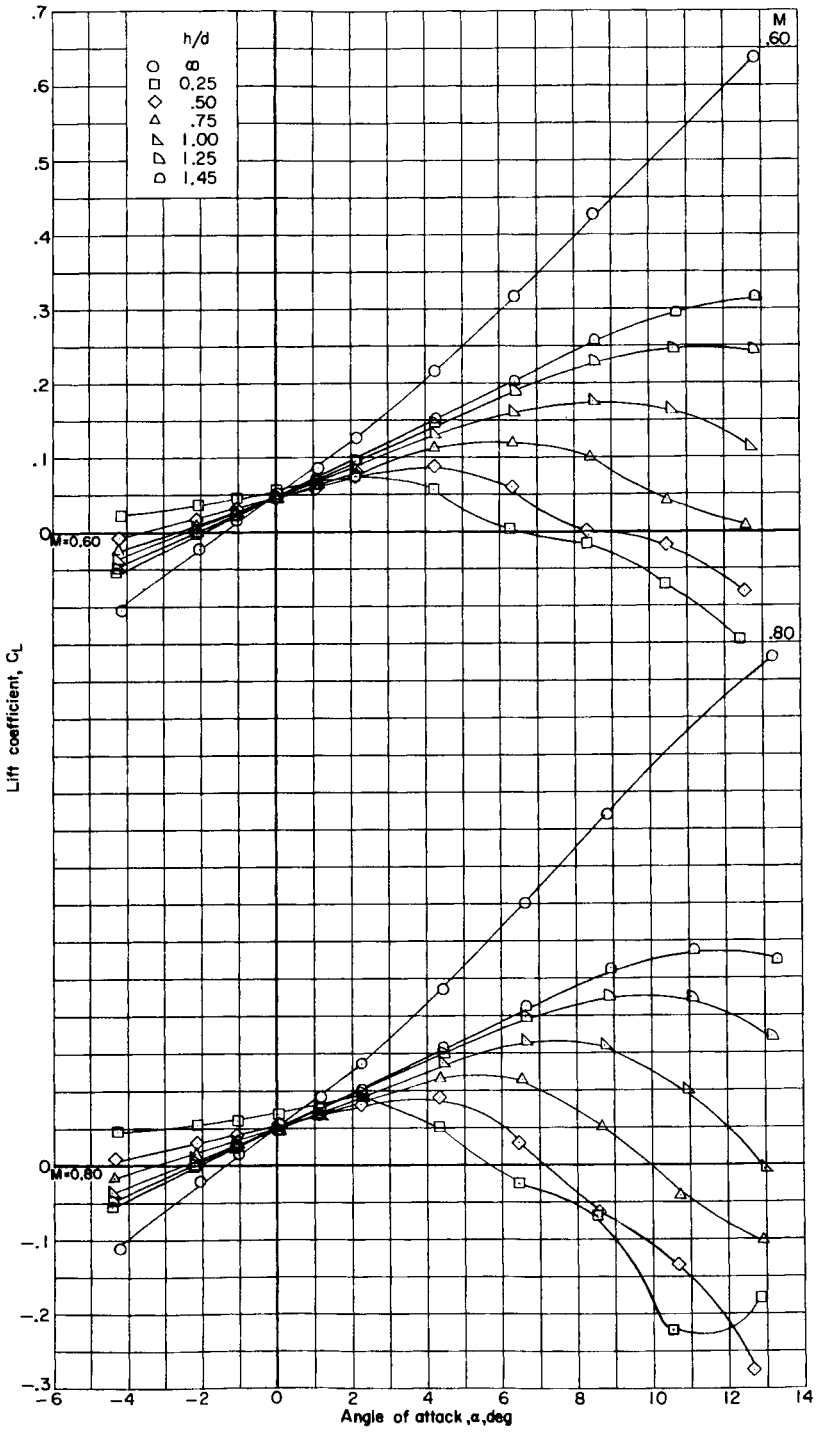

(a) Variation of lift coefficient with angle of attack.

Figure 11.- Longitudinal aerodynamic characteristics of BWFMS in presence of the complete first stage.

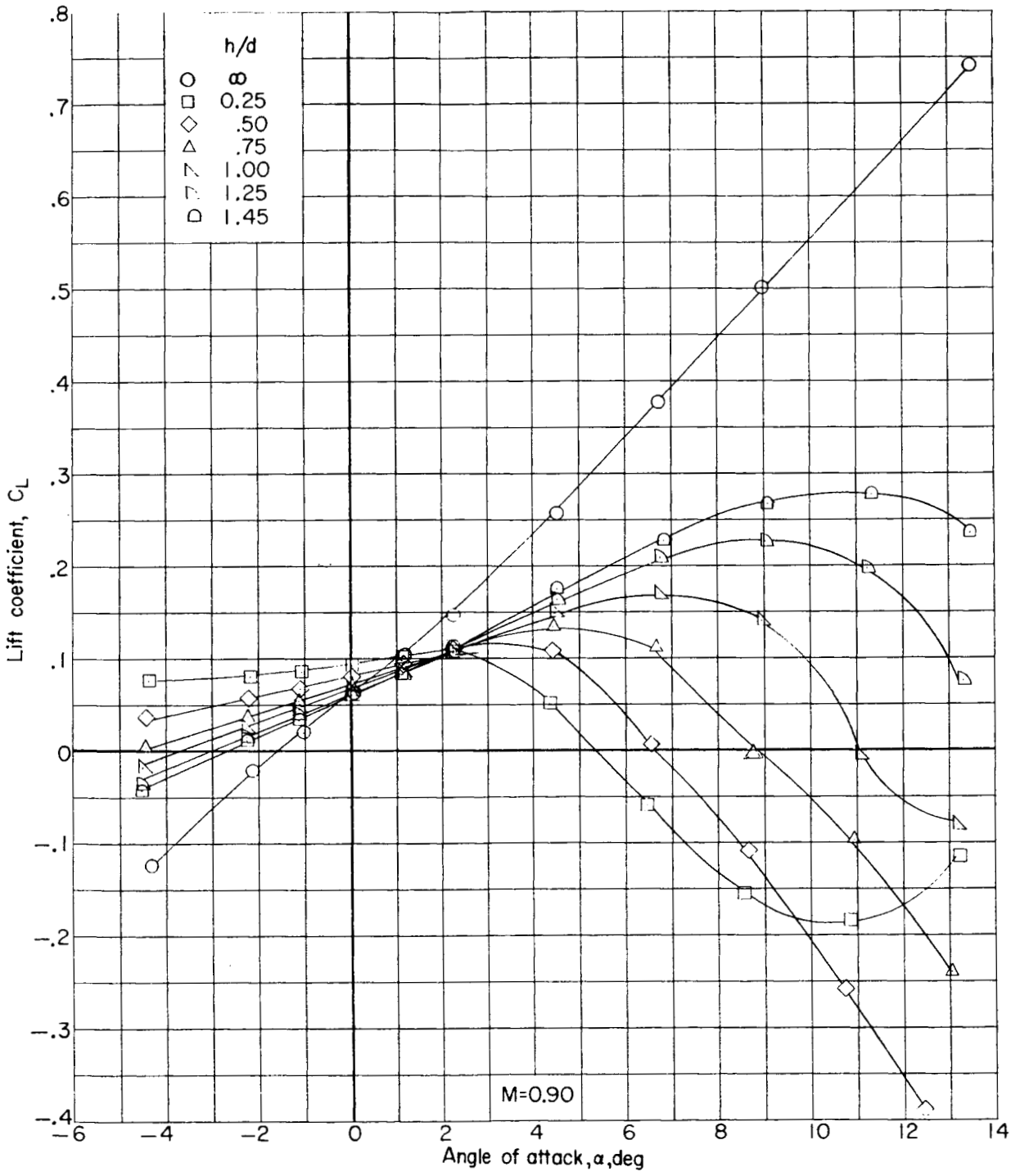

(a) Continued.

Figure 11.- Continued.

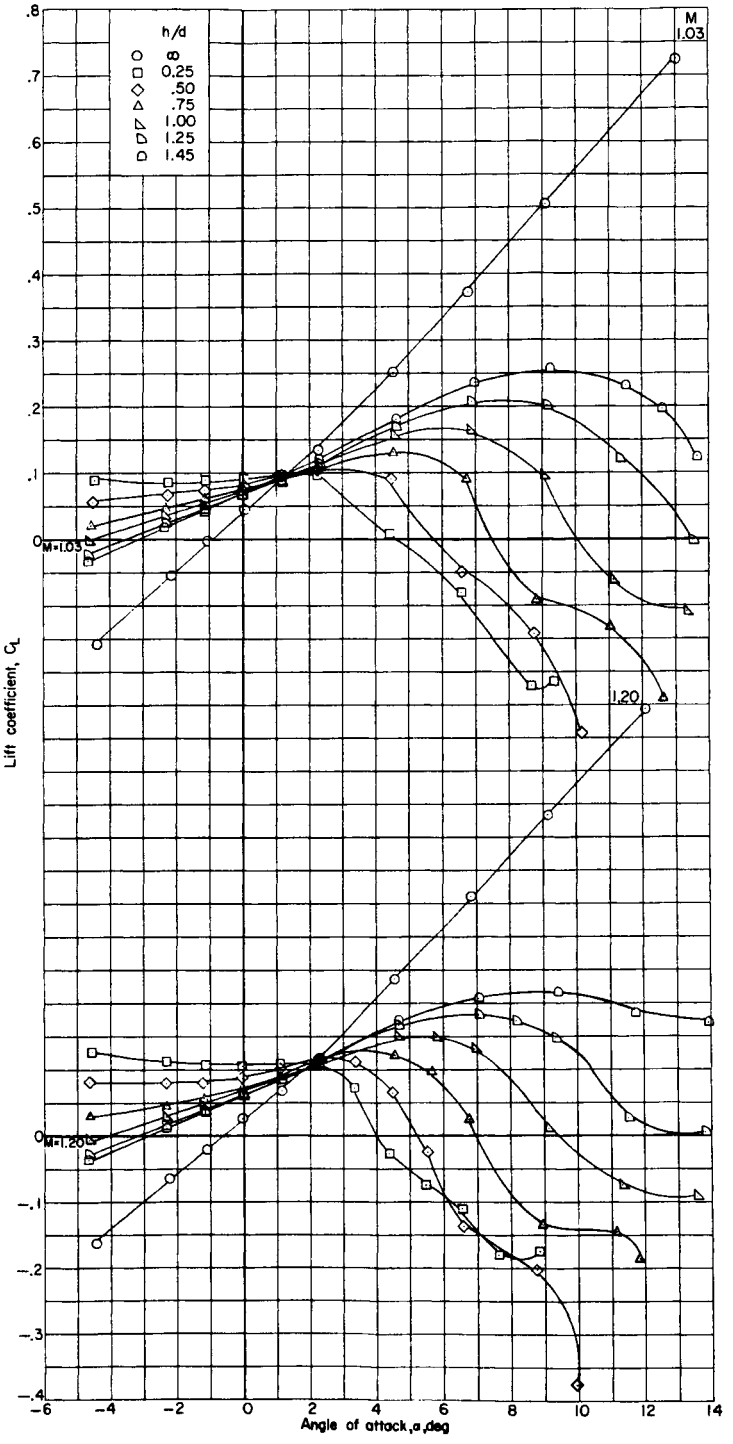

(a) Concluded.

Figure 11.- Continued.

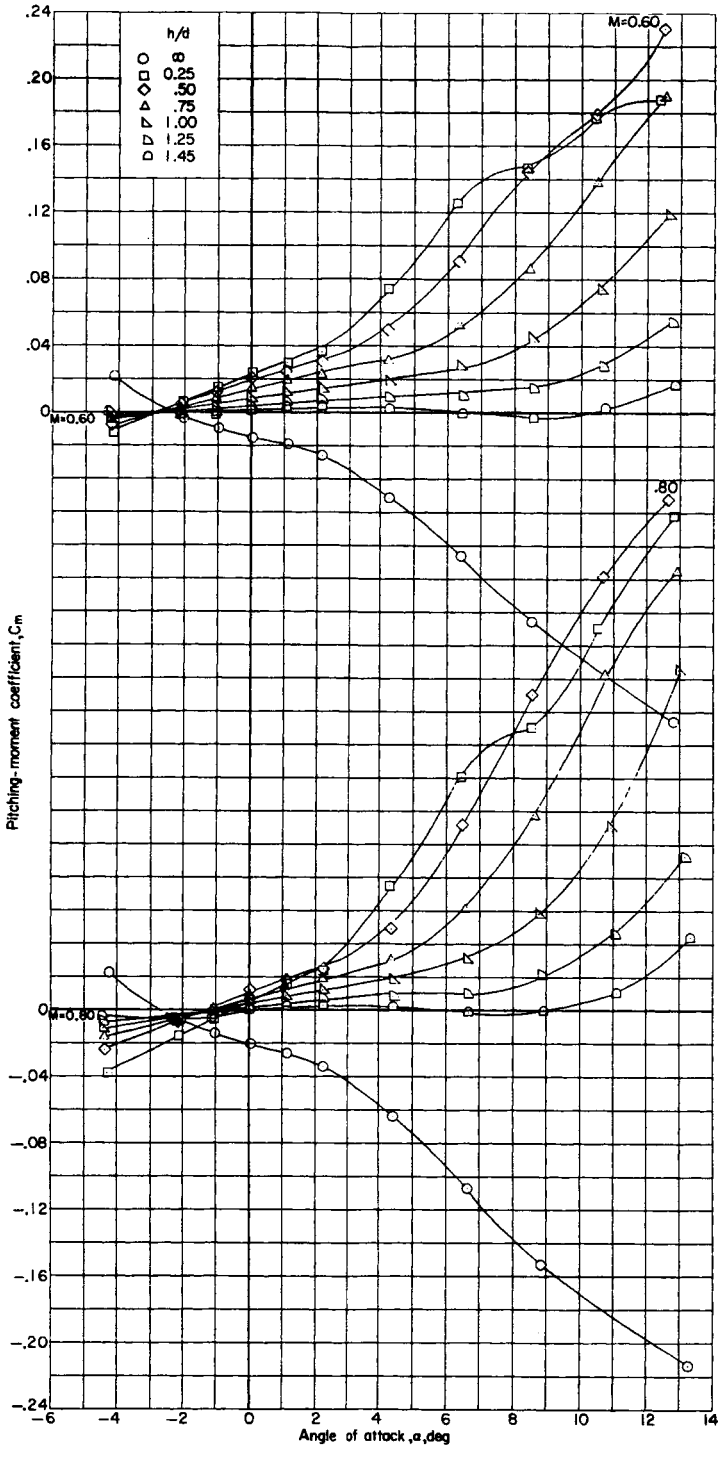

(b) Variation of pitching-moment coefficient with angle of attack.

Figure 11.- Continued.

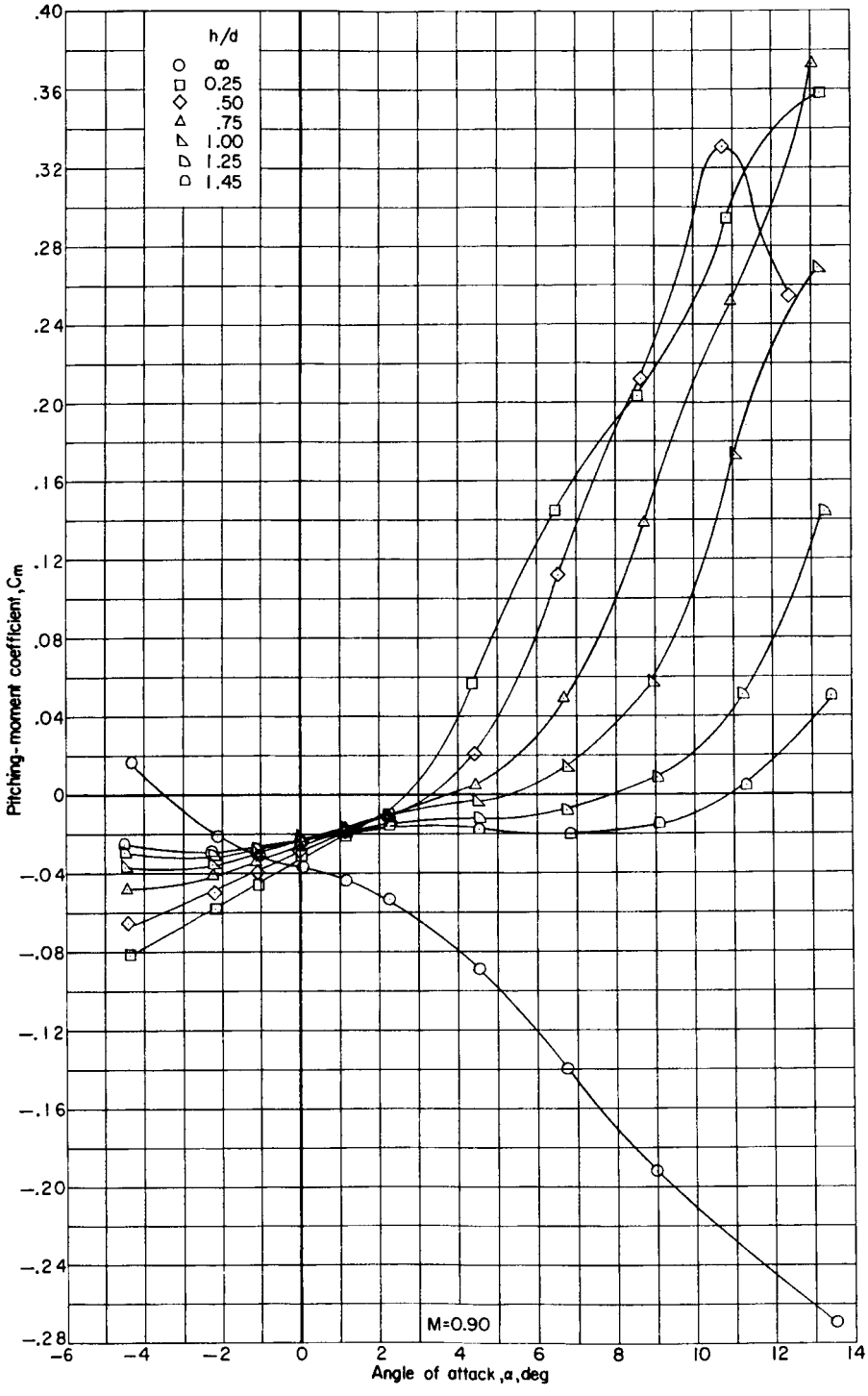

(b) Continued.

Figure 11.- Continued.

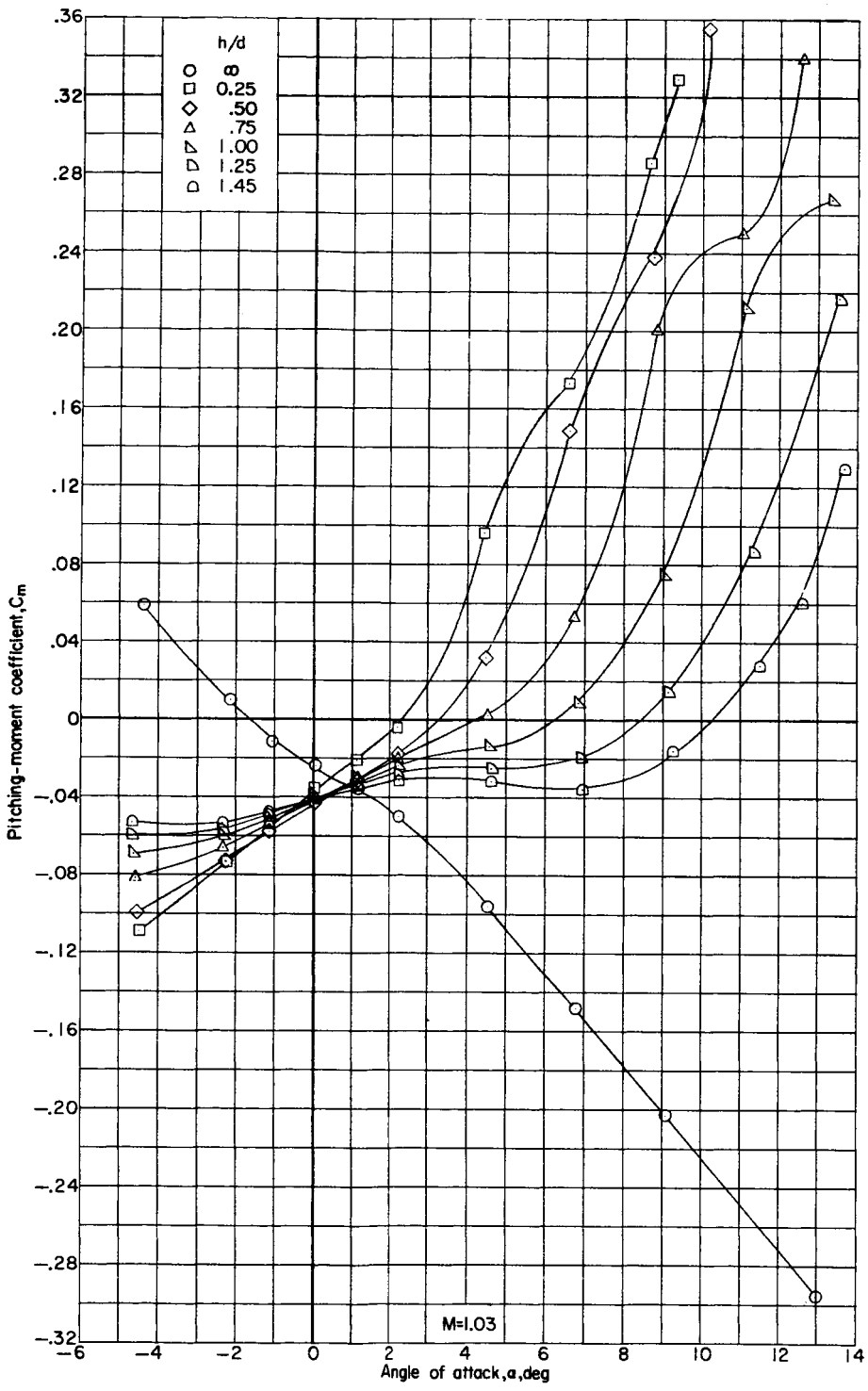

(b) Continued.

Figure 11.- Continued.

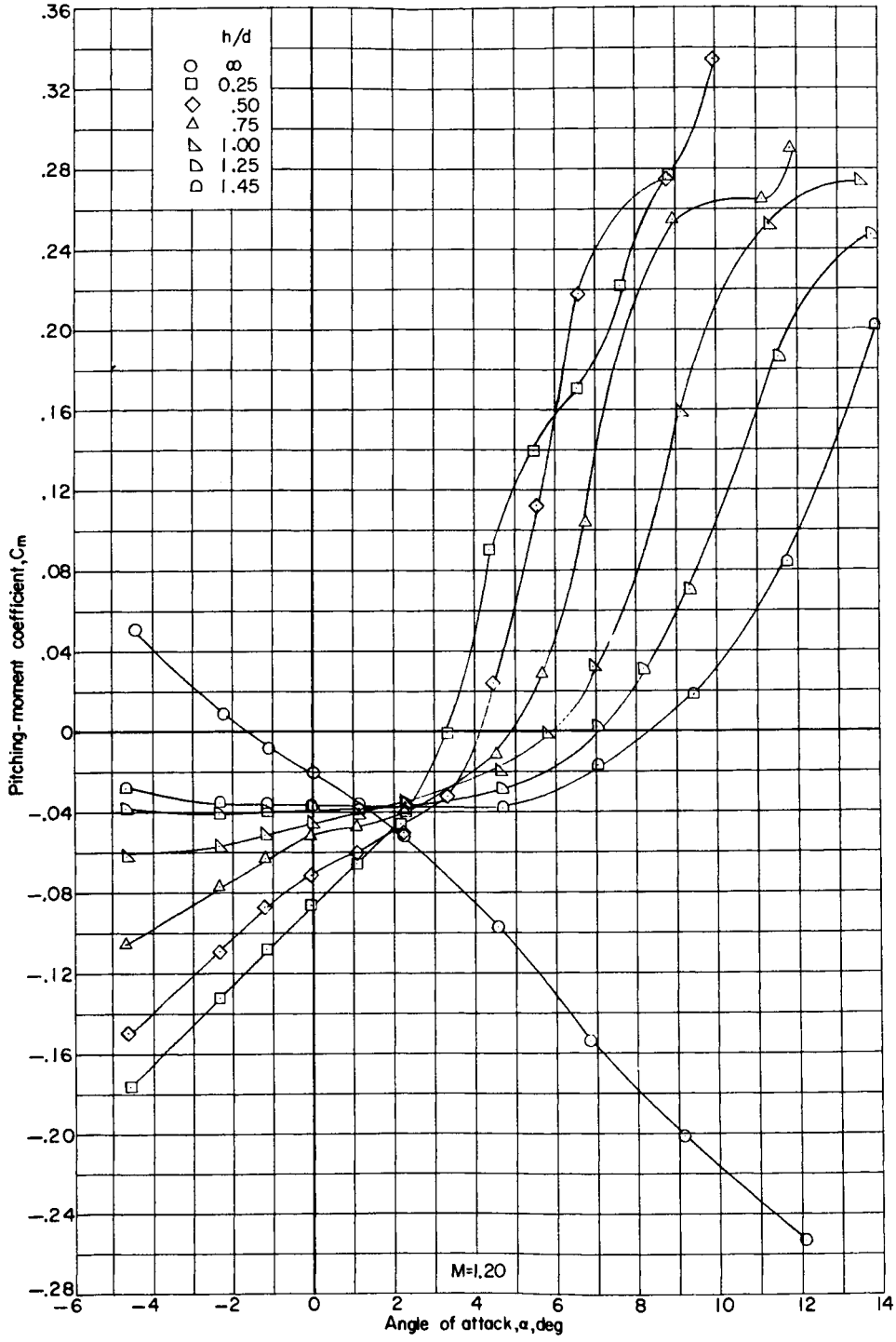

(b) Concluded.

Figure 11.- Continued.

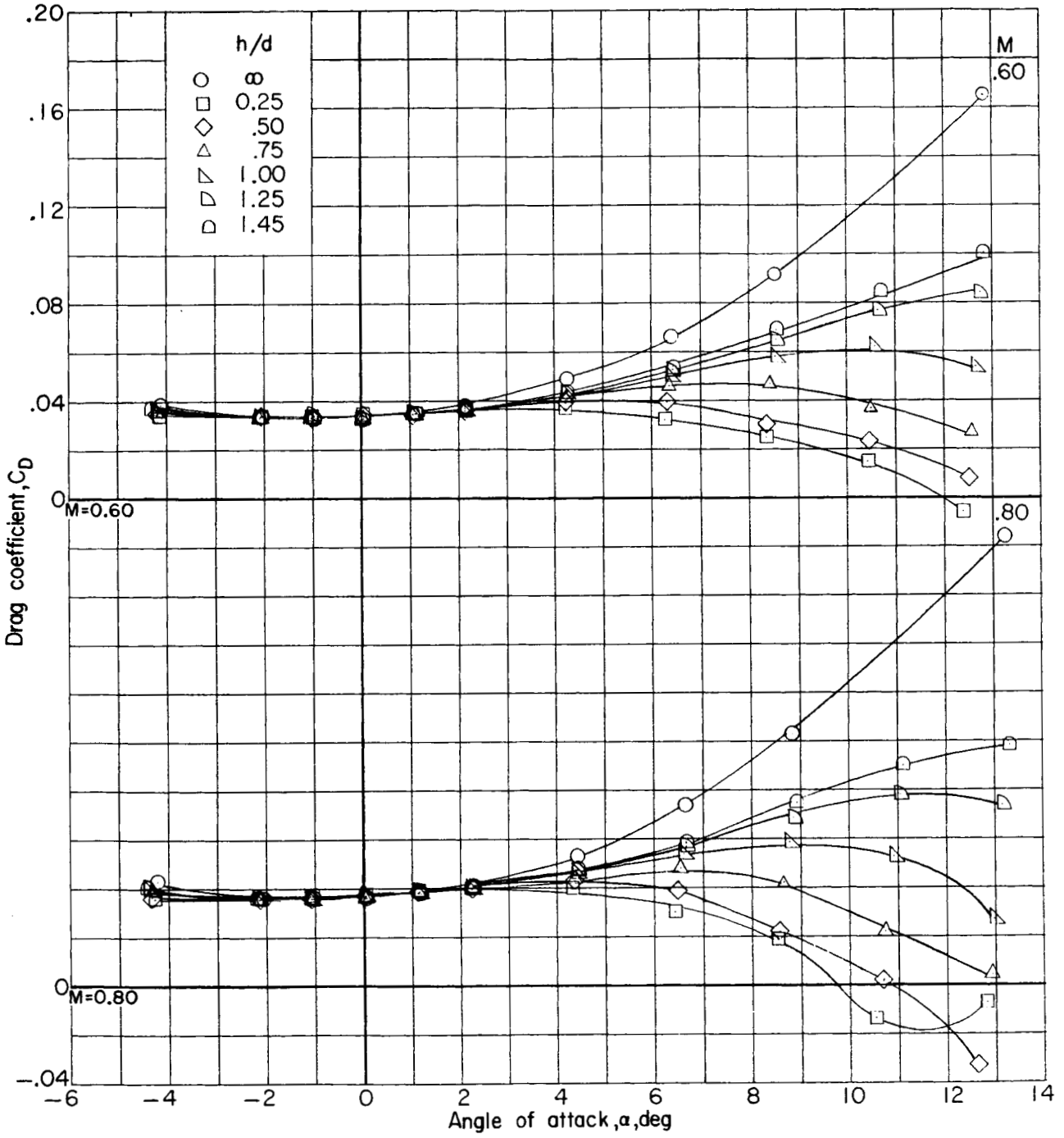

(c) Variation of drag coefficient with angle of attack.

Figure 11.- Continued.

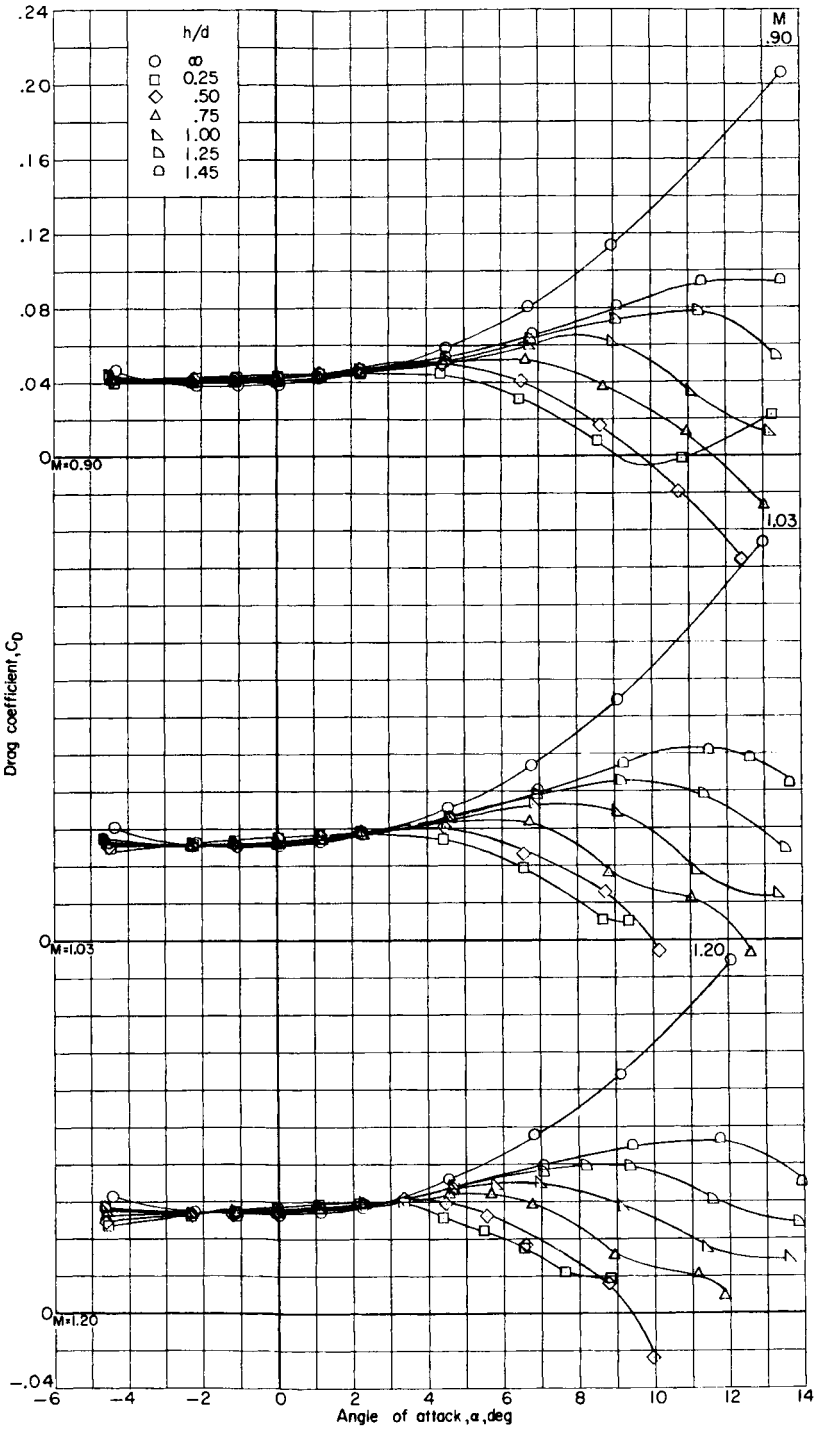

(c) Concluded.

Figure 11.- Concluded.

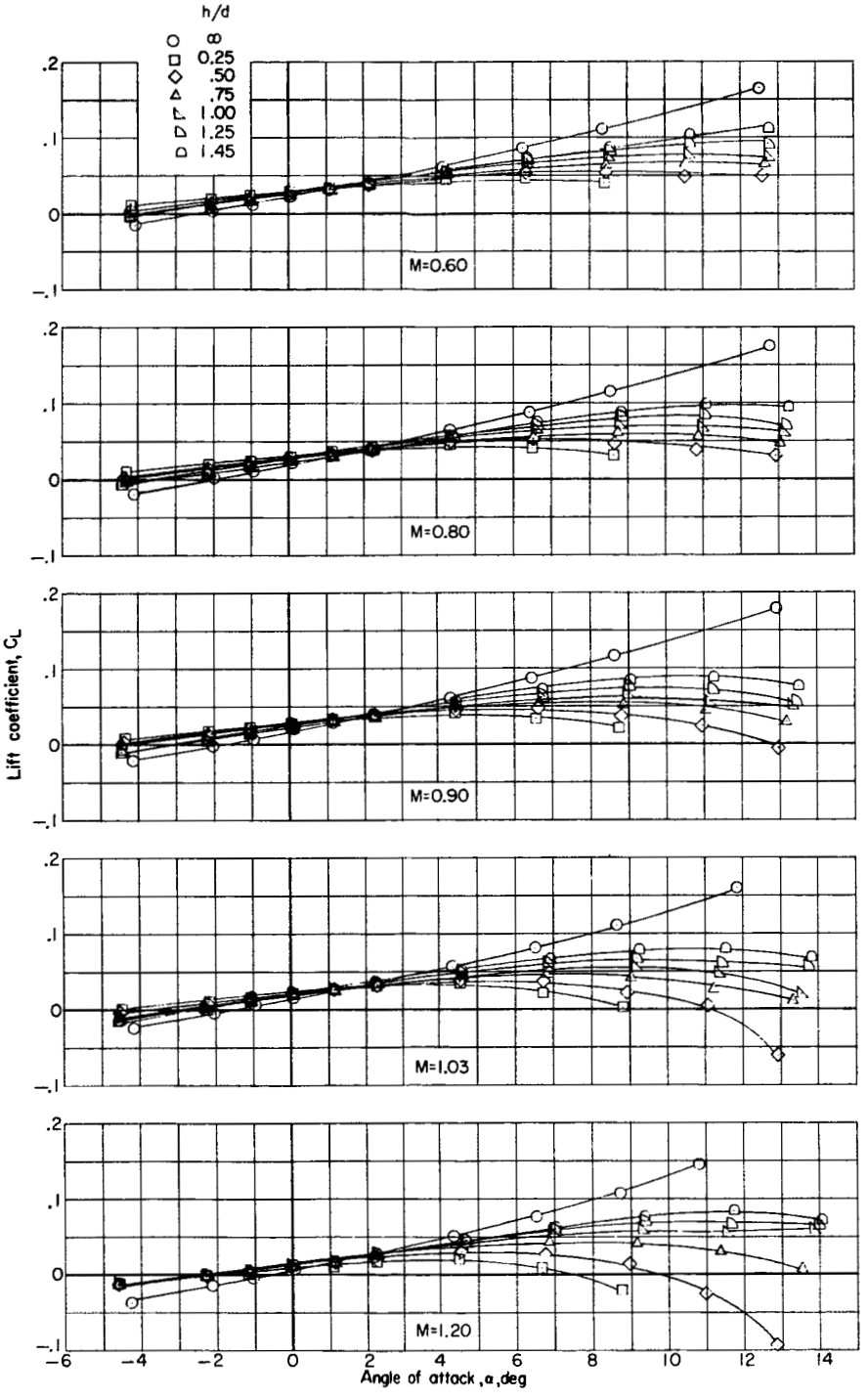

(a) Variation of lift coefficient with angle of attack.

Figure 12.- Longitudinal aerodynamic characteristics of BMS in presence of the complete first stage.

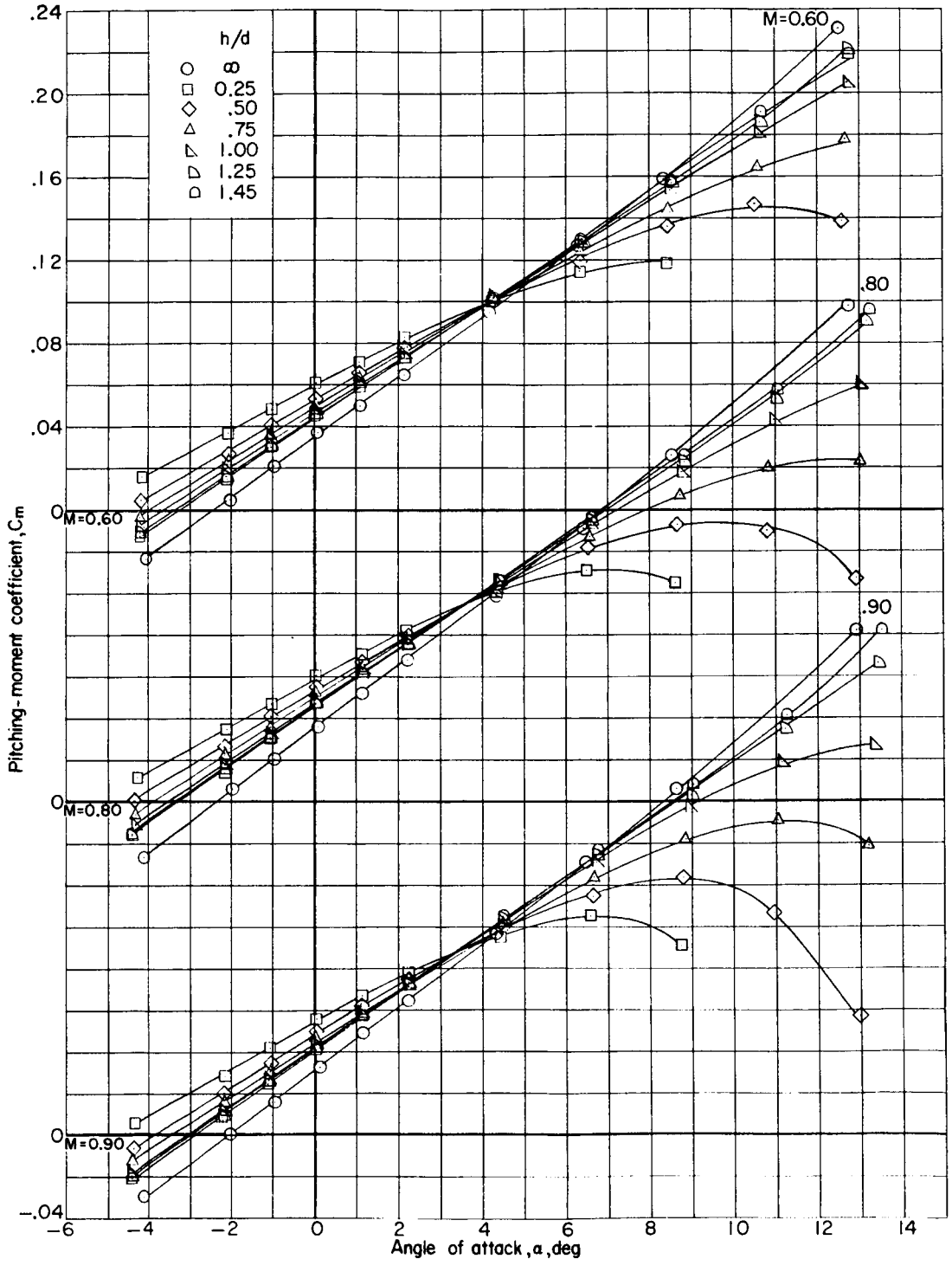

(b) Variation of pitching-moment coefficient with angle of attack.

Figure 12.- Continued.

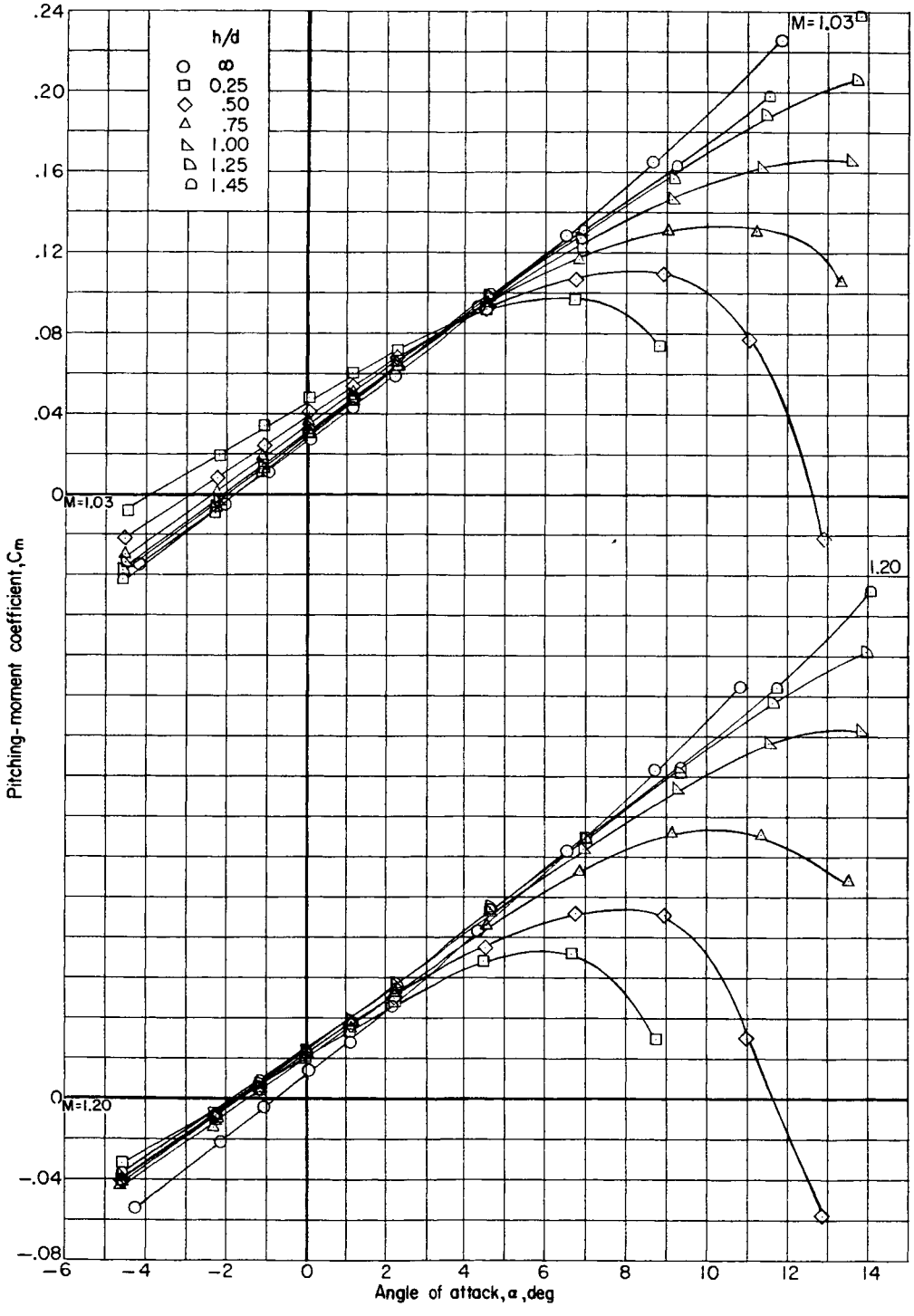

(b) Concluded.

Figure 12.- Continued.

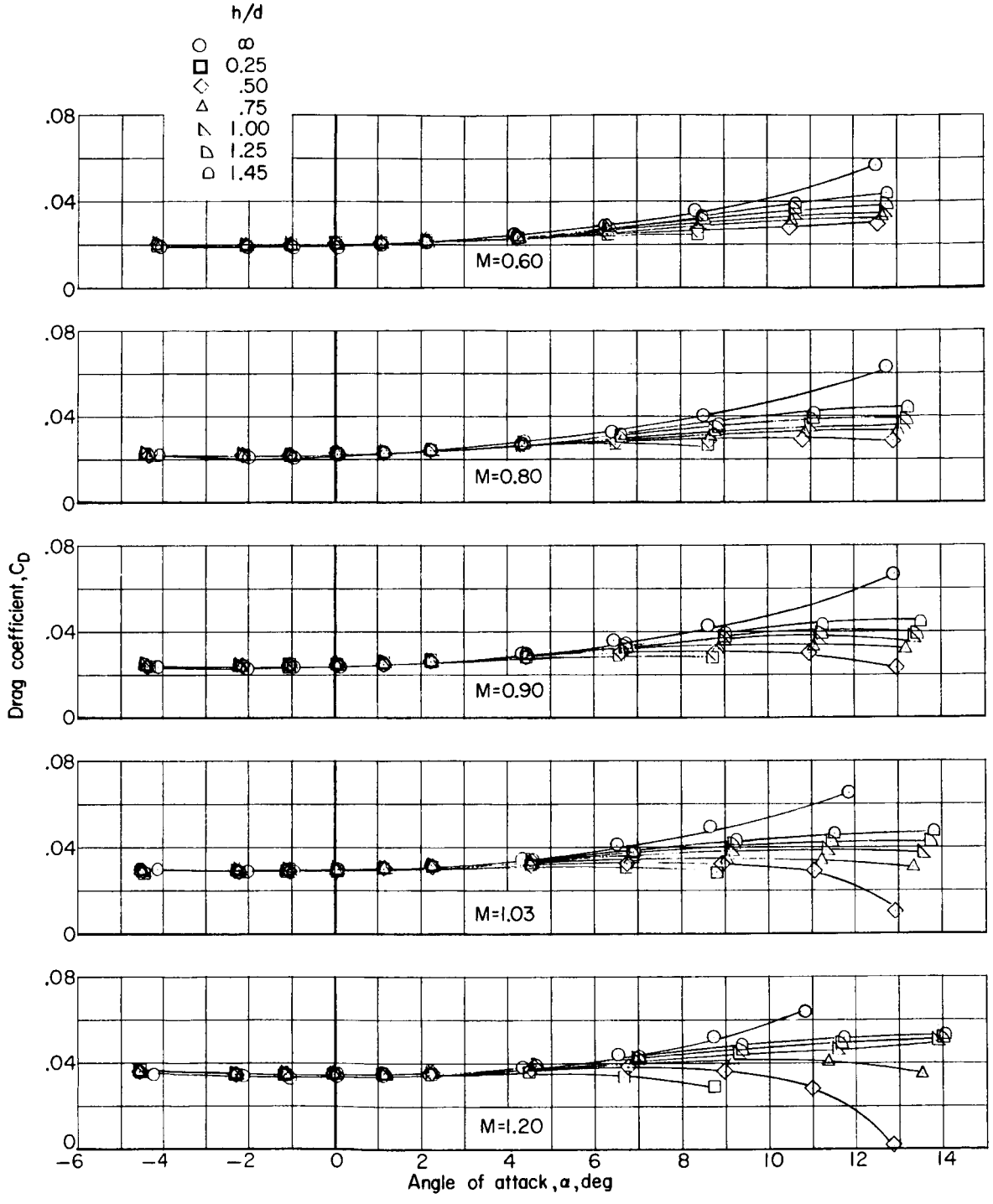

(c) Variation of drag coefficient with angle of attack.

Figure 12.- Concluded.

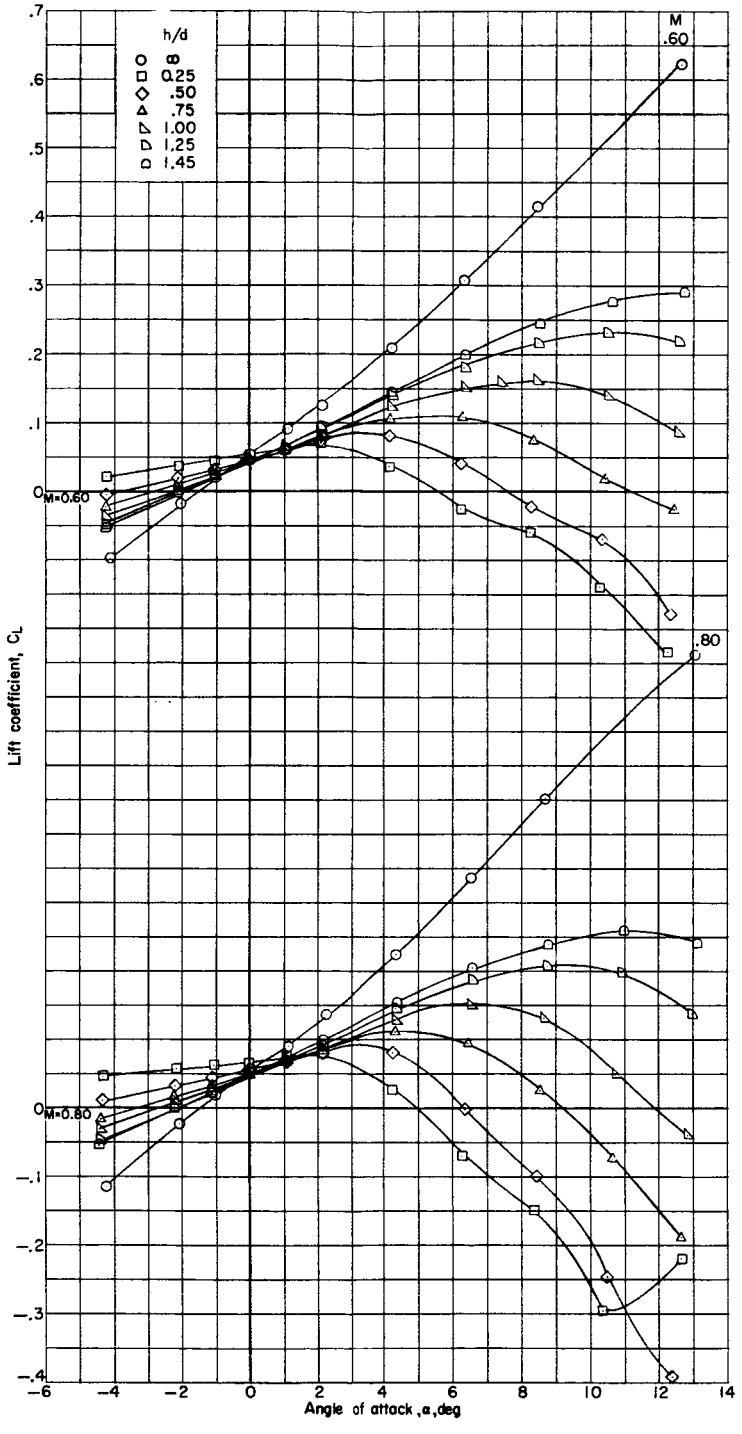

(a) Variation of lift coefficient with angle of attack.

Figure 13.- Longitudinal aerodynamic characteristics of BWFS in presence of the complete first stage.

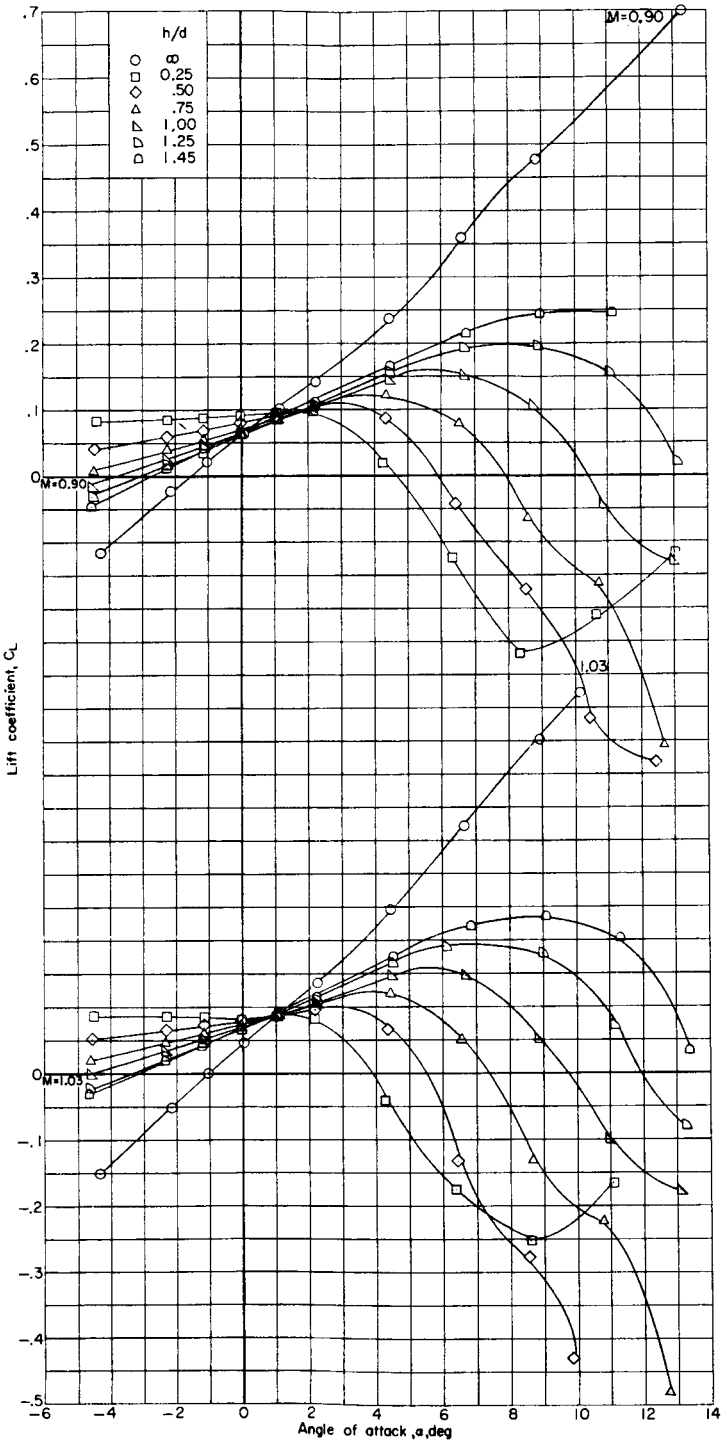

(a) Continued.

Figure 13.- Continued.

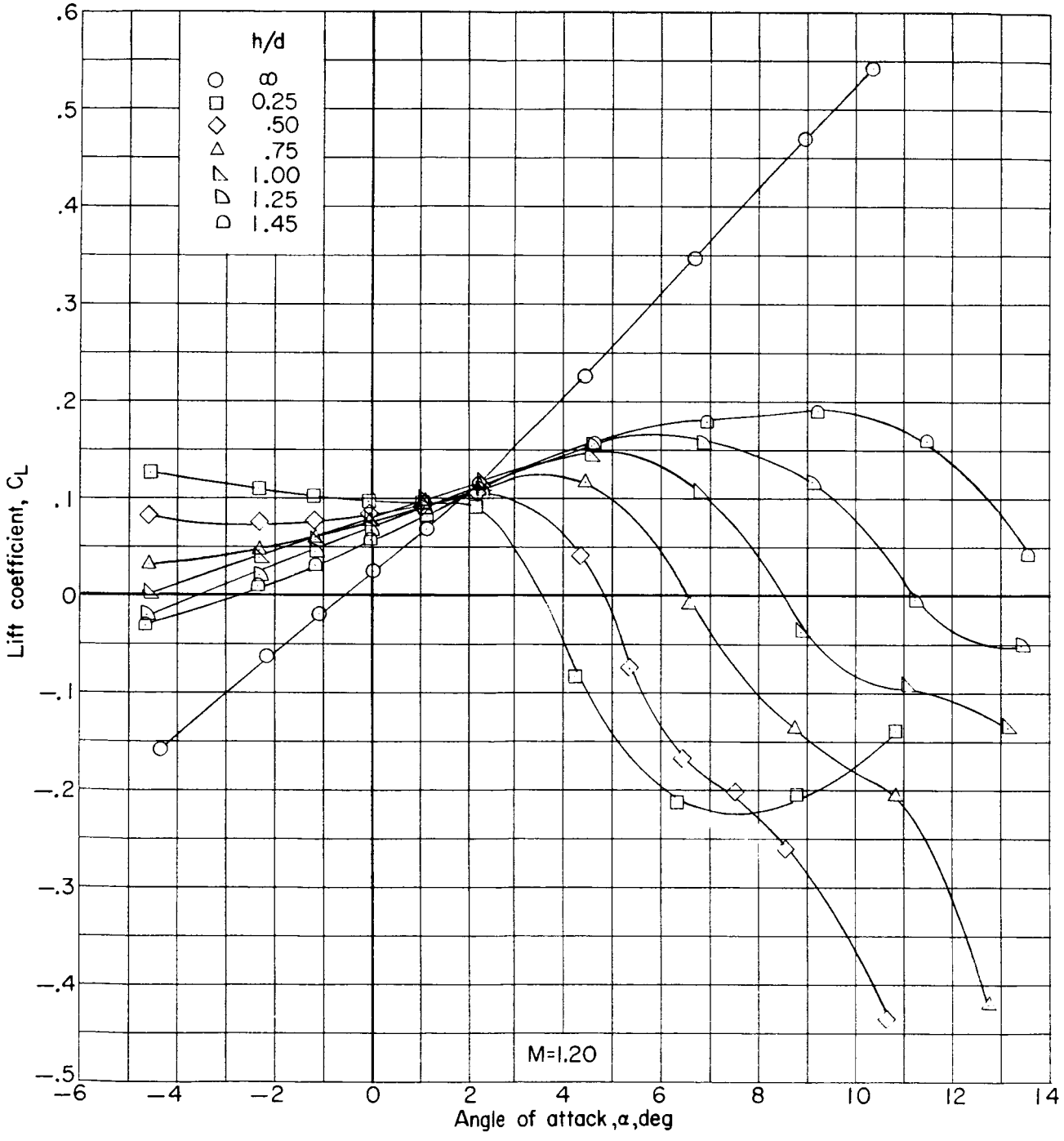

(a) Concluded.

Figure 13.- Continued.

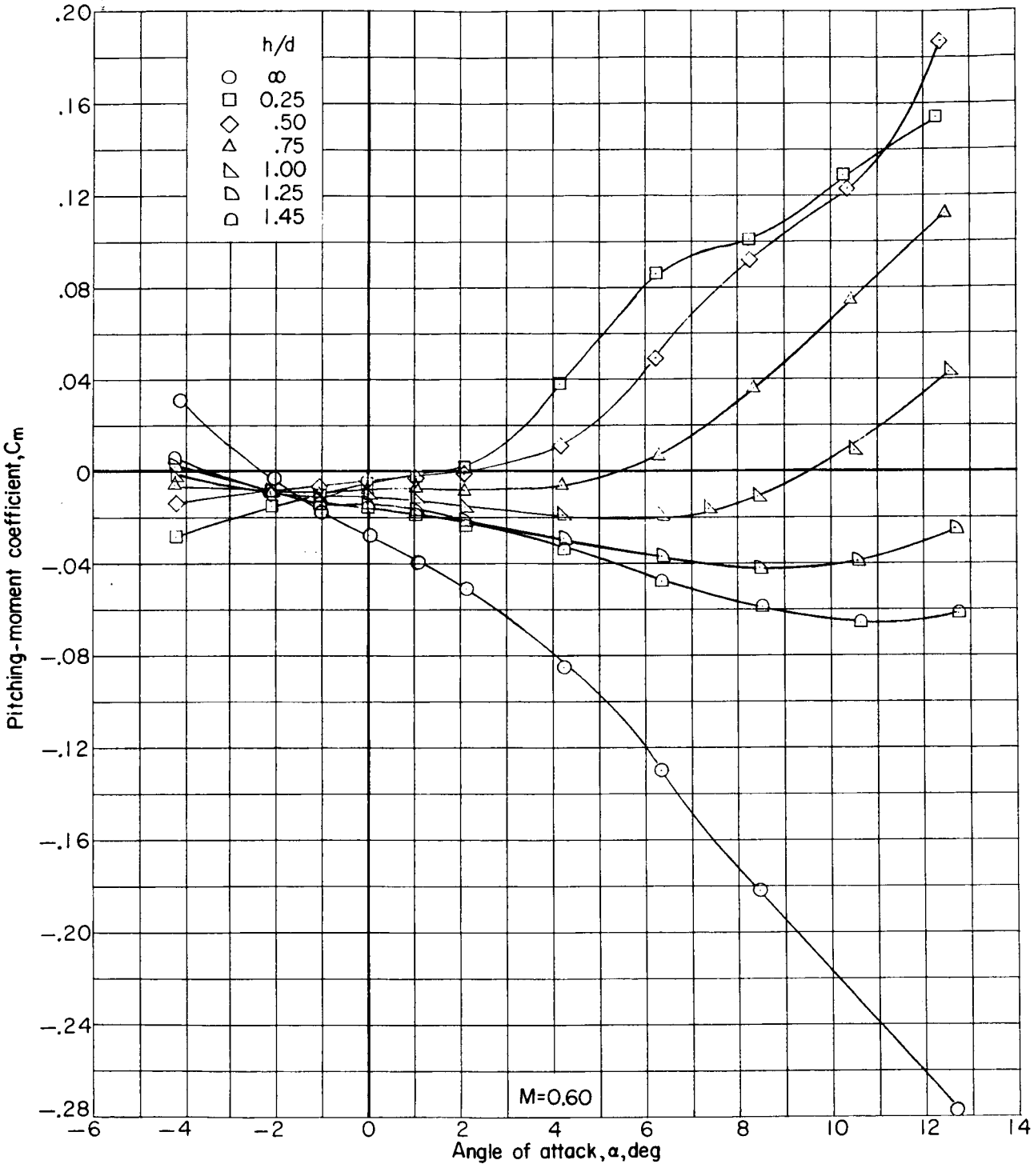

(b) Variation of pitching-moment coefficient with angle of attack.

Figure 13.- Continued.

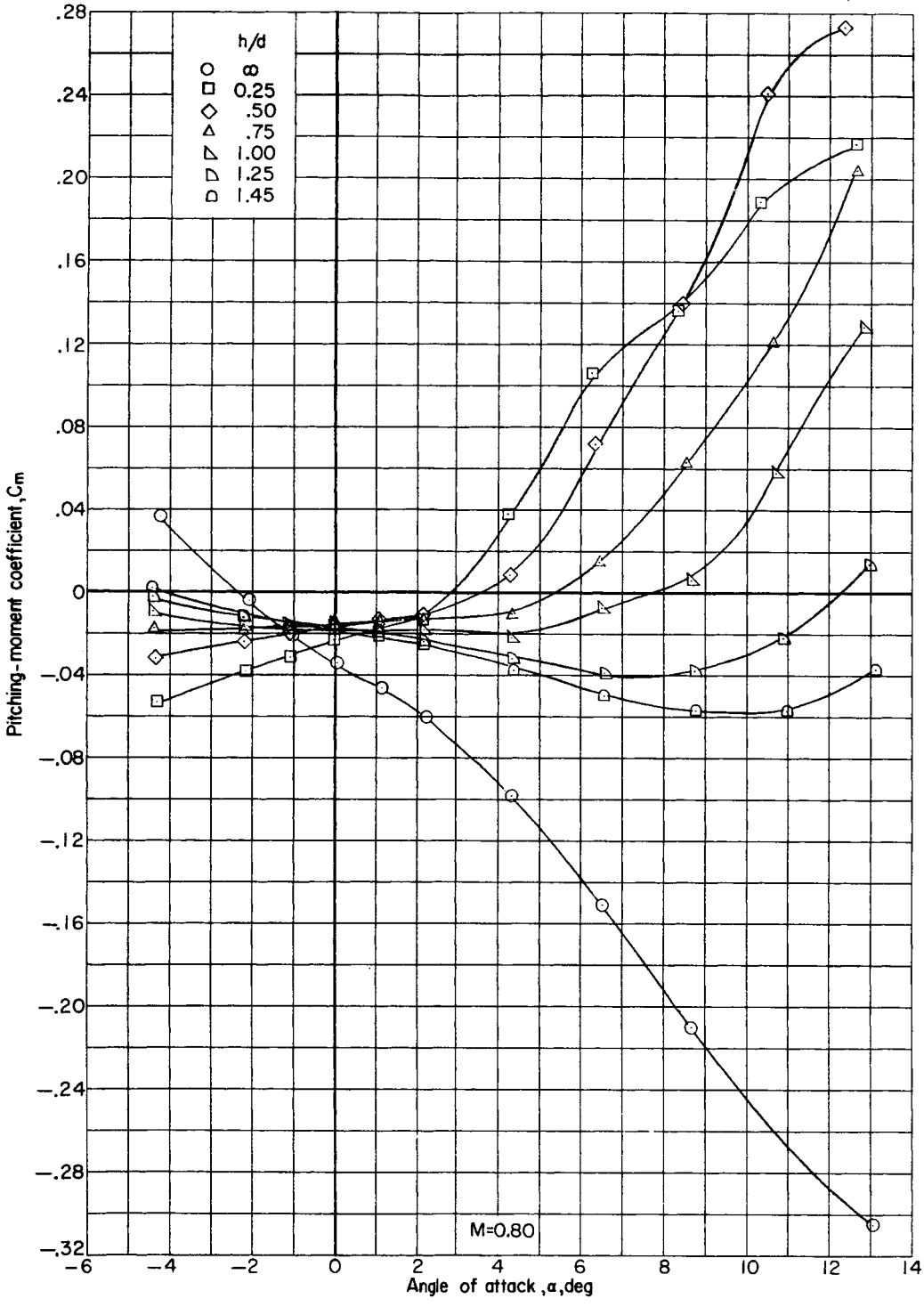

(b) Continued.

Figure 13.- Continued.

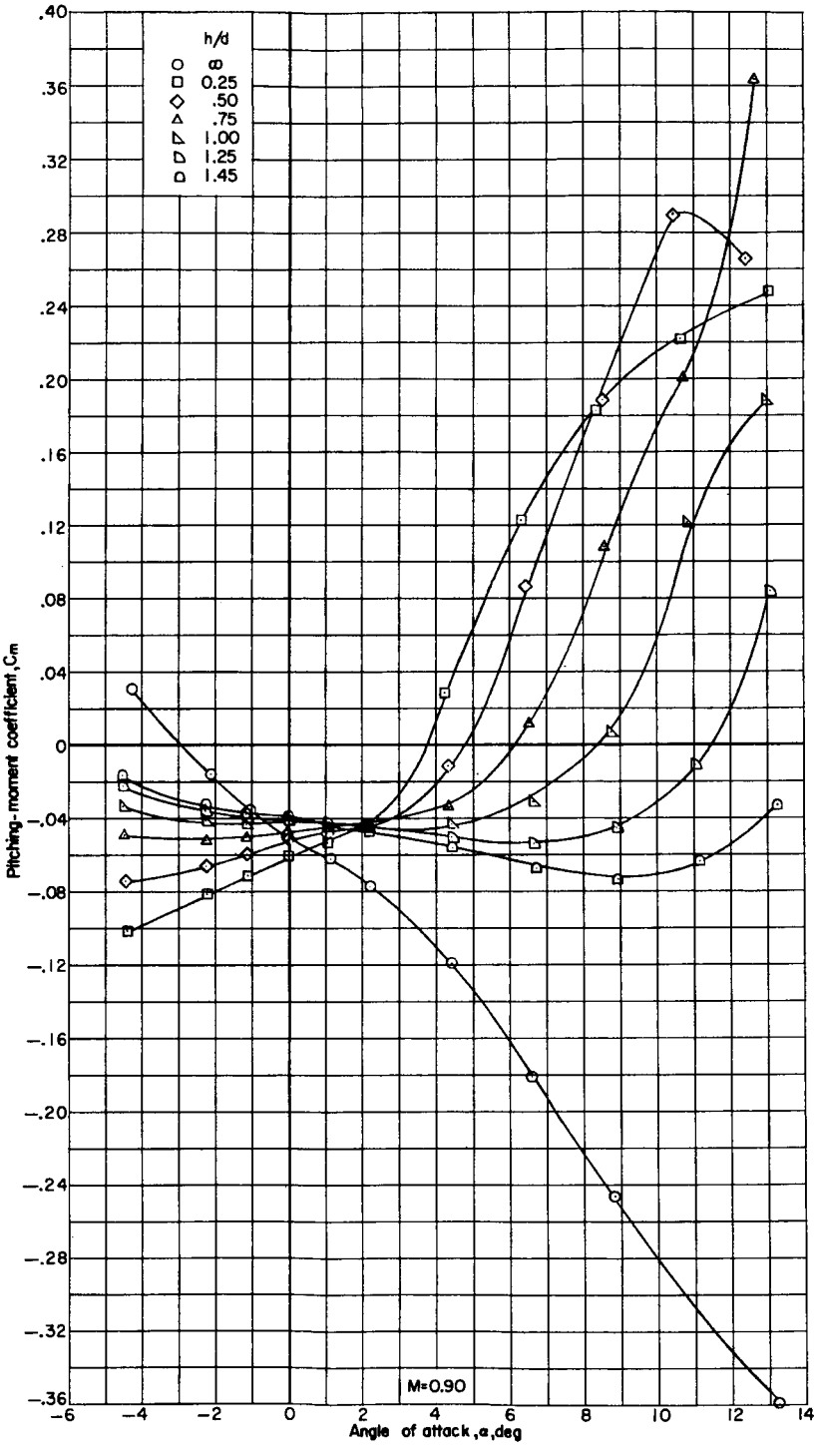

(b) Continued.

Figure 13.- Continued.

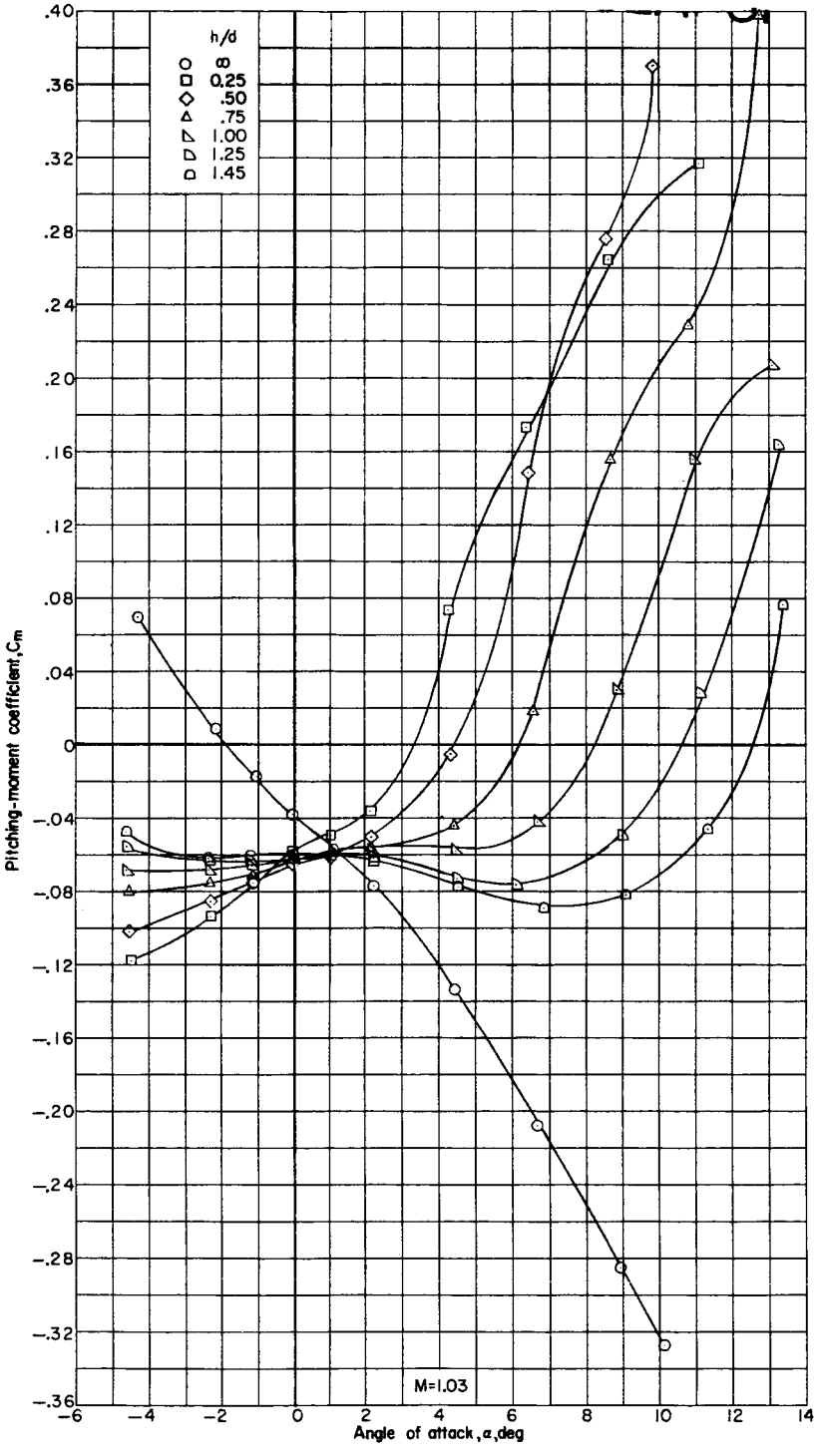

(b) Continued.

Figure 13.- Continued.

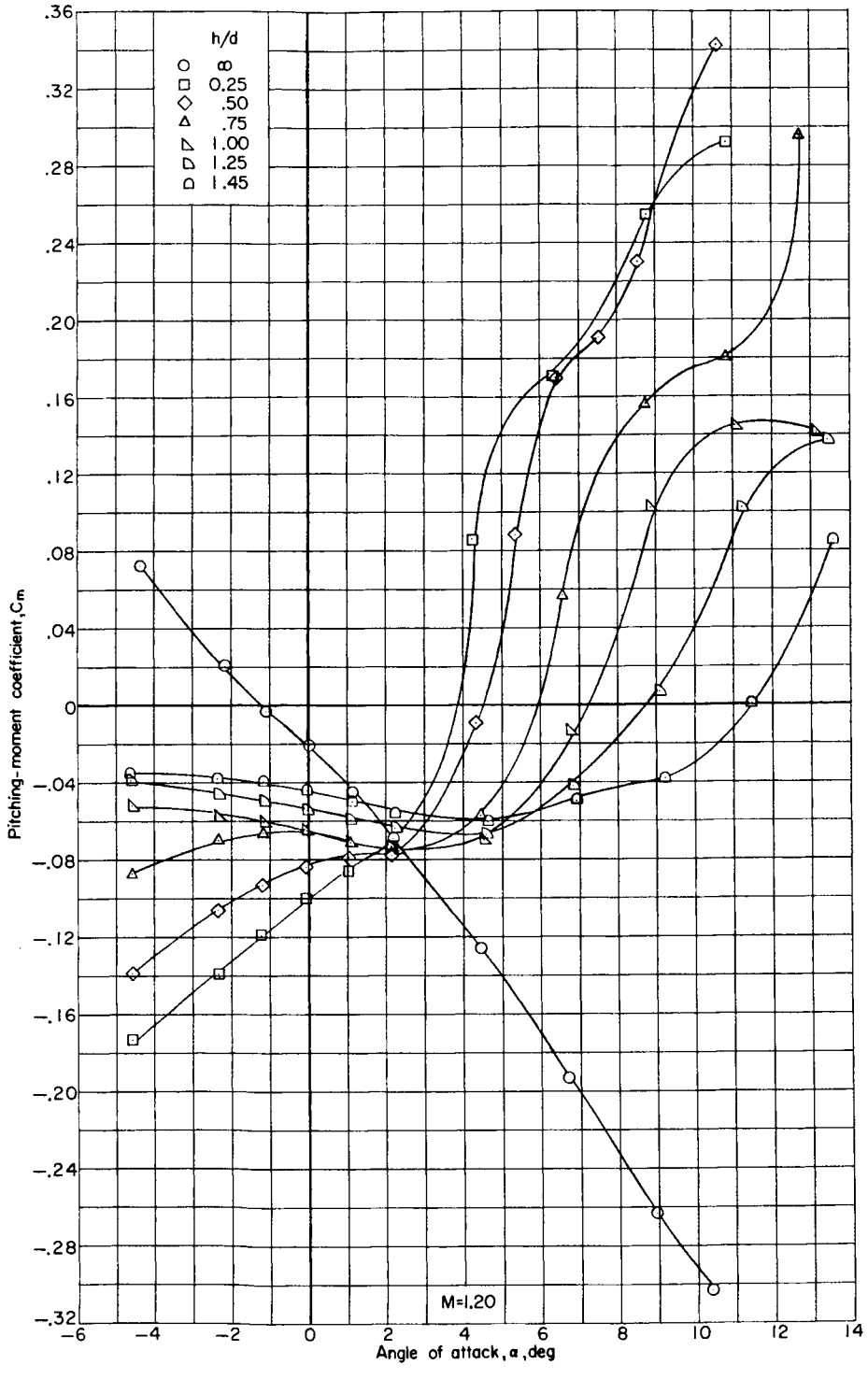

(b) Concluded.

Figure 13.- Continued.

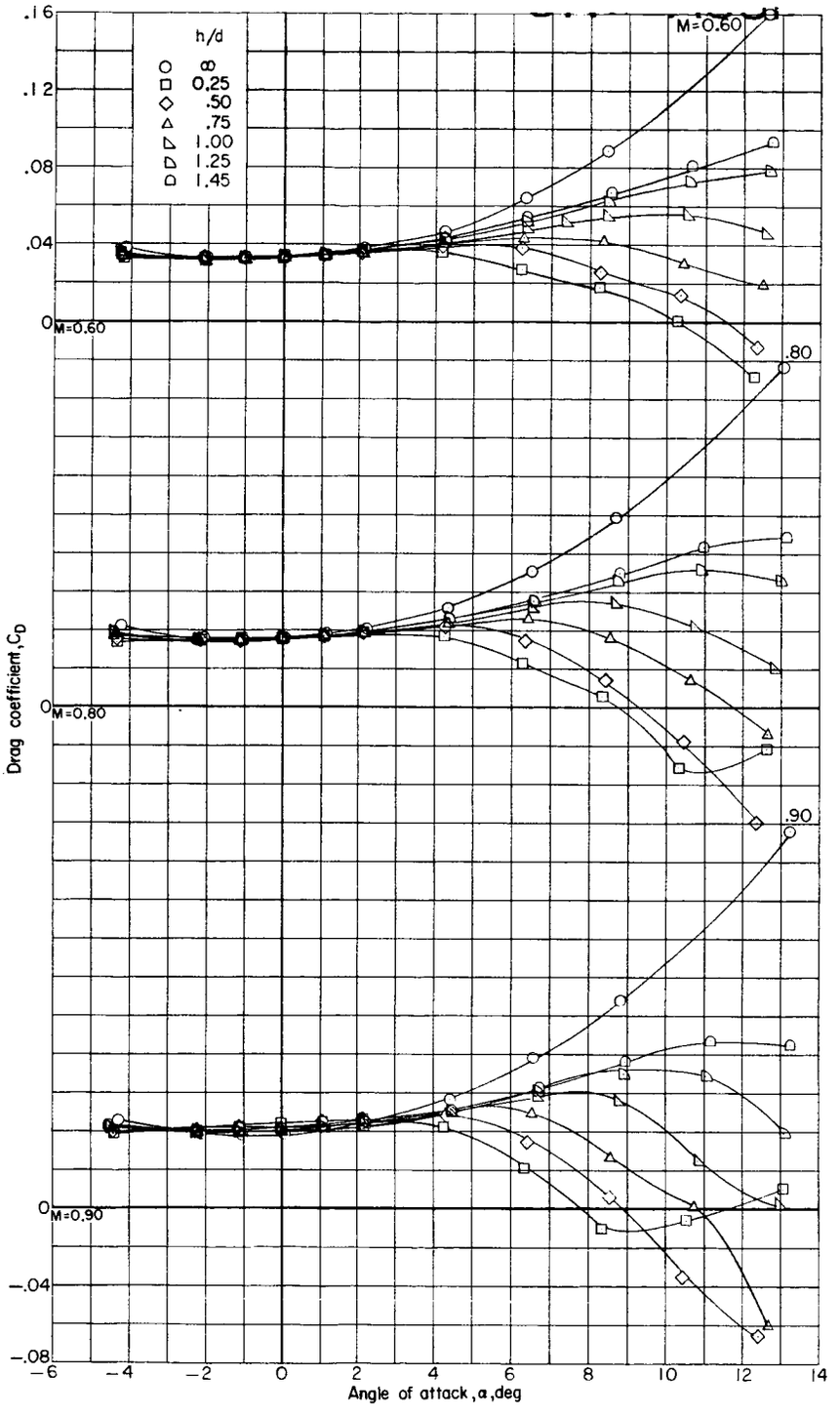

(c) Variation of drag coefficient with angle of attack.

Figure 13.- Continued.

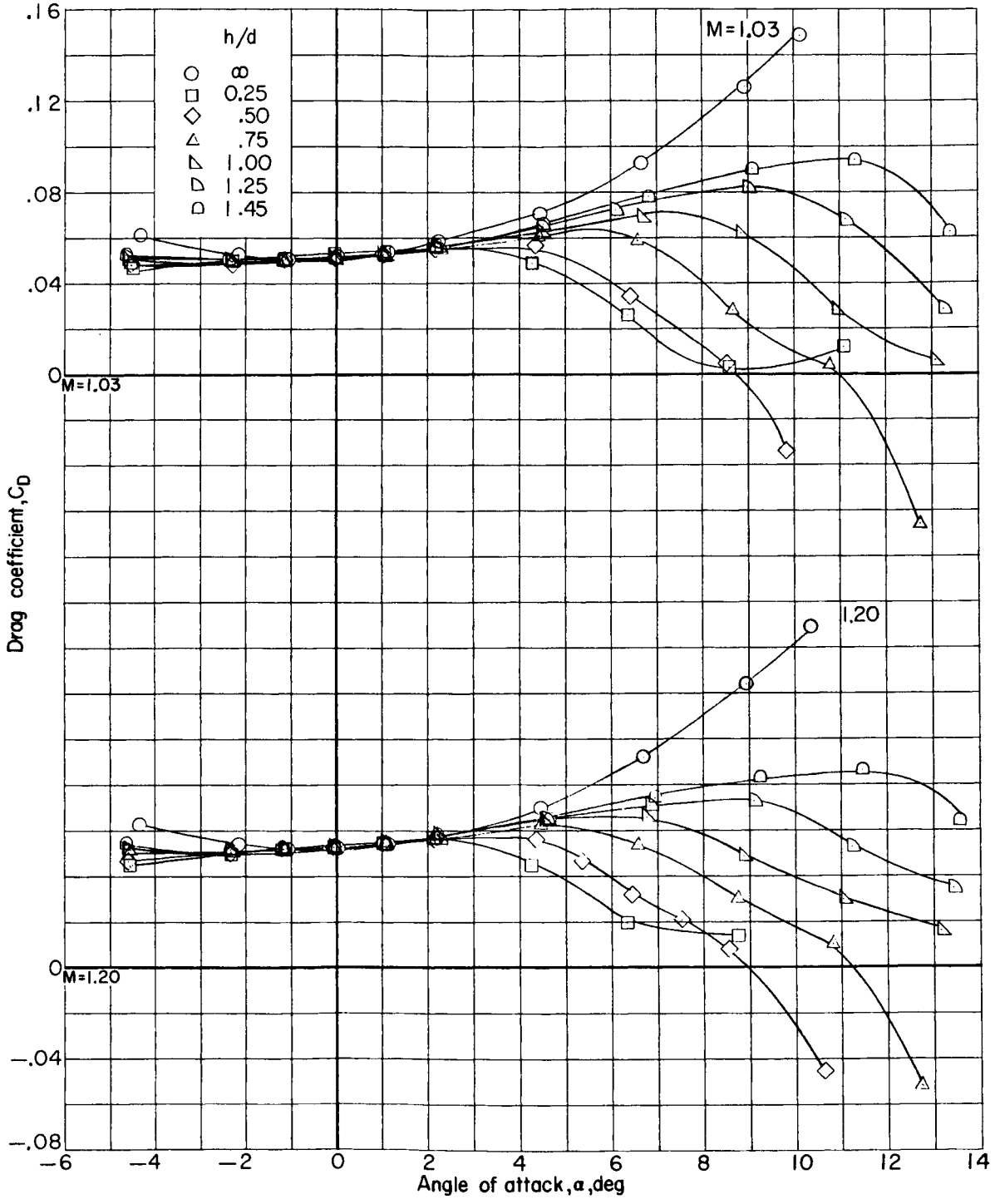

(c) Concluded.

Figure 13.- Concluded.

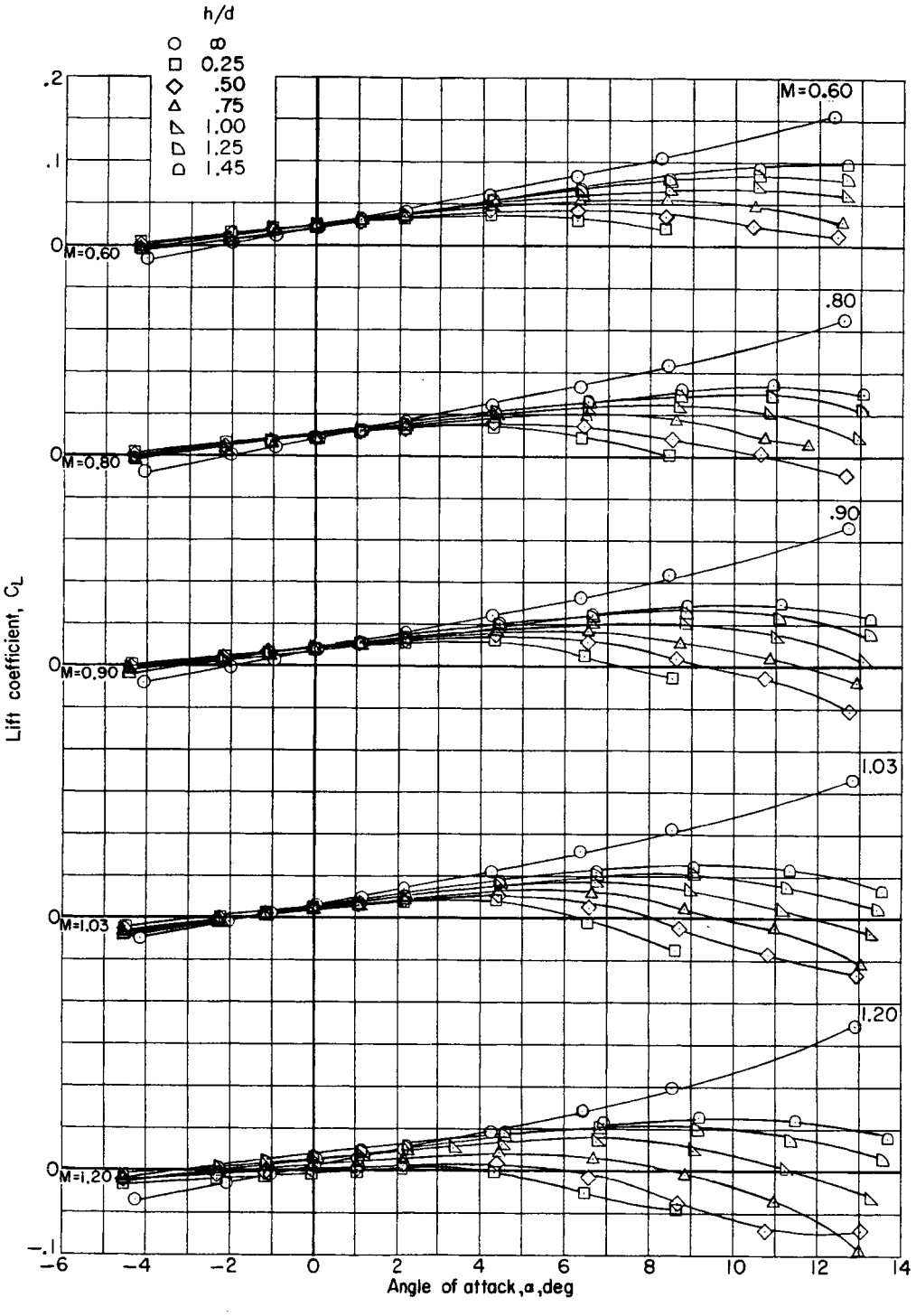

(a) Variation of lift coefficient with angle of attack.

Figure 14.- Longitudinal aerodynamic characteristics of BS in presence of the complete first stage.

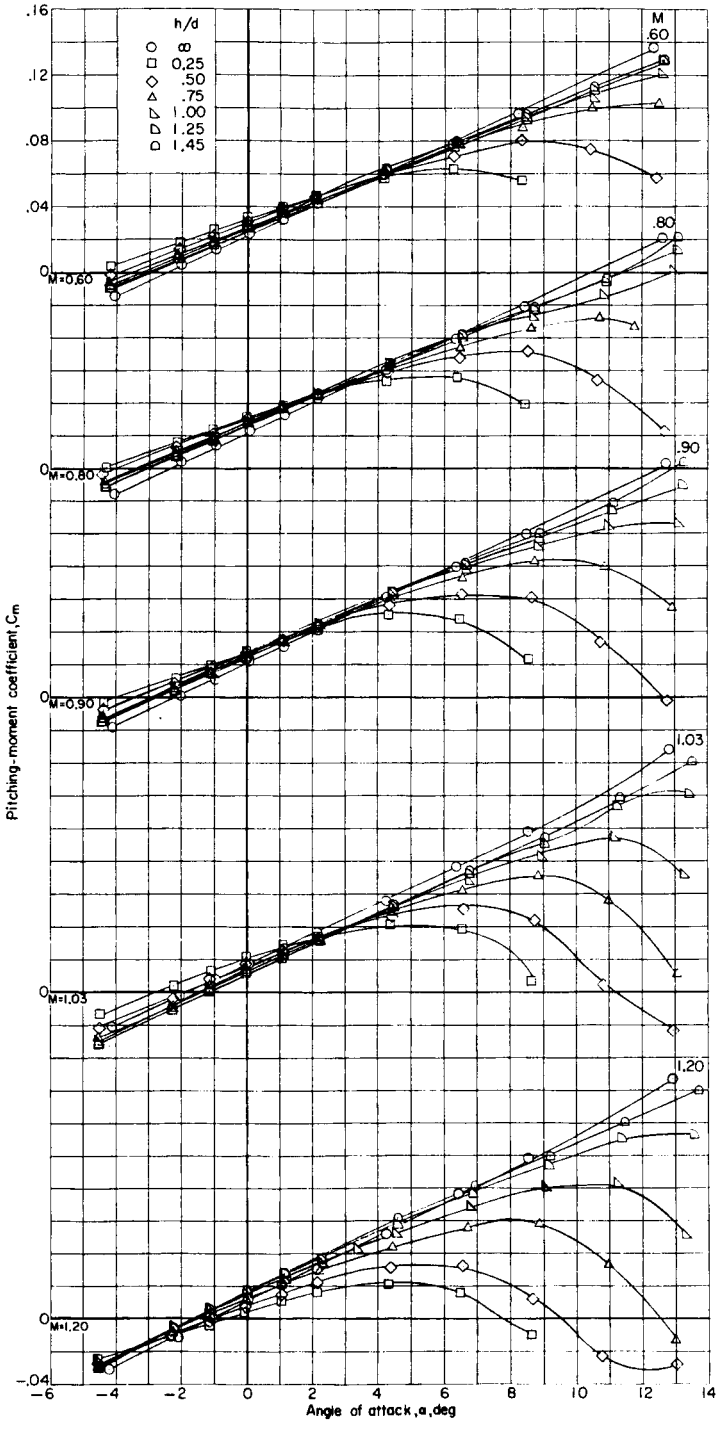

(b) Variation of pitching-moment coefficient with angle of attack.

Figure 14.- Continued.

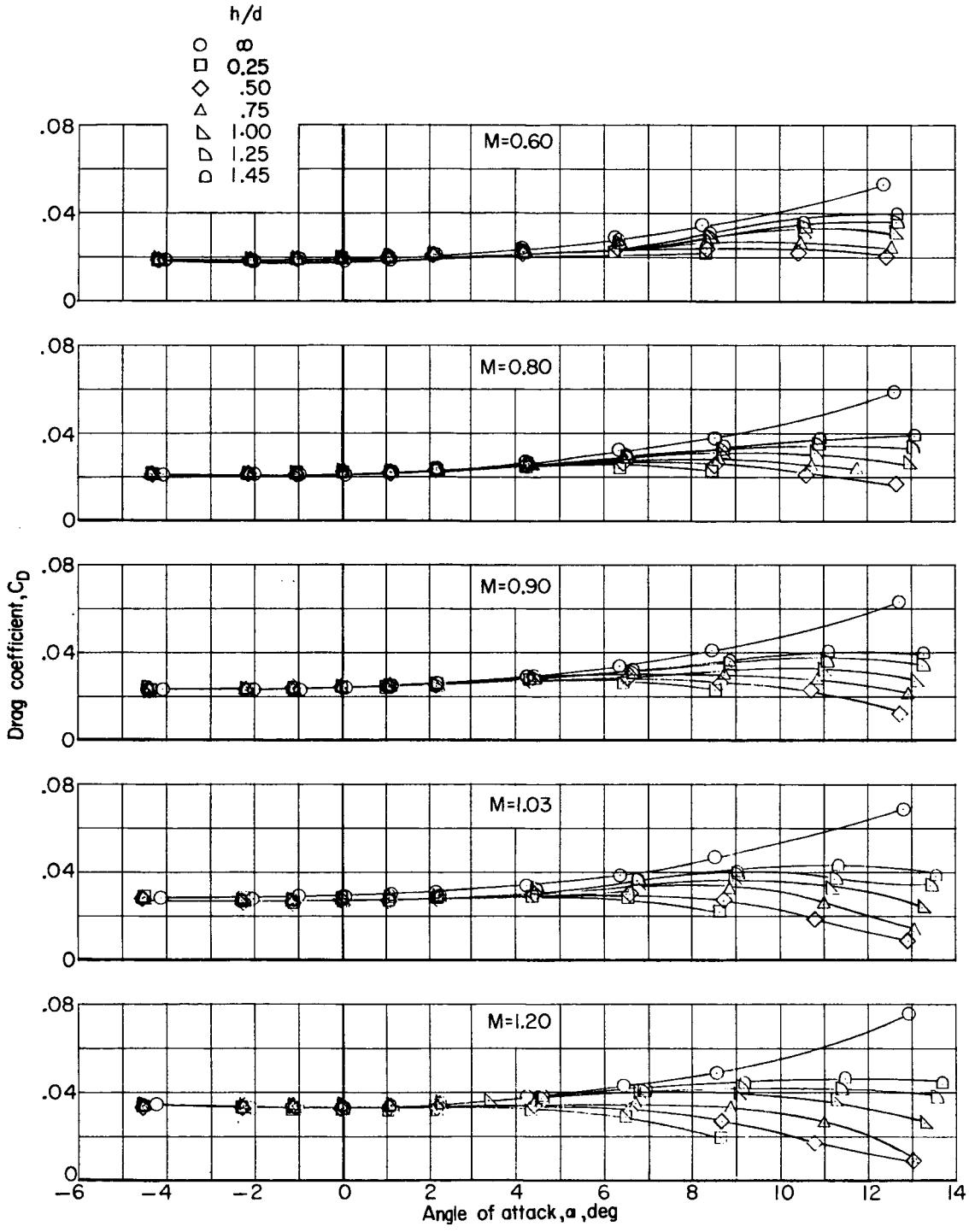

(c) Variation of drag coefficient with angle of attack.

Figure 14.- Concluded.

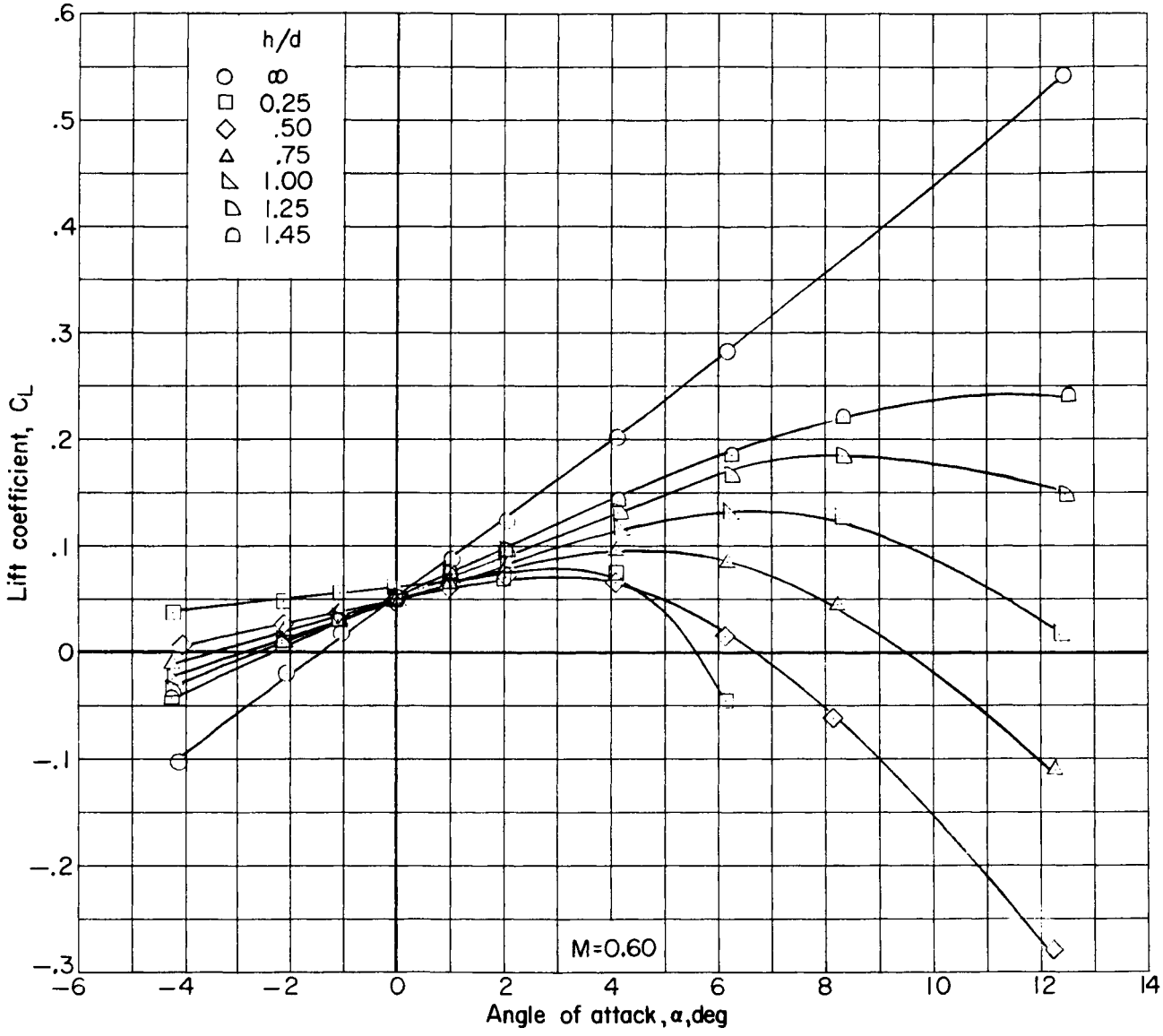

(a) Variation of lift coefficient with angle of attack.

Figure 15.- Longitudinal aerodynamic characteristics of BWFMS' in presence of the complete first stage.

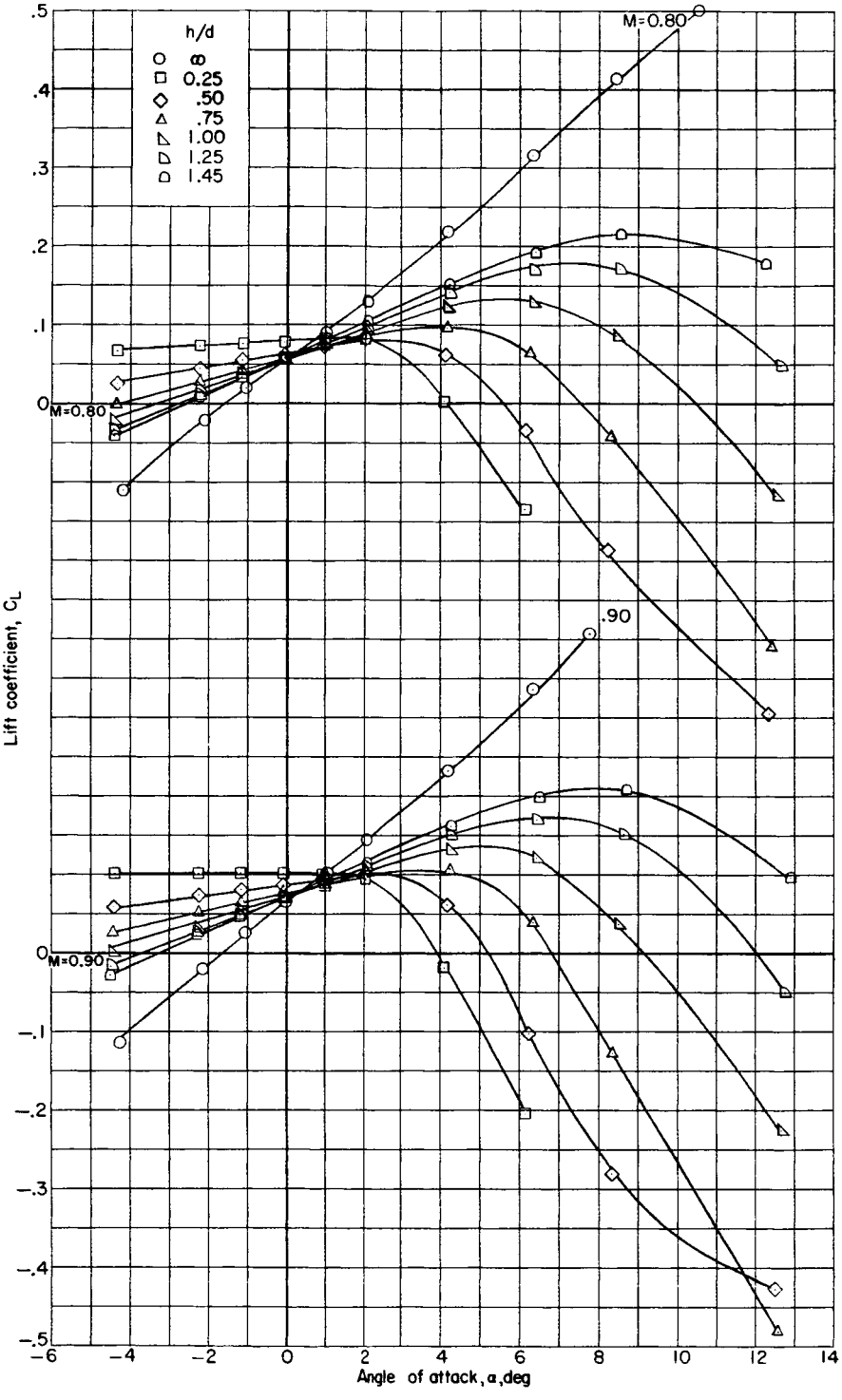

(a) Continued.

Figure 15.- Continued.

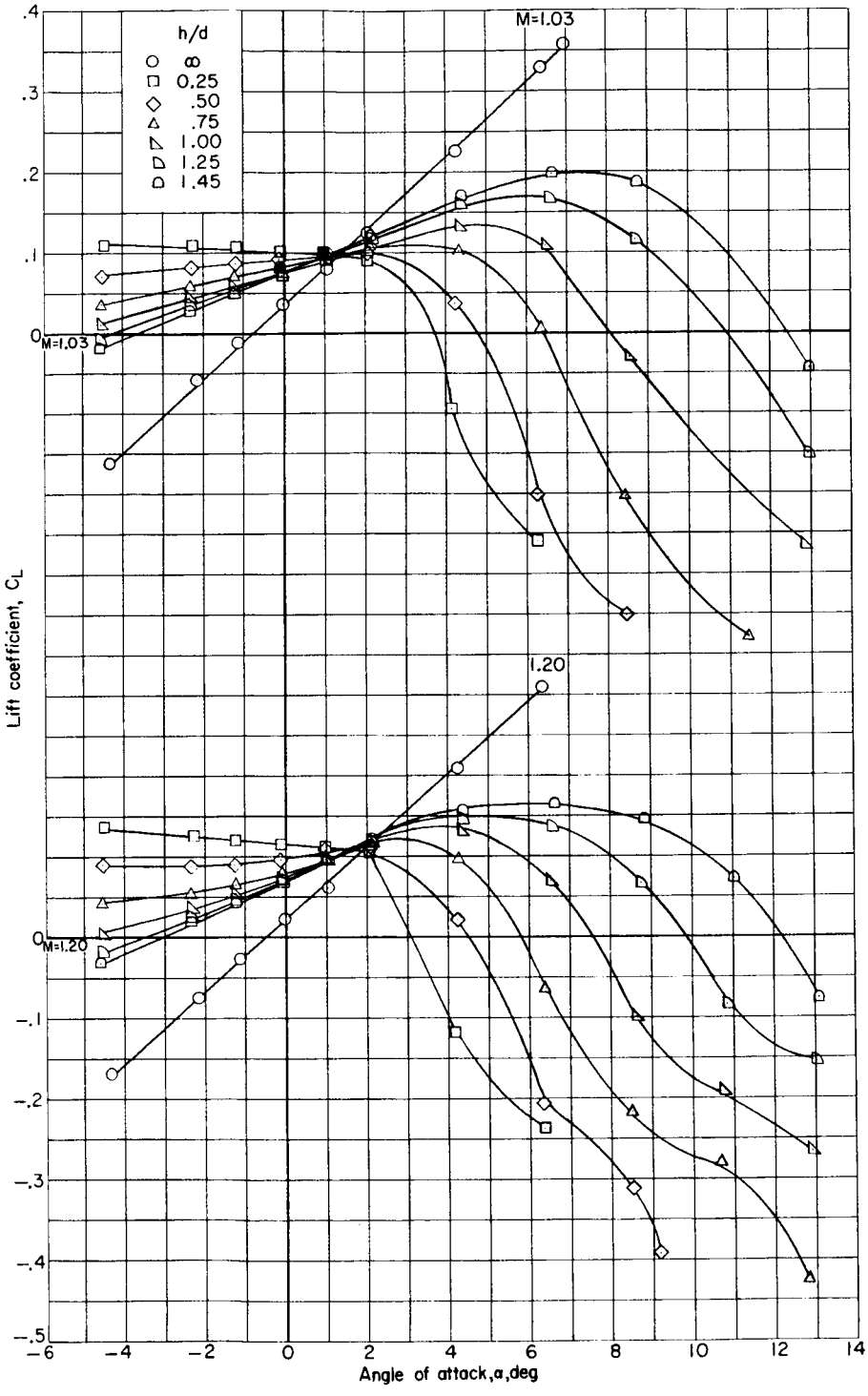

(a) Concluded.

Figure 15.- Continued.

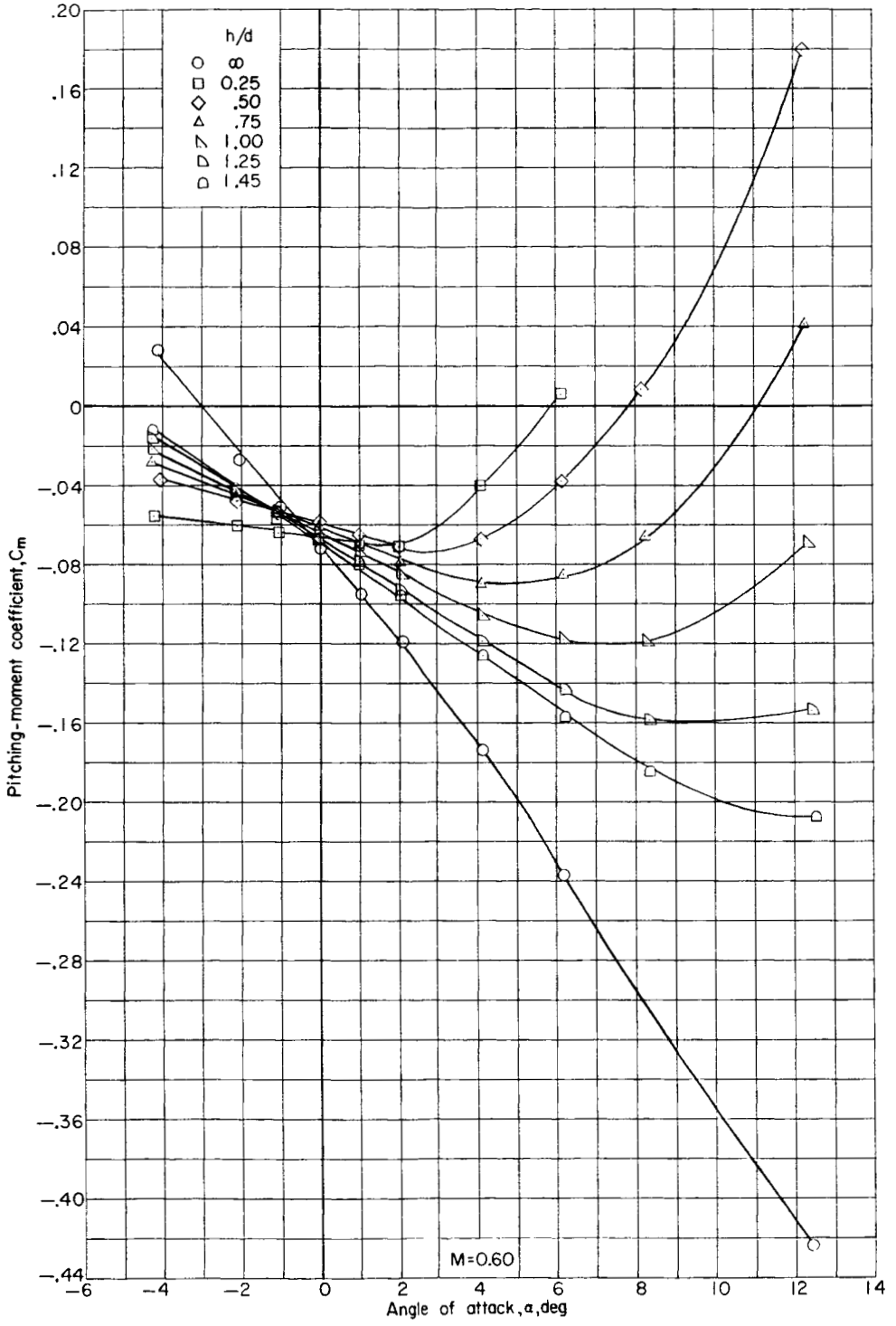

(b) Variation of pitching-moment coefficient with angle of attack.

Figure 15.- Continued.

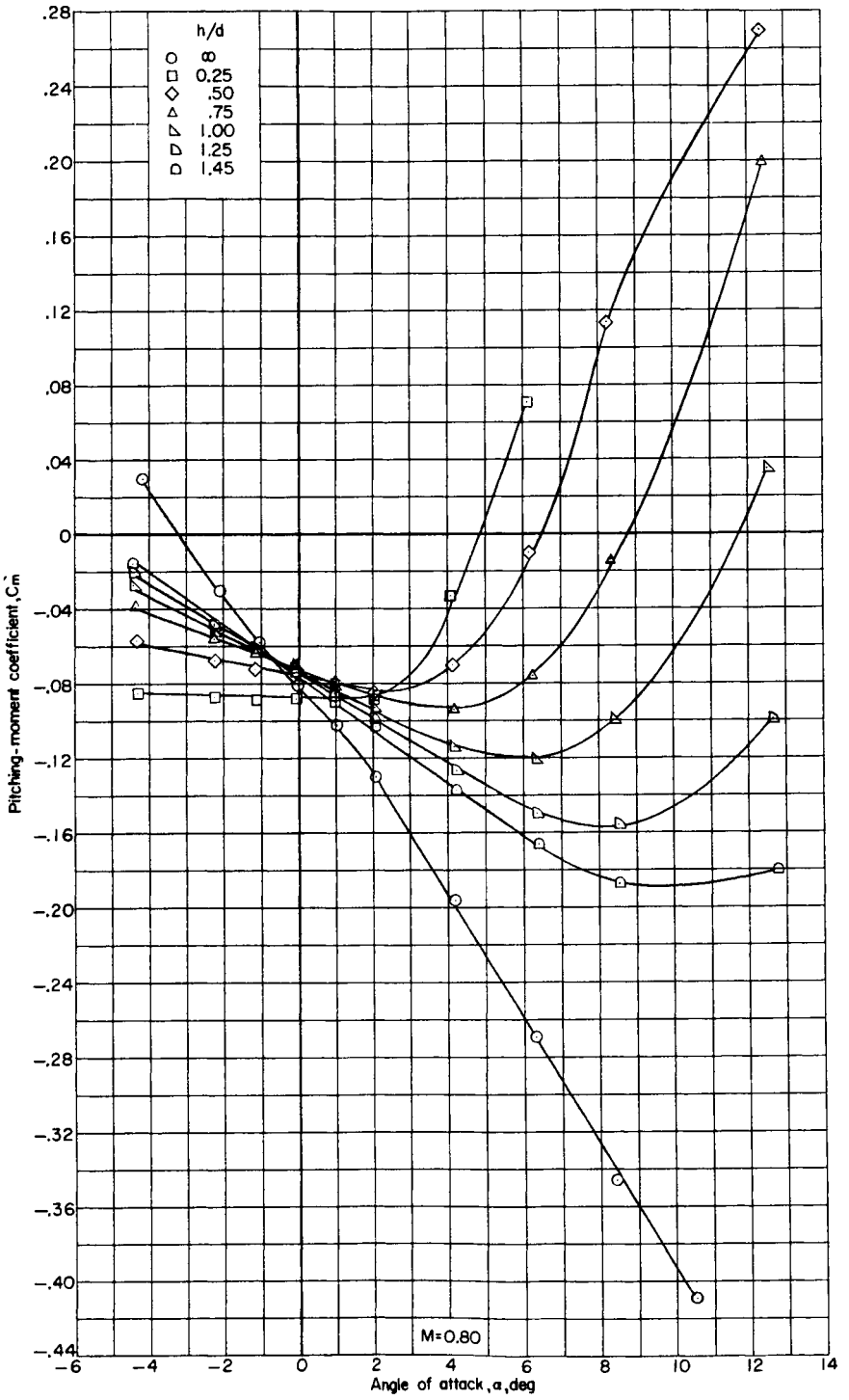

(b) Continued.

Figure 15.- Continued.

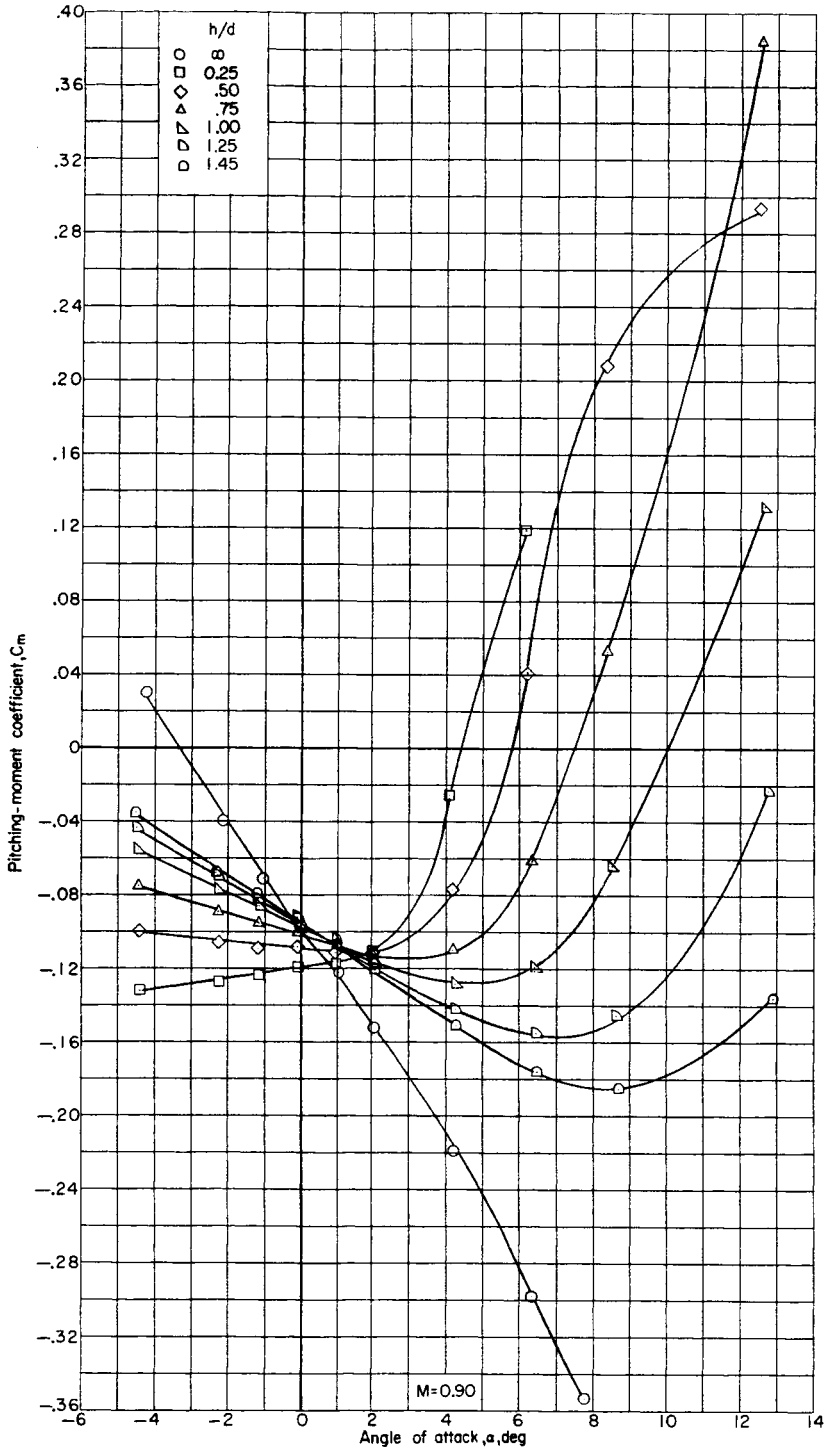

(b) Continued.

Figure 15.- Continued.

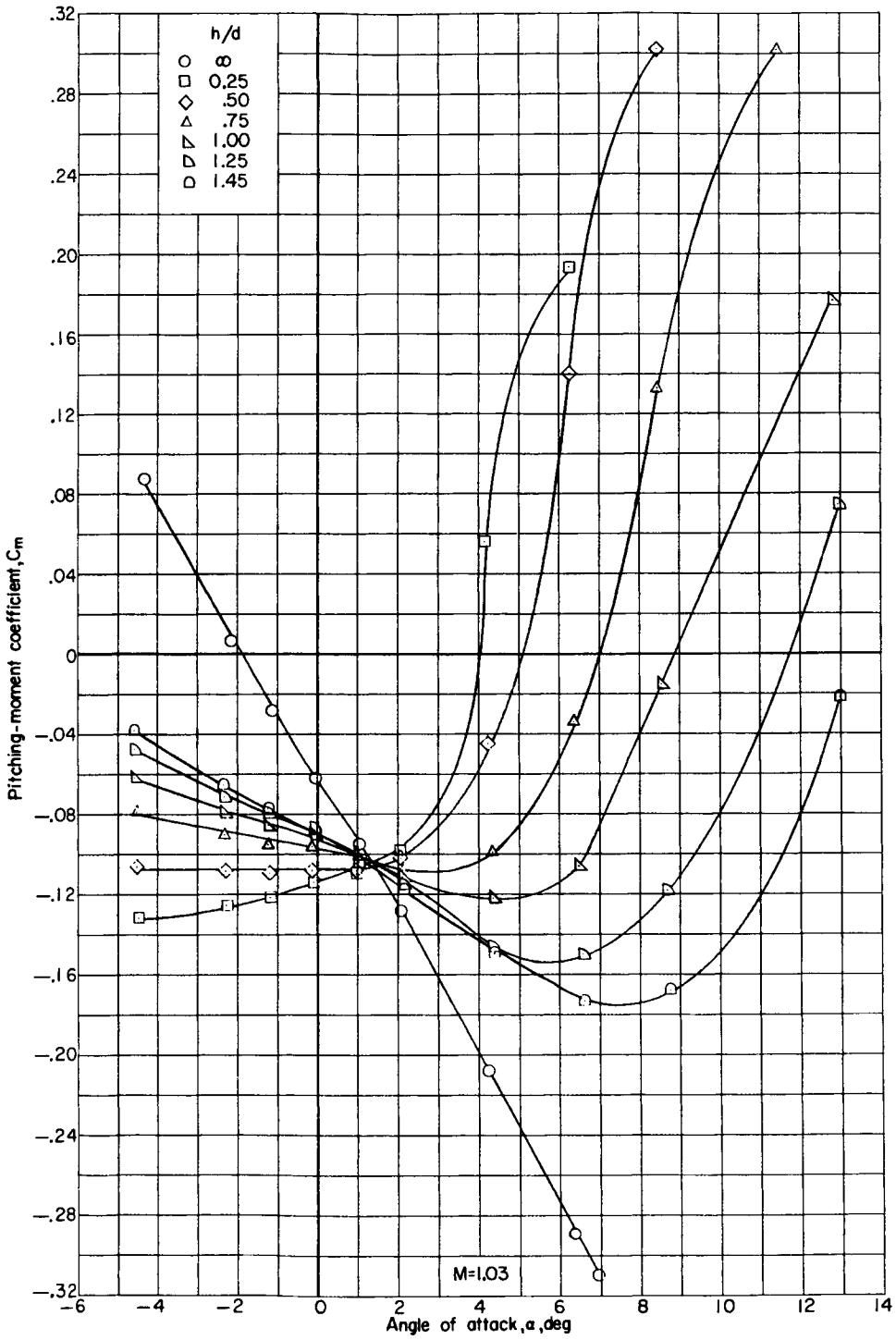

(b) Continued.

Figure 15.- Continued.

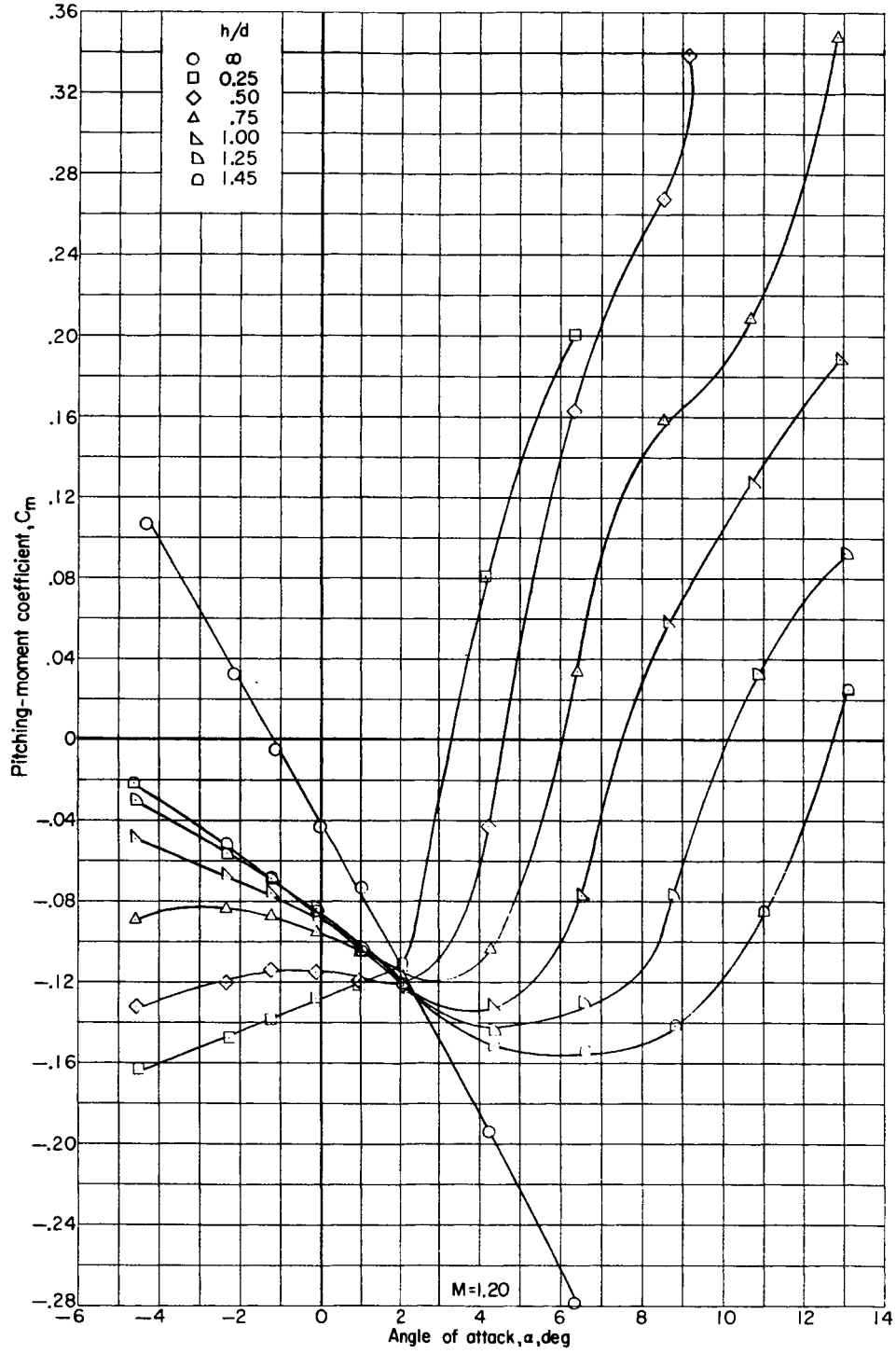

(b) Concluded.

Figure 15.- Continued.

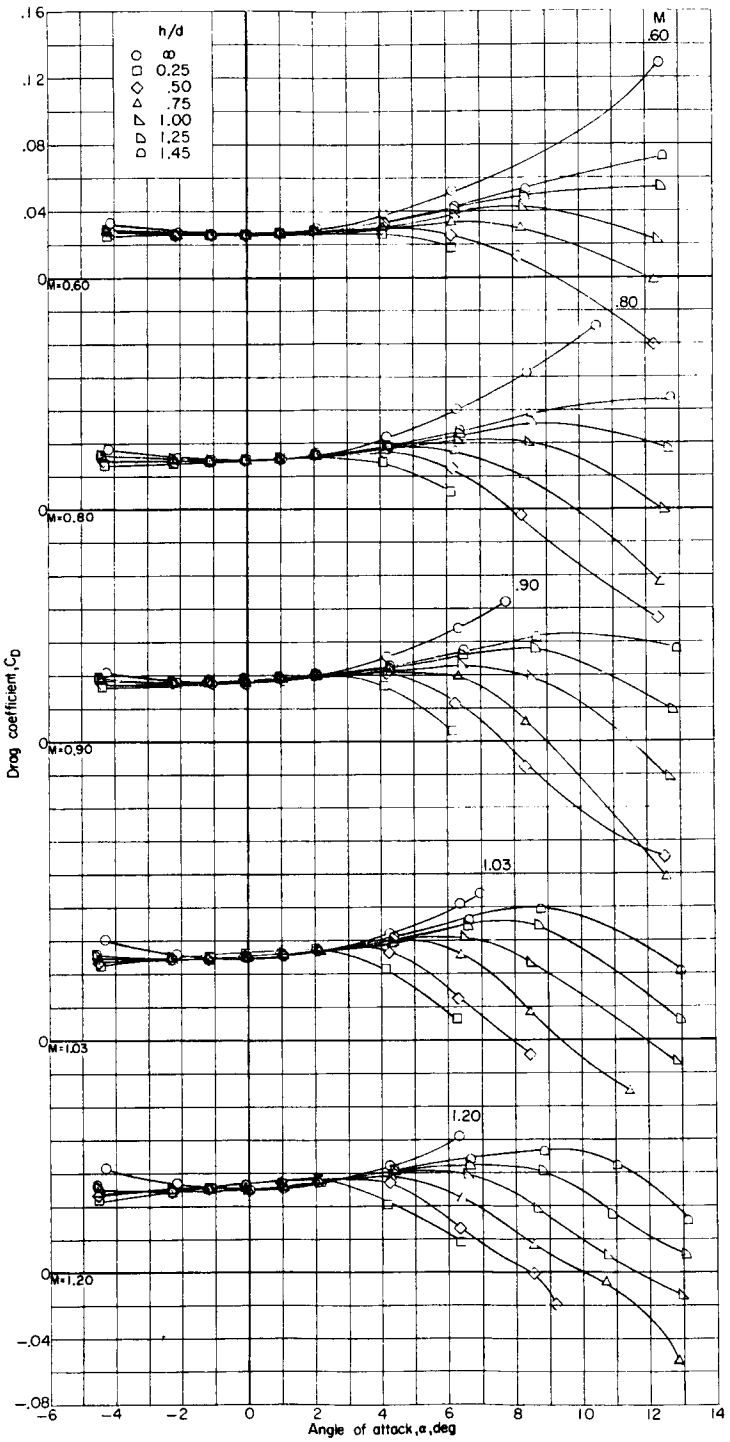

(c) Variation of drag coefficient with angle of attack.

Figure 15.- Concluded.

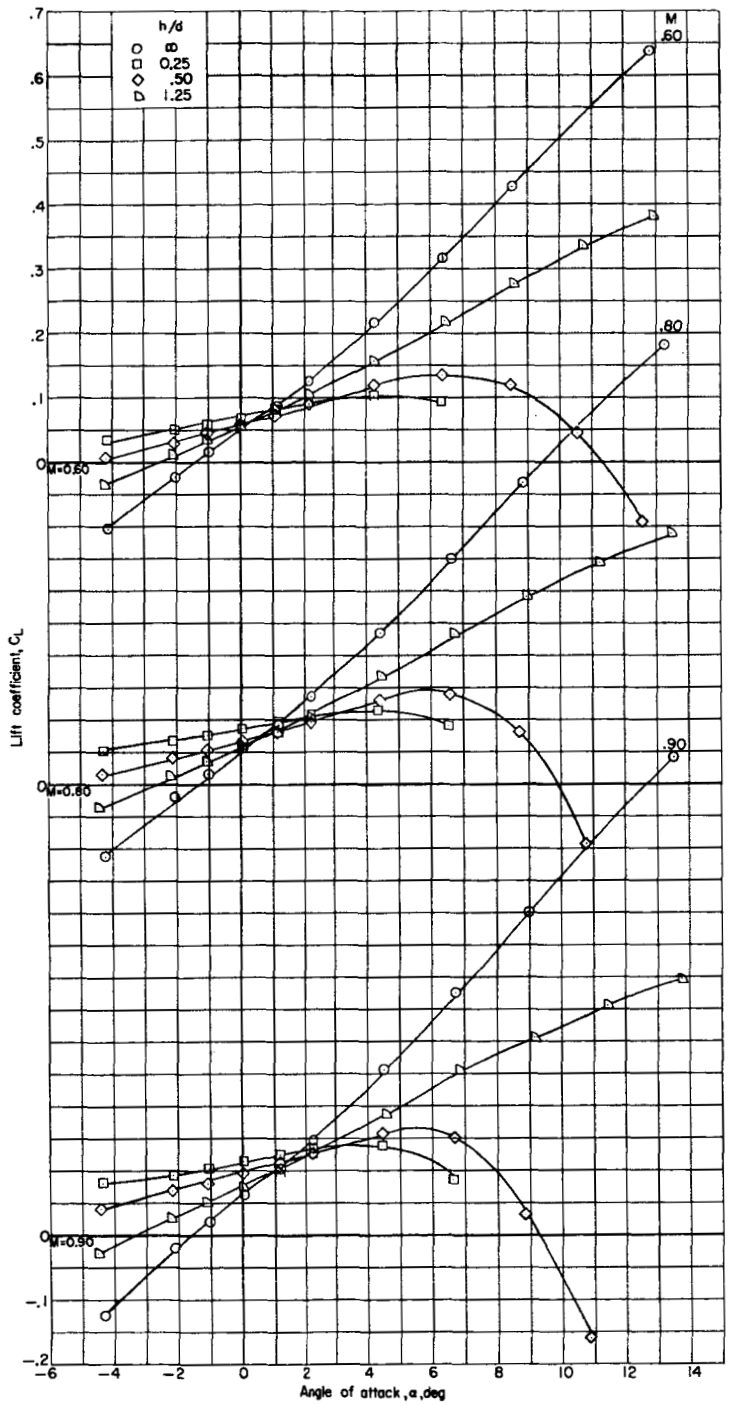

(a) Variation of lift coefficient with angle of attack.

Figure 16.- Longitudinal aerodynamic characteristics of BWFMS in presence of the first stage without the canard.

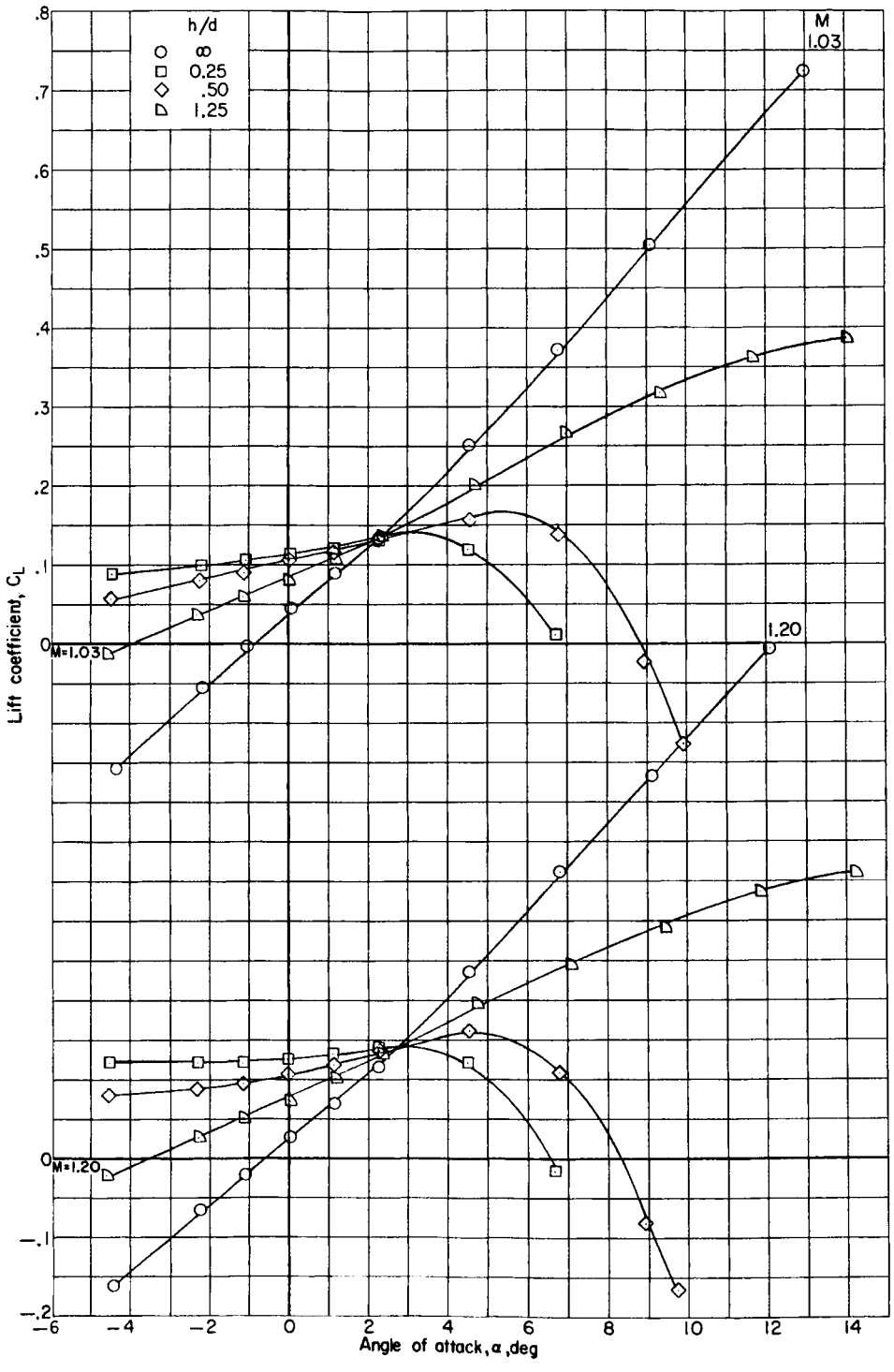

(a) Concluded.

Figure 16.- Continued.

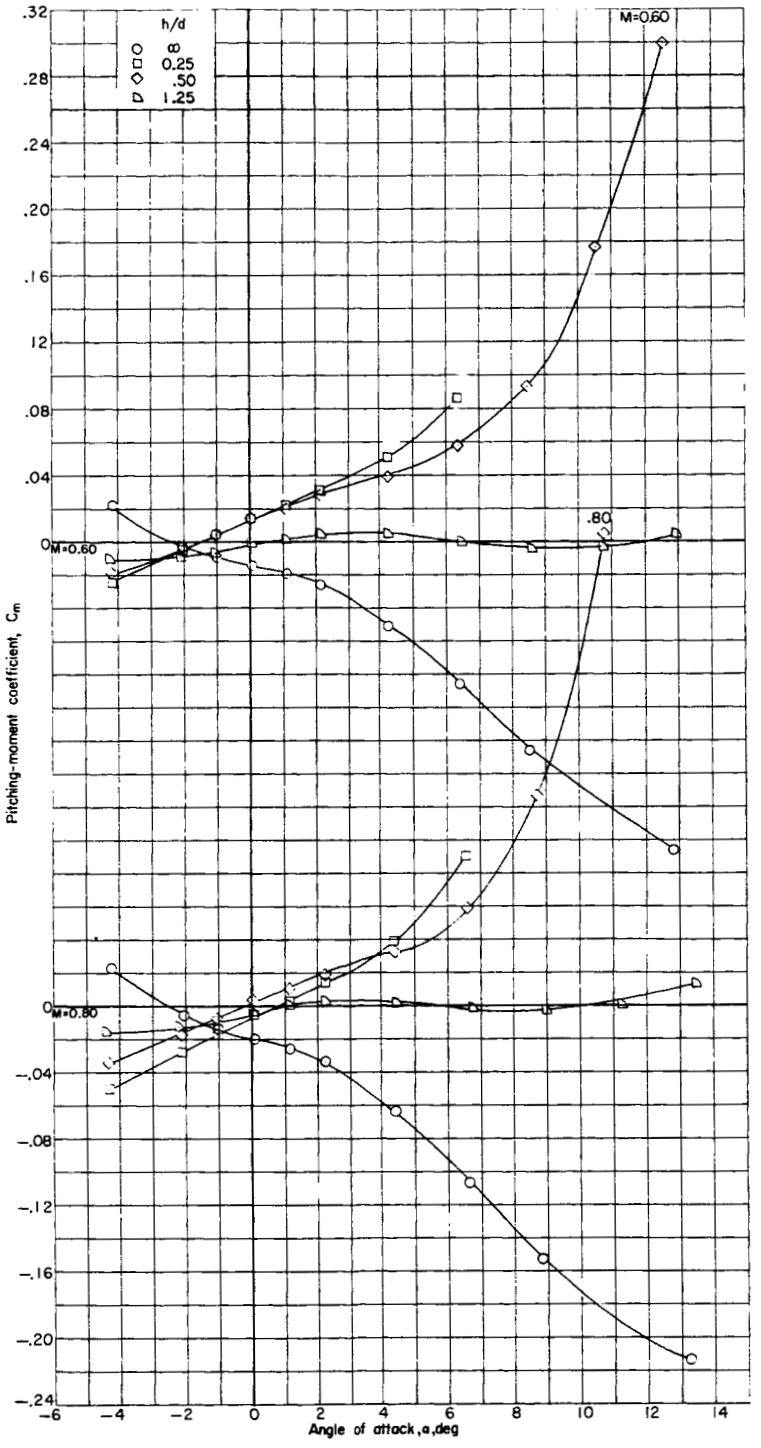

(b) Variation of pitching-moment coefficient with angle of attack.

Figure 16.- Continued.

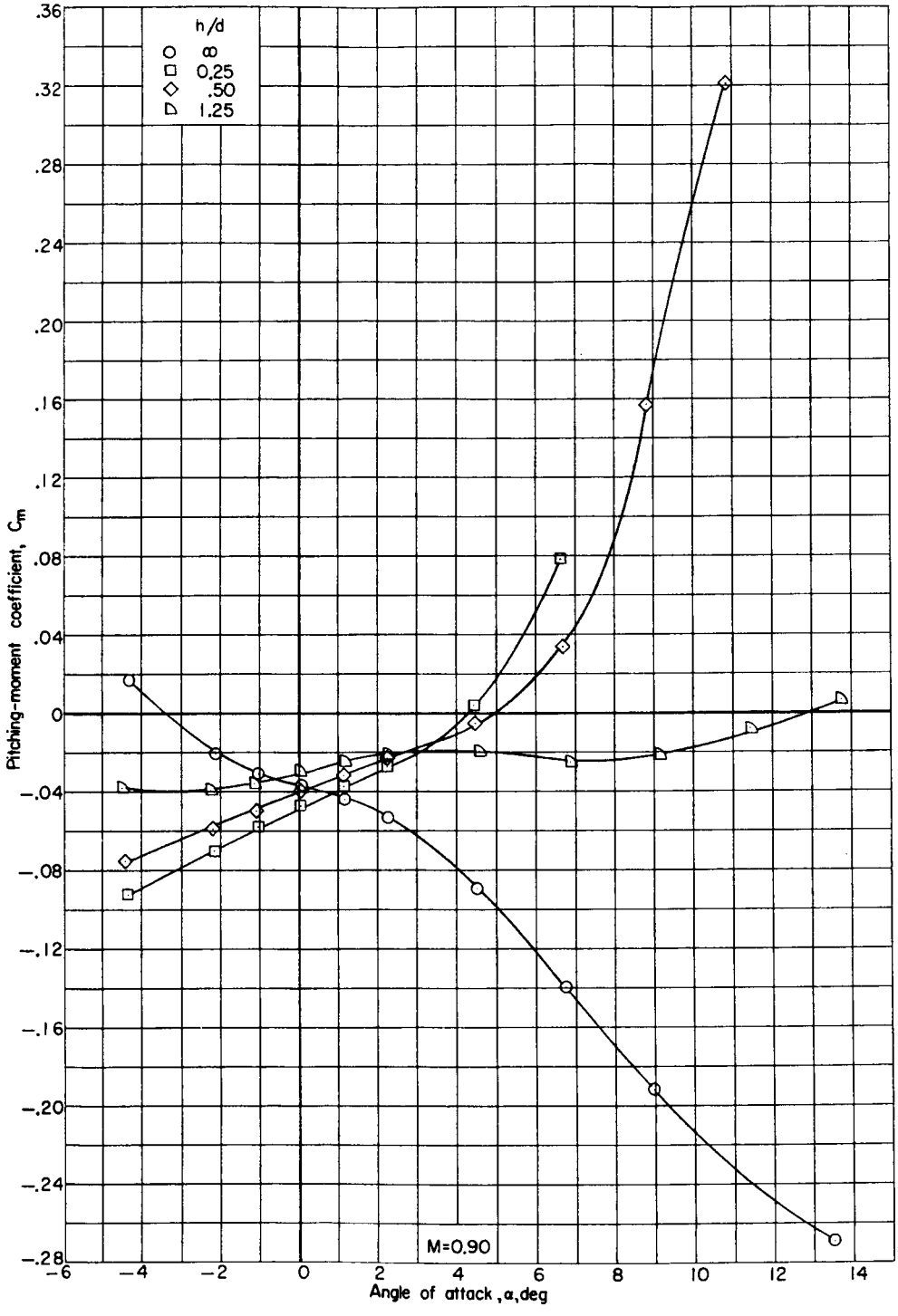

(b) Continued.

Figure 16.- Continued.

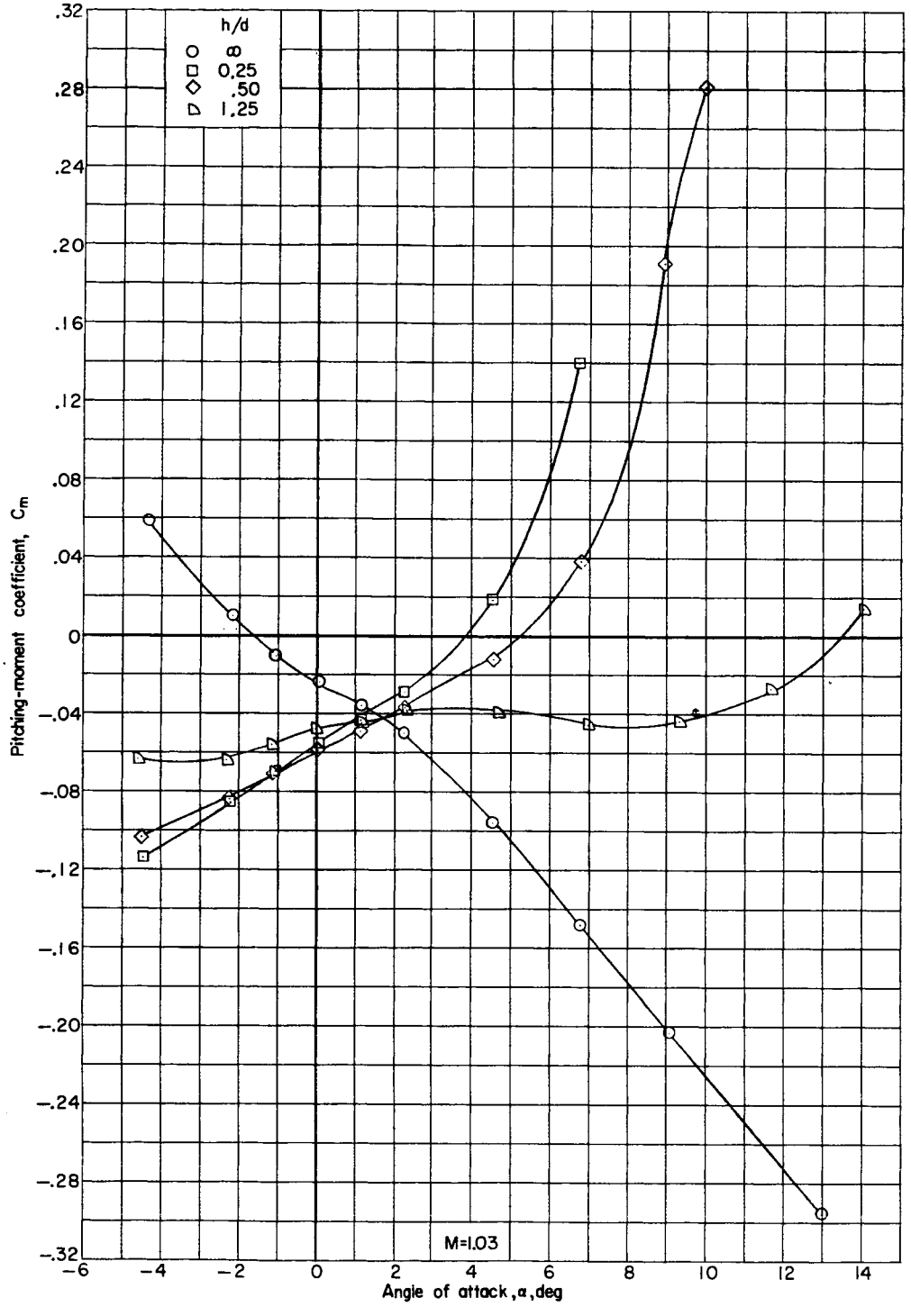

(b) Continued.

Figure 16.- Continued.

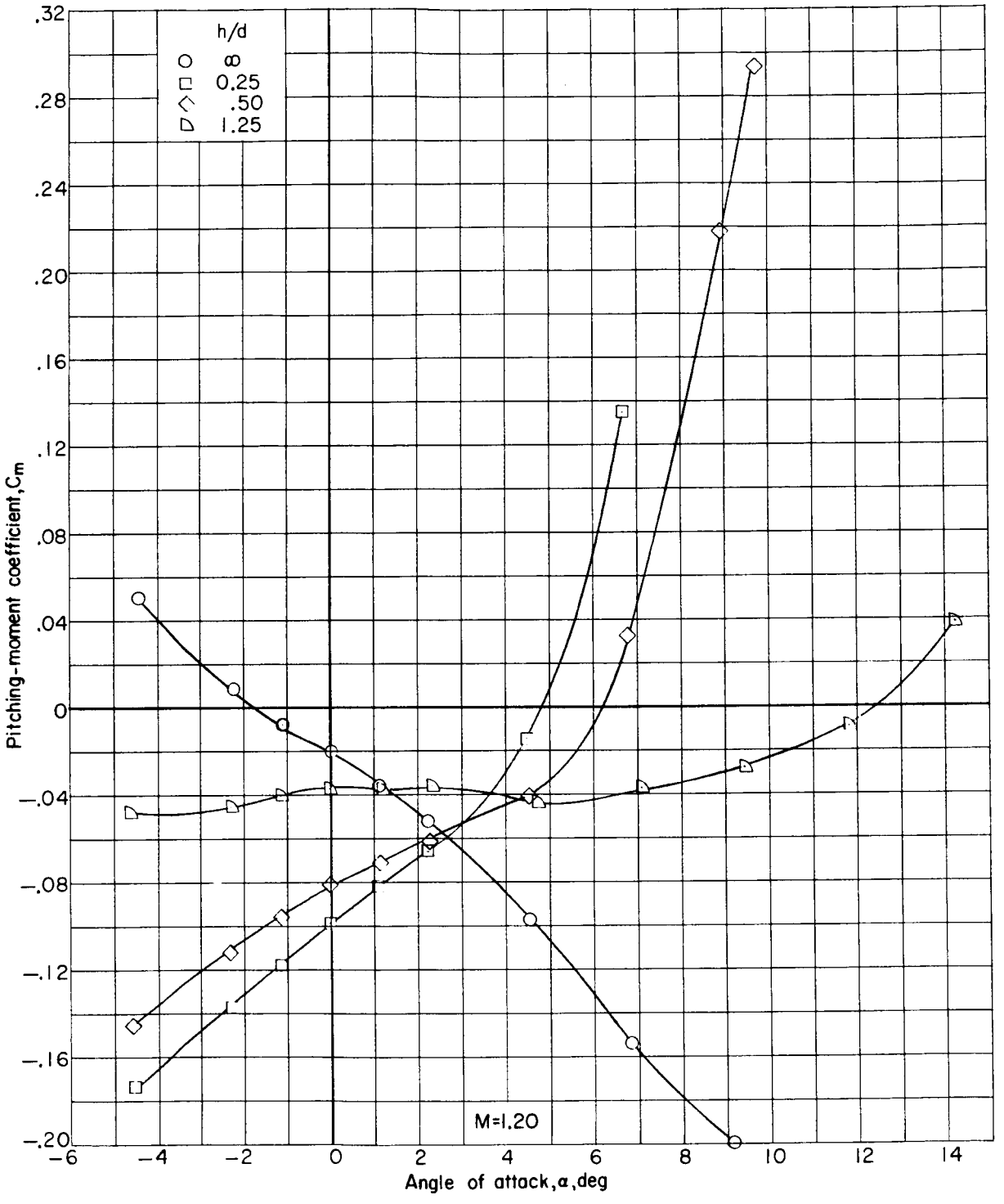

(b) Concluded.

Figure 16.- Continued.

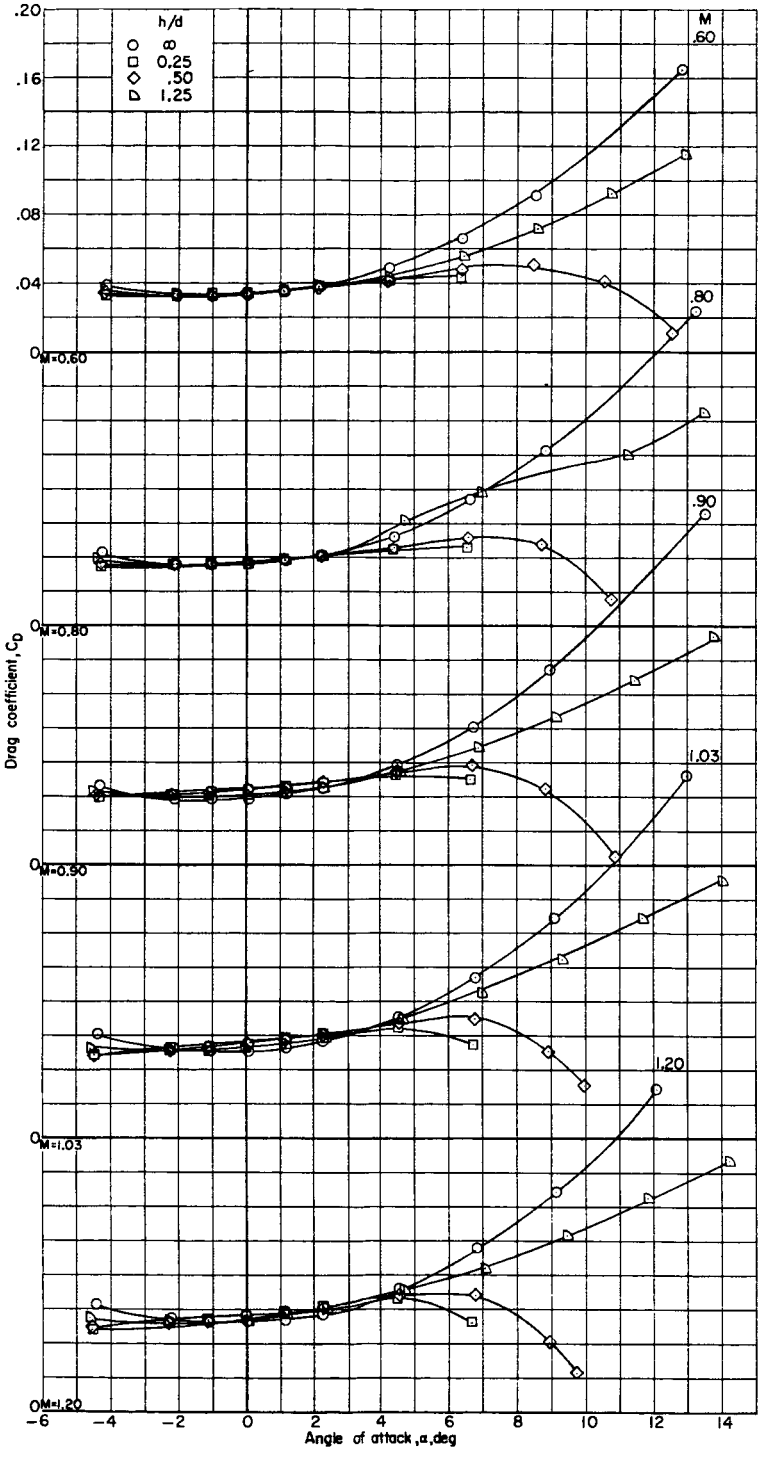

(c) Variation of drag coefficient with angle of attack.

Figure 16.- Concluded.

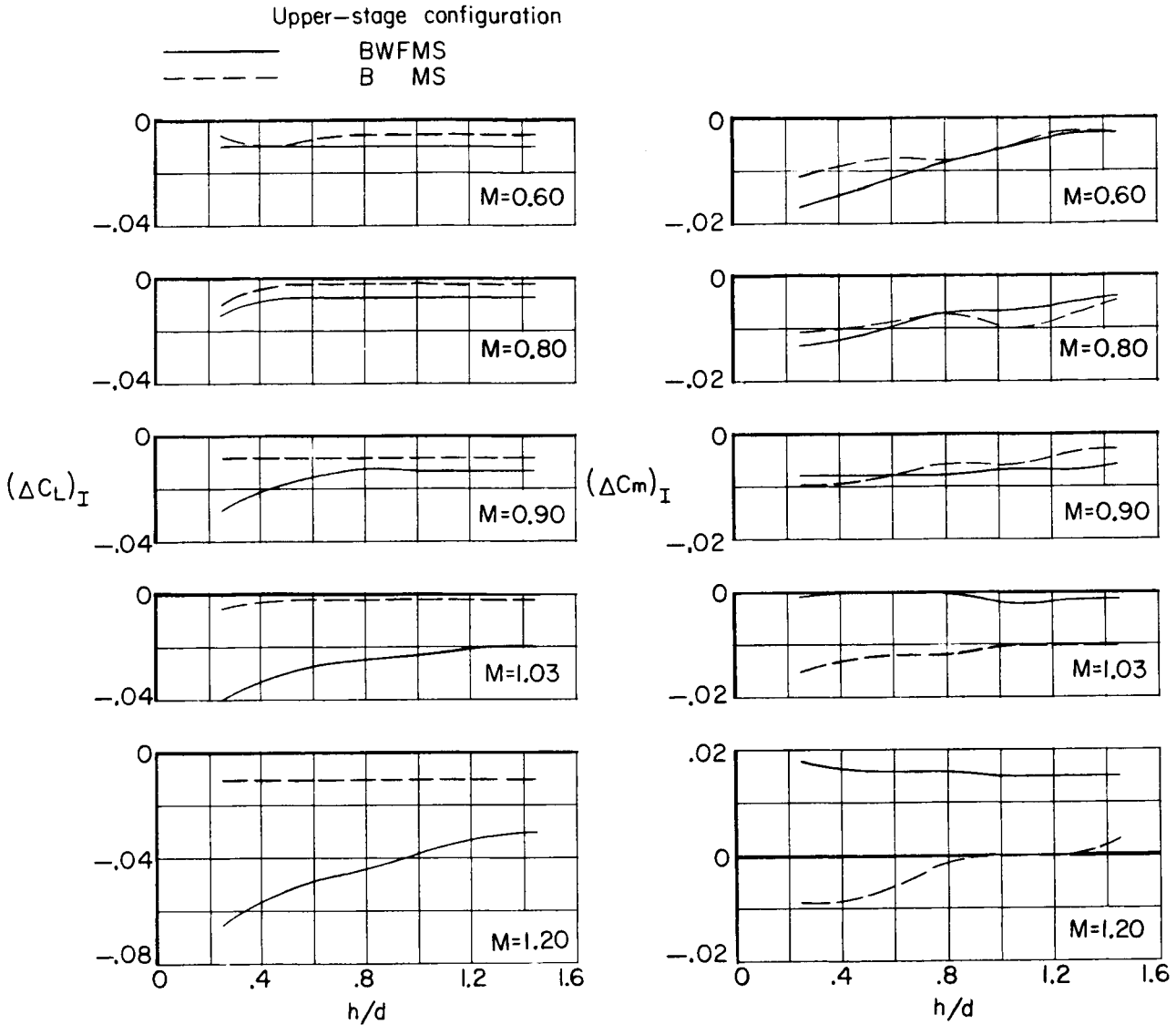

(a) $\alpha = 0^\circ$.

Figure 17.- Variation with spacing distance of the incremental changes in lift and pitching-moment coefficients for the complete first stage in presence of two upper-stage configurations.

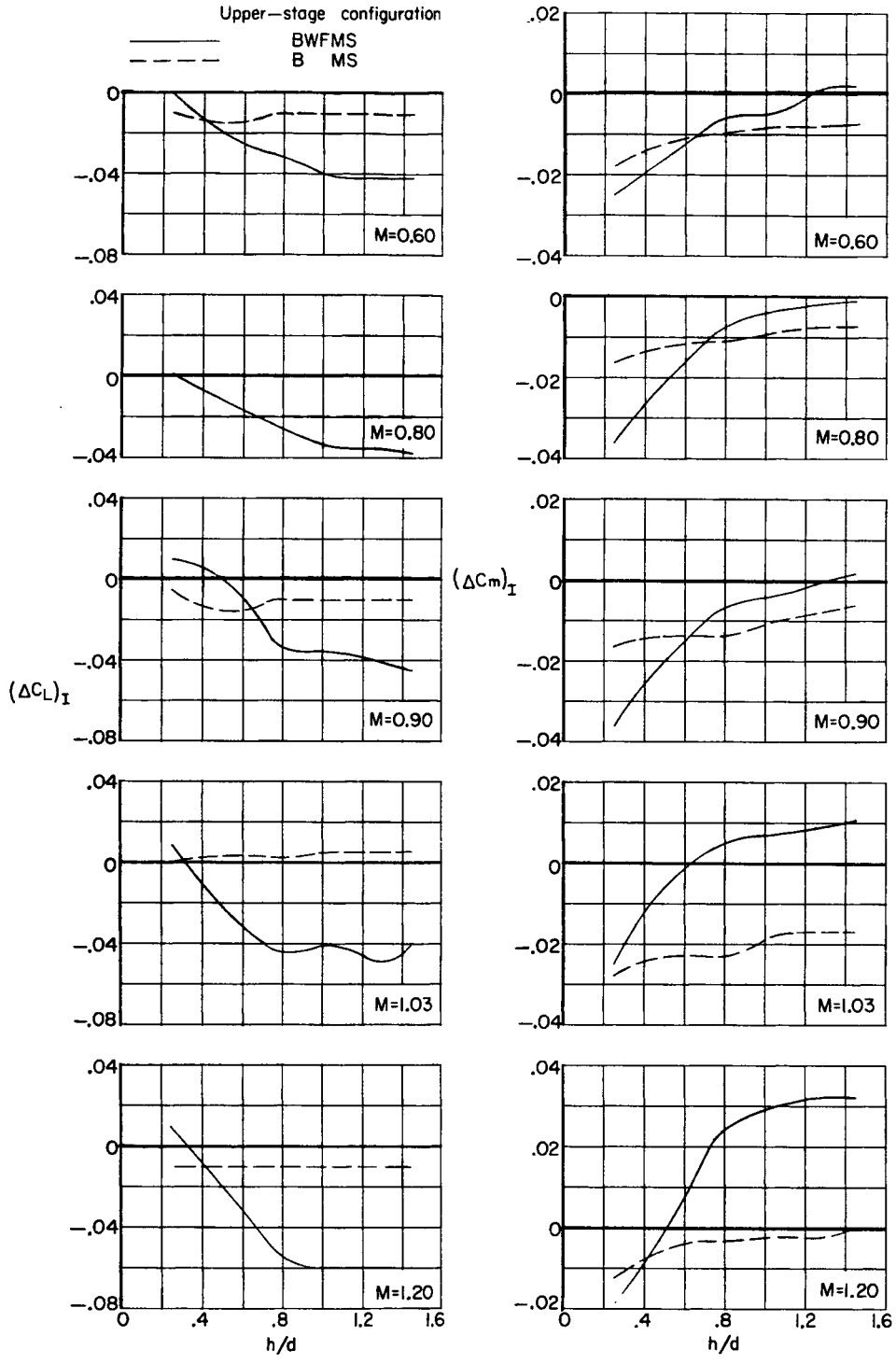

(b) $\alpha = 6^\circ$.

Figure 17.- Concluded.

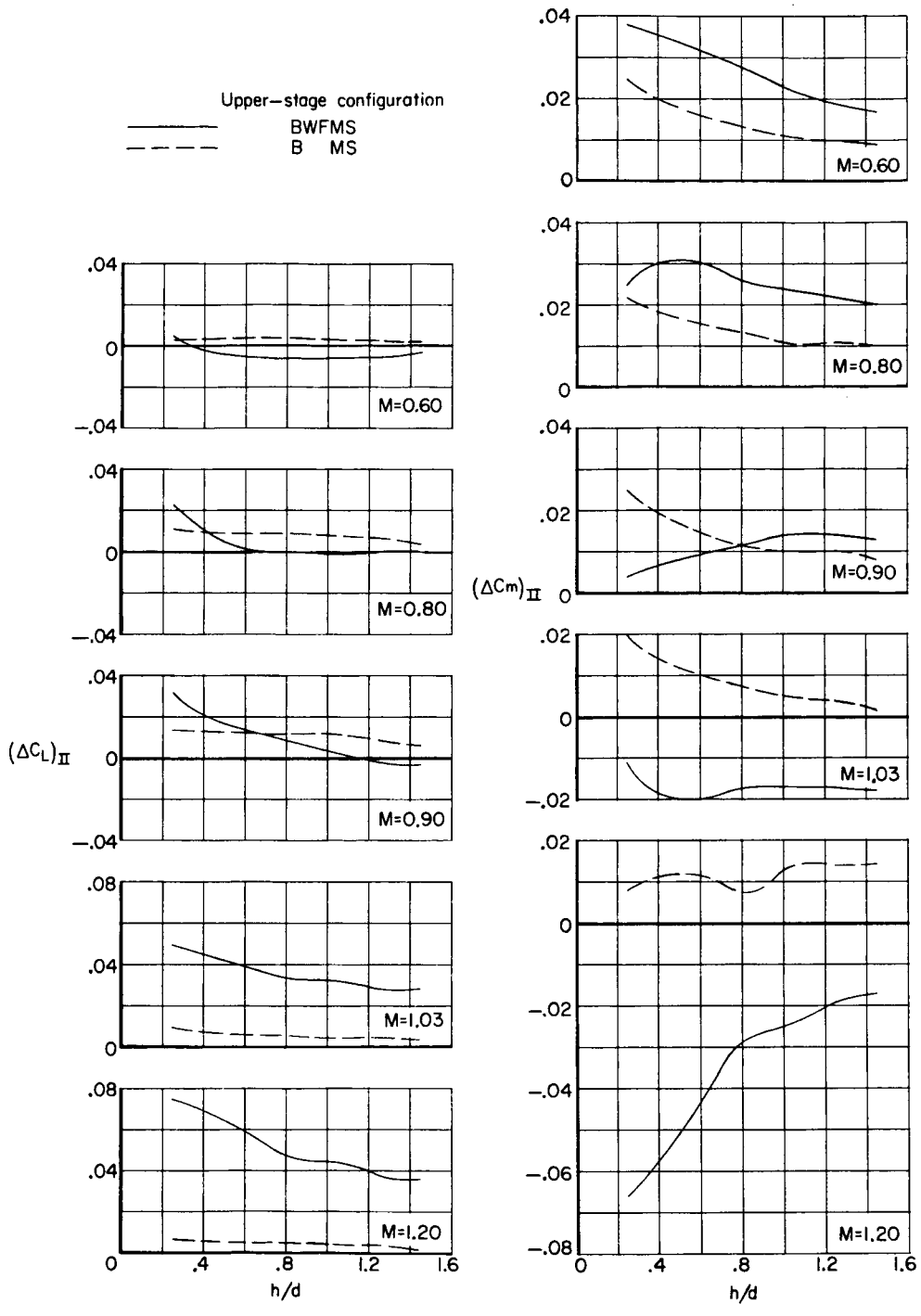

(a) $\alpha = 0^{\circ}$.

Figure 18.- Variation with spacing distance of the incremental changes in lift and pitching-moment coefficients for two upper-stage configurations in presence of the complete first stage.

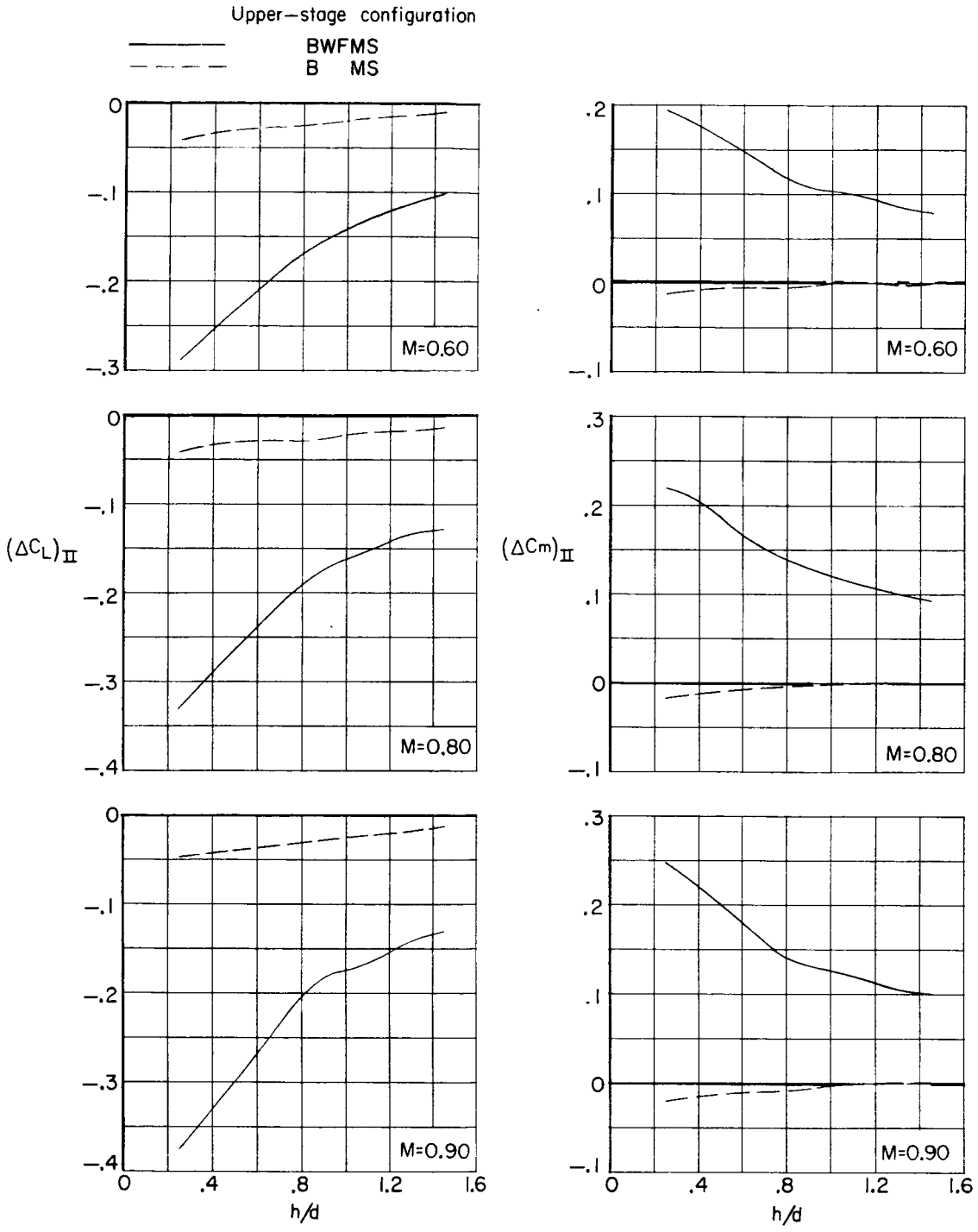

(b) $\alpha = 6^{\circ}$.

Figure 18.- Continued.

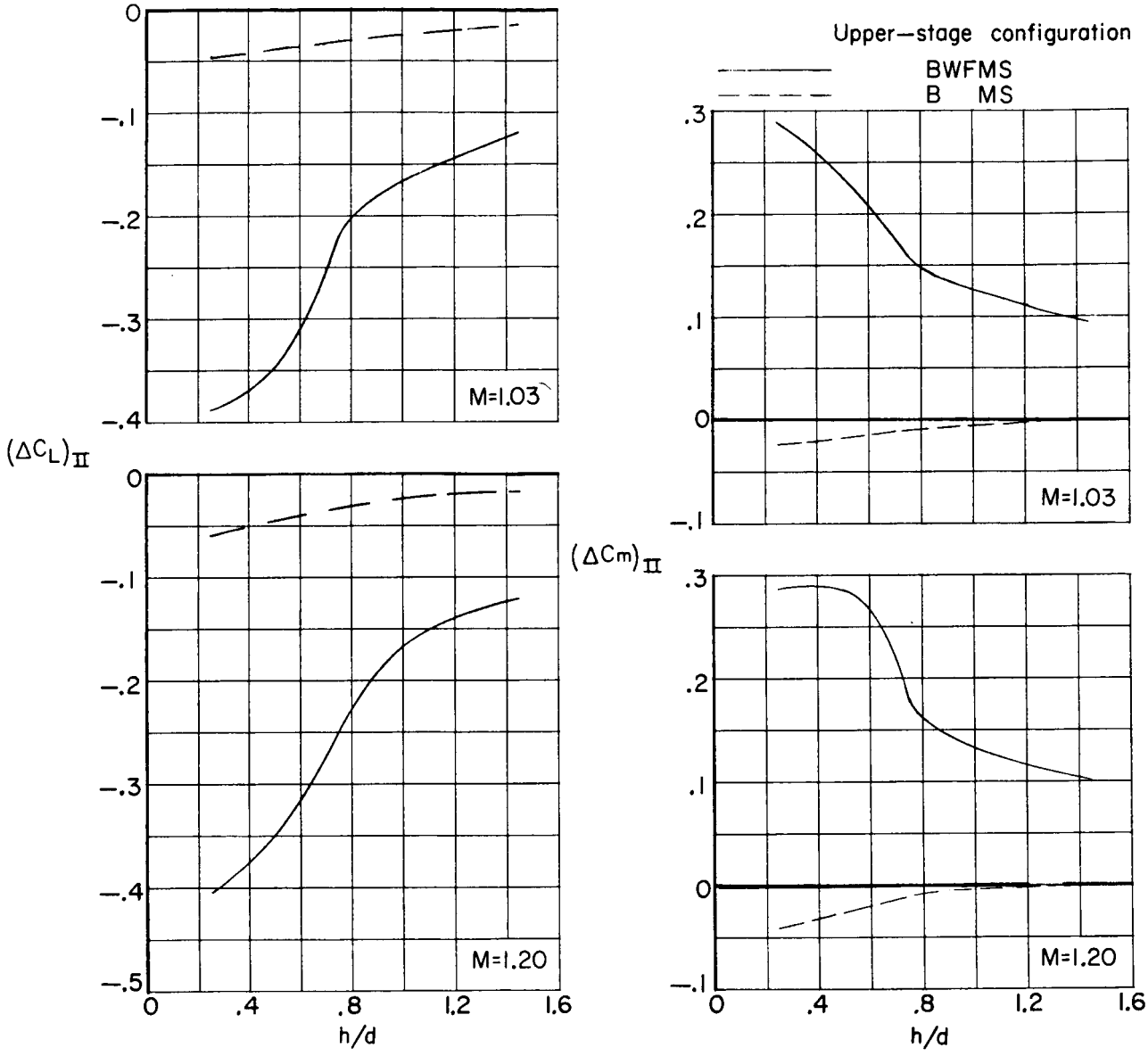

(b) $\alpha = 6^{\circ}$. Concluded.

Figure 18.- Concluded.

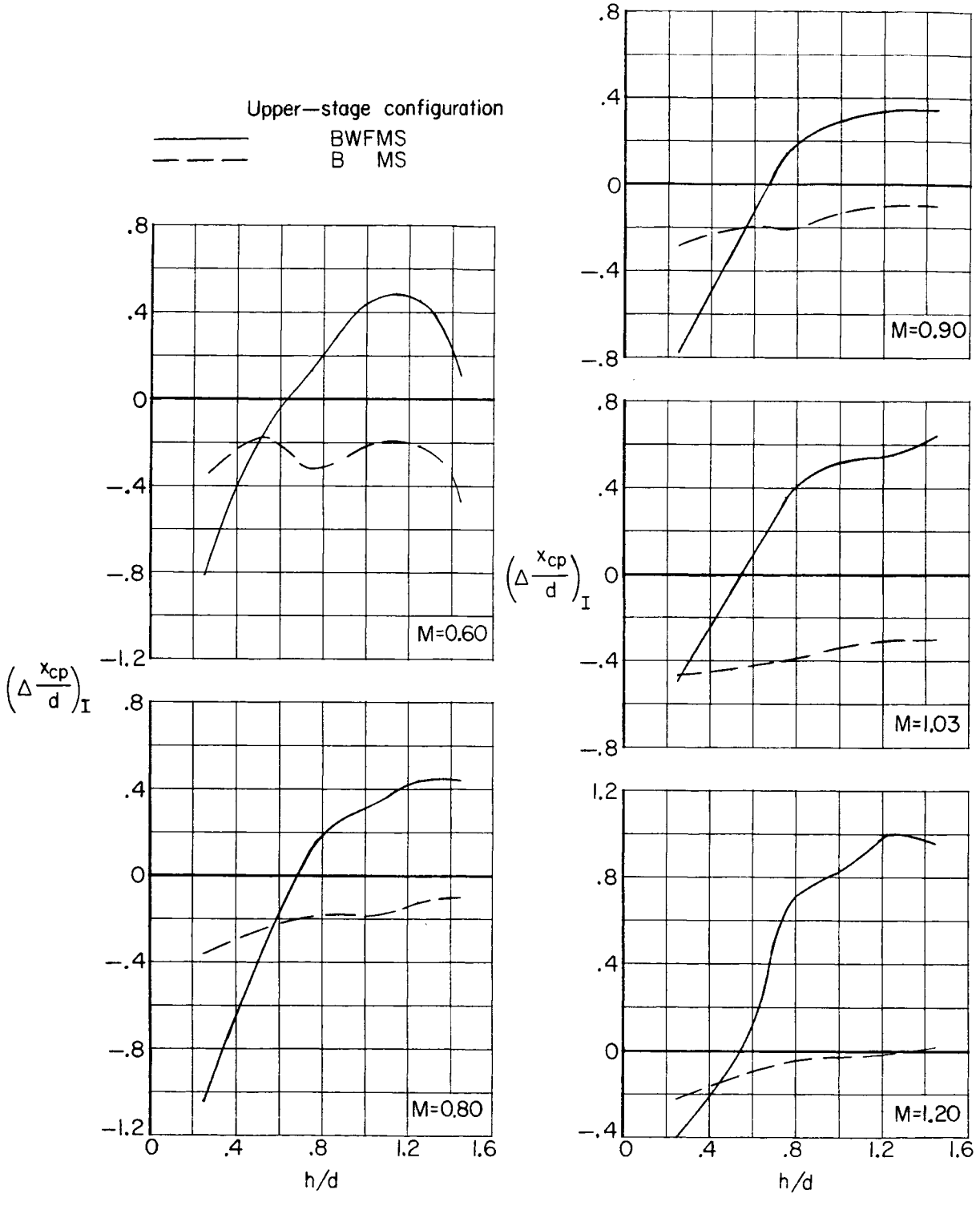

Figure 19.- Variation with spacing distance of the incremental changes in center of pressure at $\alpha = 6^{\circ}$ for the complete first stage in presence of two upper-stage configurations.

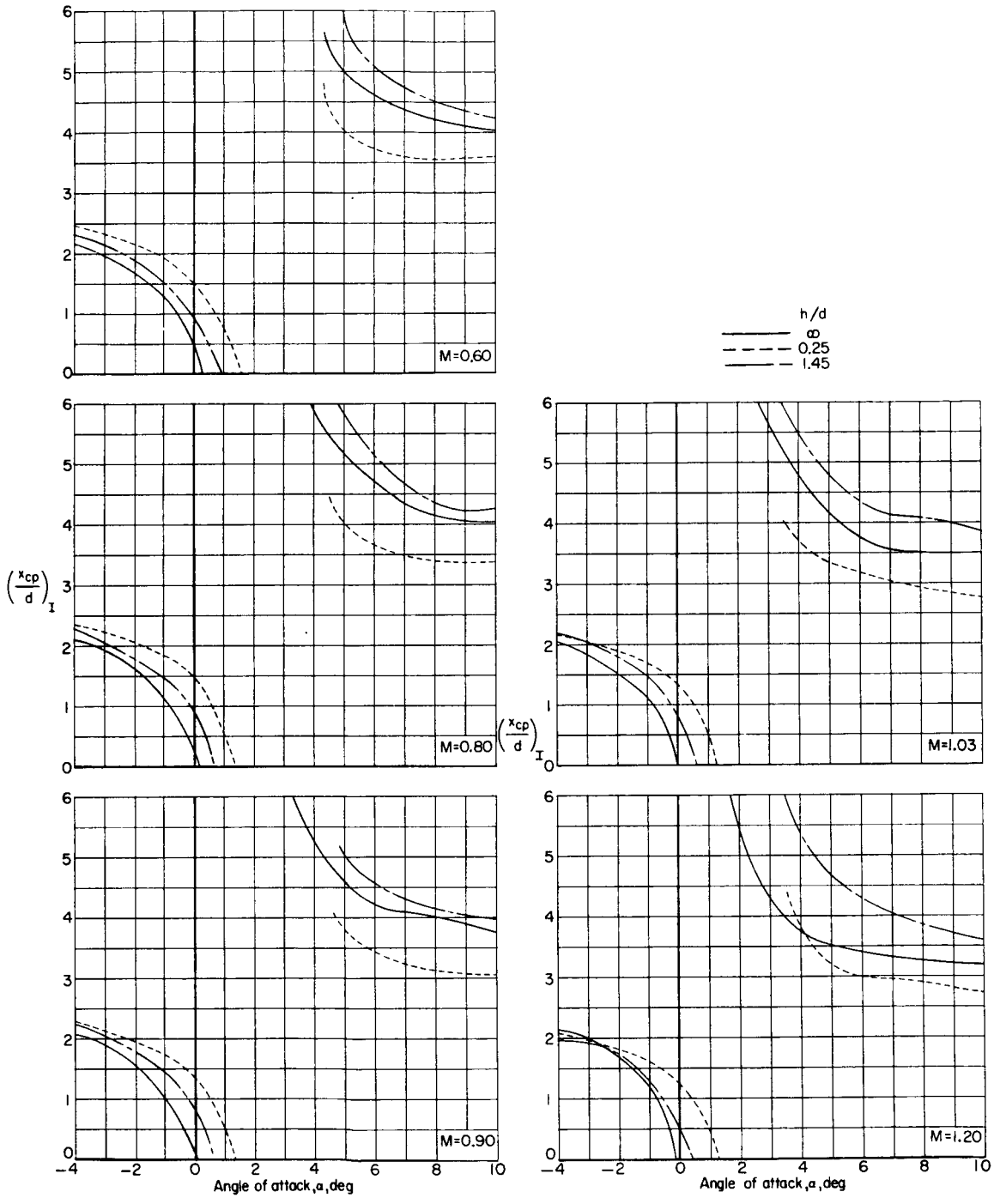

(a) Variation for complete first stage in presence of BWFMS.

Figure 20.- Variation of the center of pressure with angle of attack for the complete first stage in presence of two upper-stage configurations.

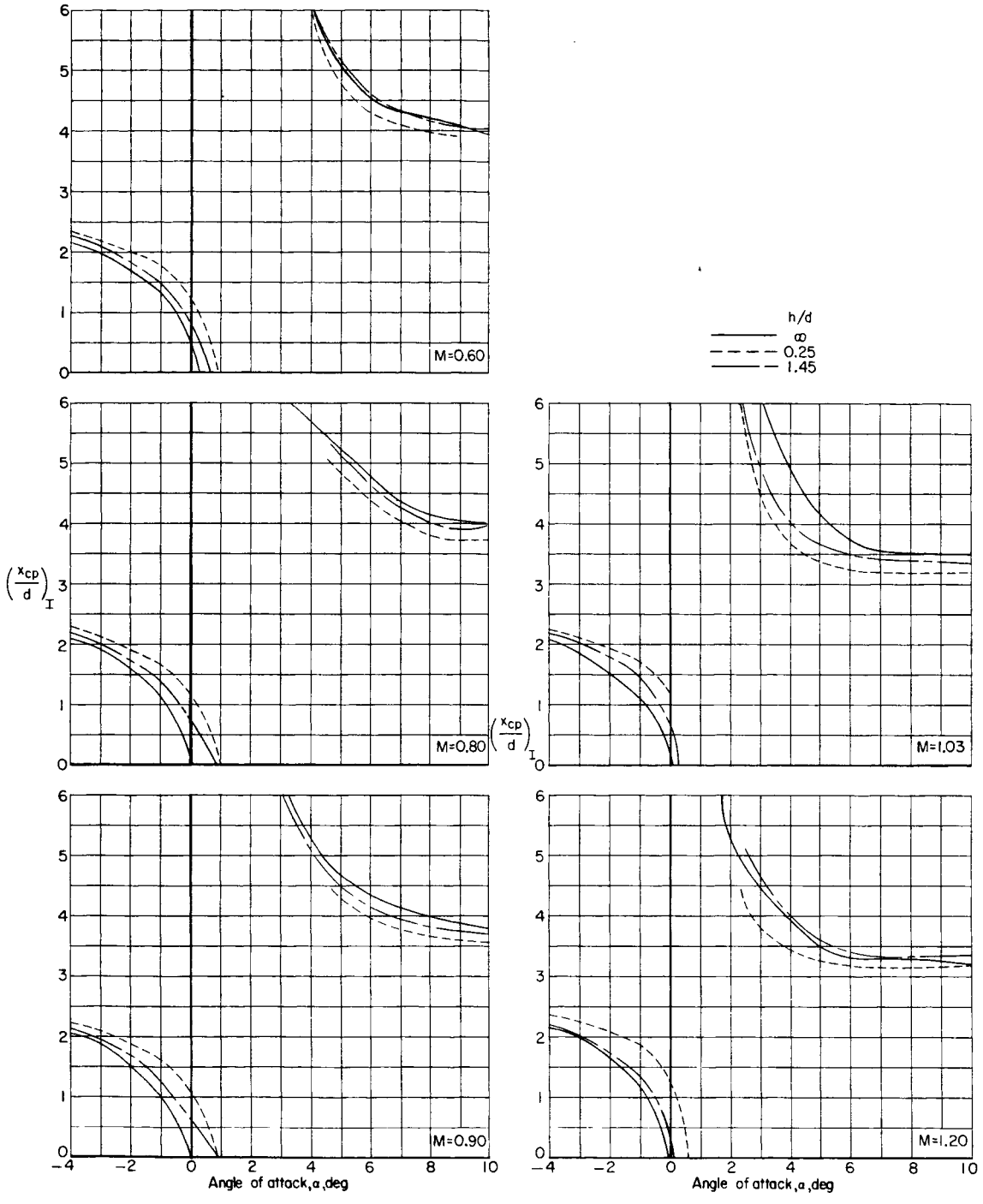

(b) Variation for complete first stage in presence of BMS.

Figure 20.- Concluded.

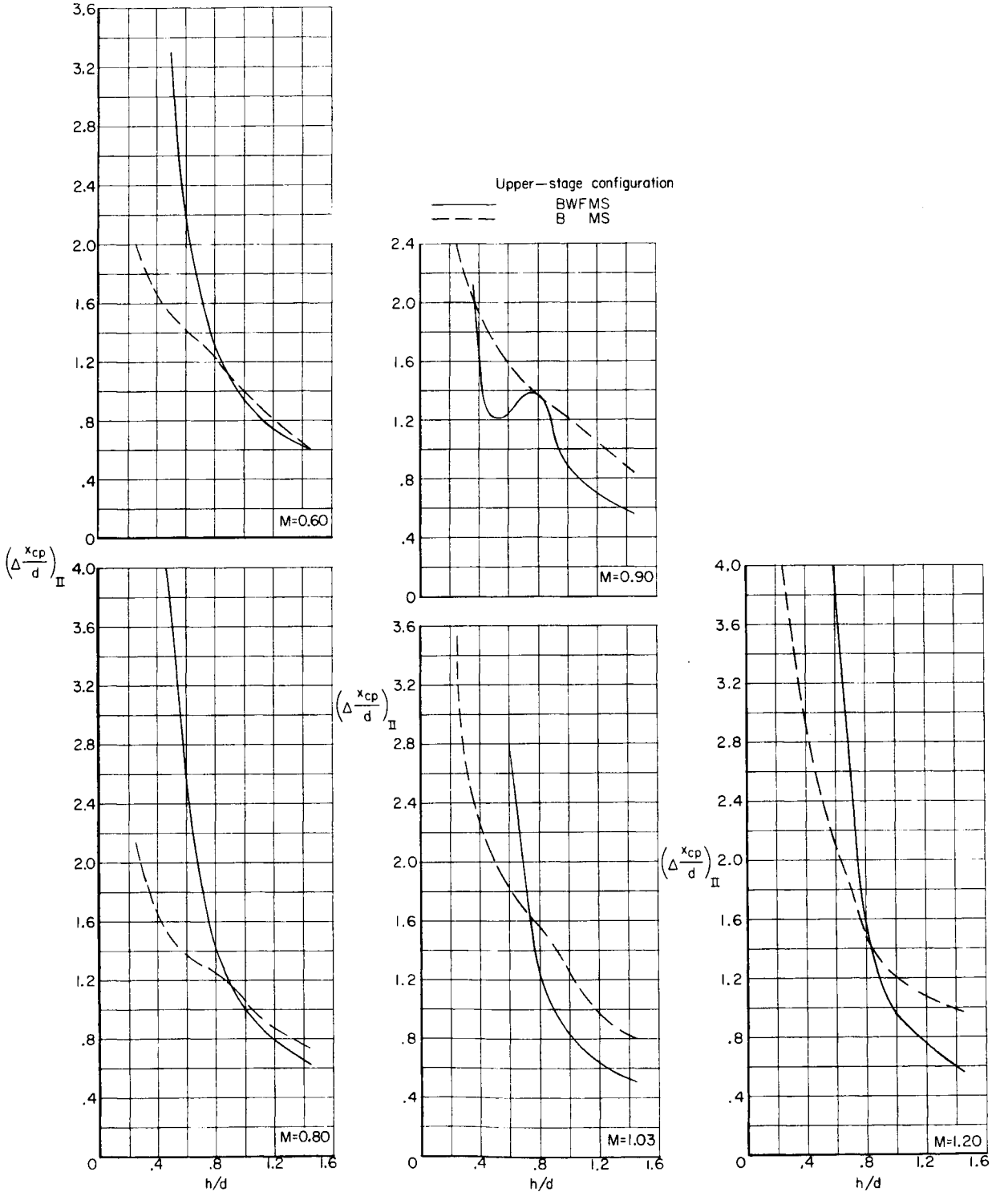

Figure 21.- Variation with spacing distance of the incremental changes in center of pressure at $\alpha = 6^{\circ}$ for two upper-stage configurations in presence of the complete first stage.

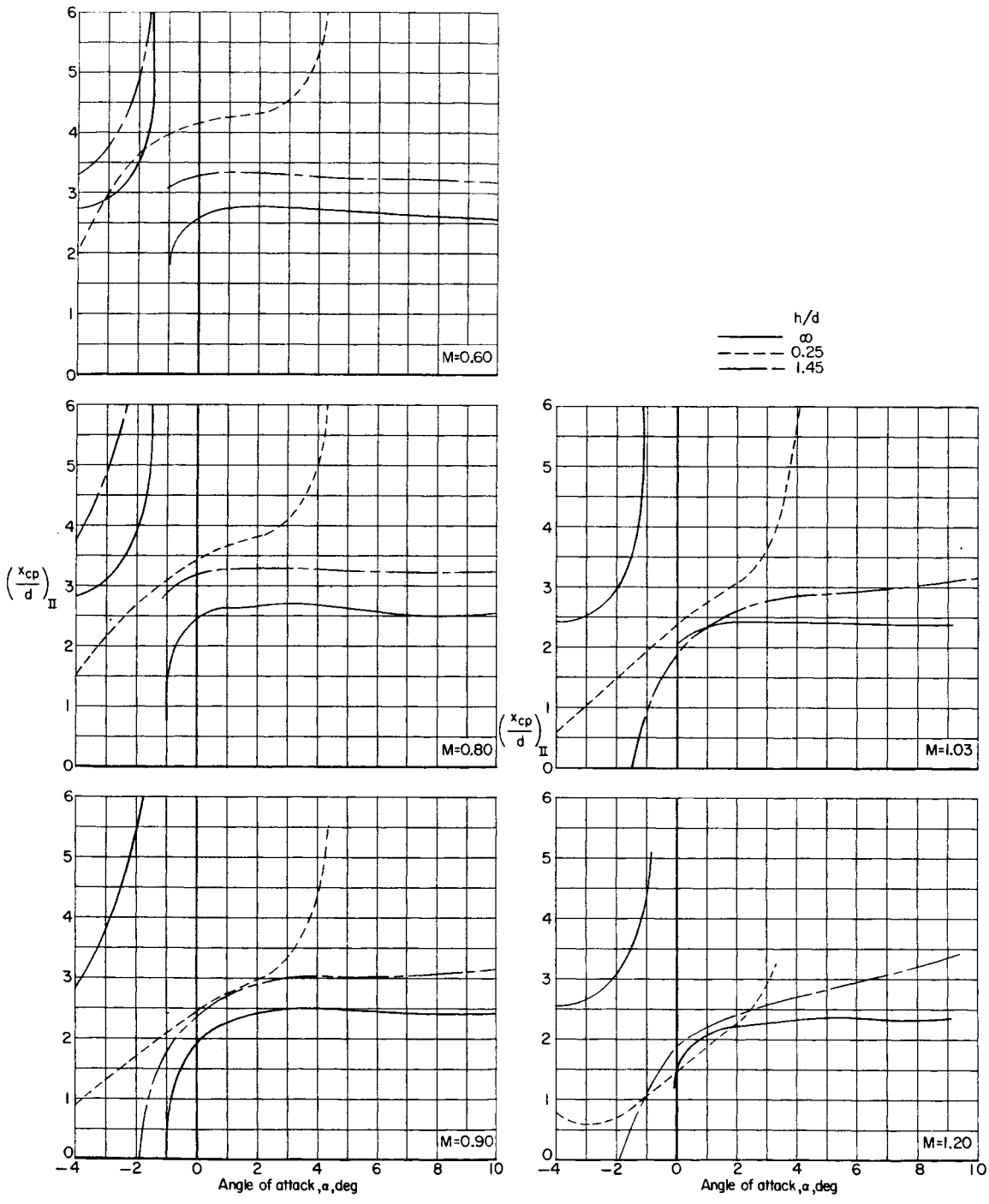

(a) Variation for BWFMS in presence of complete first stage.

Figure 22.- Variation of center of pressure with angle of attack for two upper-stage configurations in presence of the complete first stage.

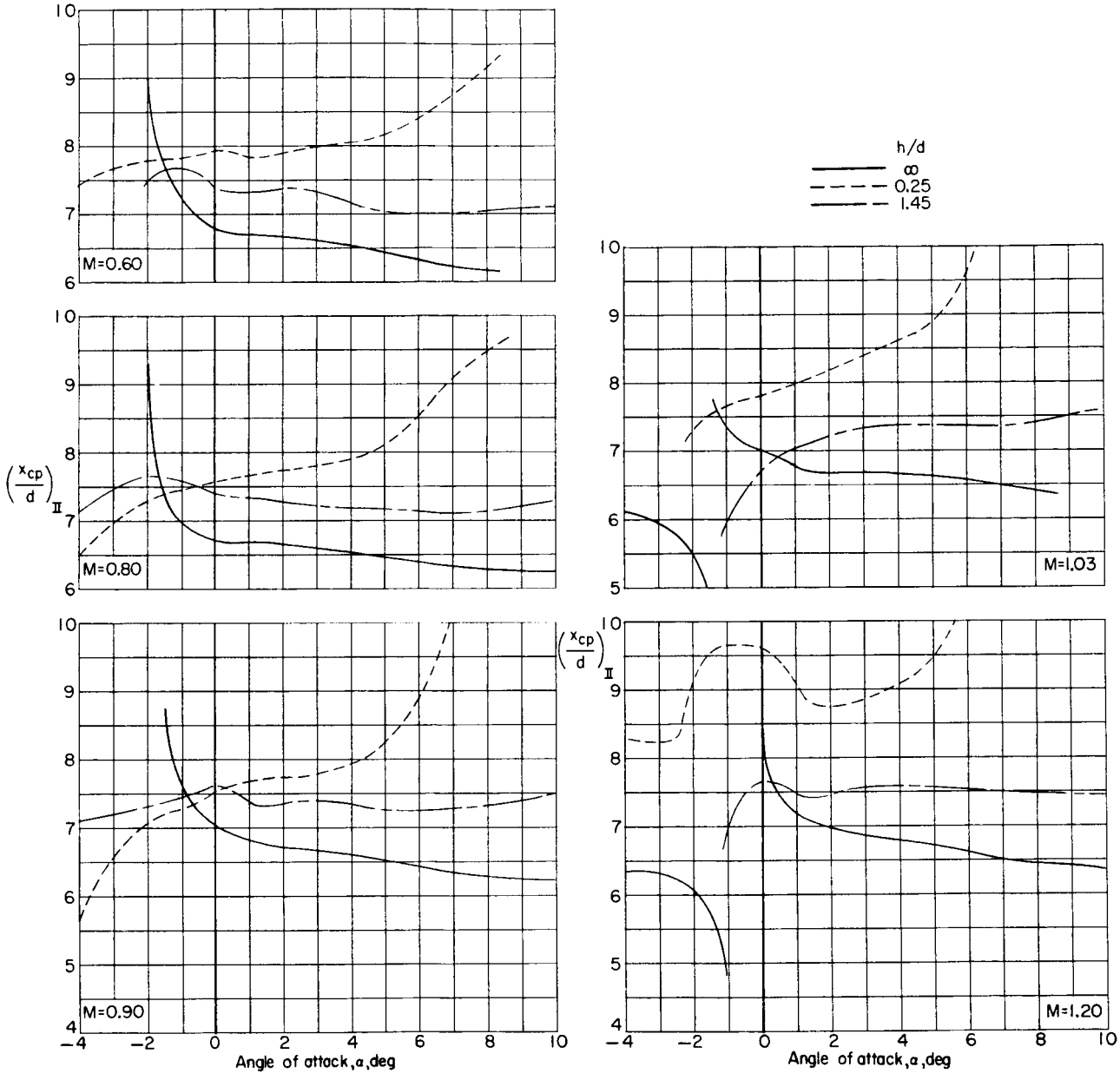

(b) Variation for BMS in presence of complete first stage.

Figure 22.- Concluded.

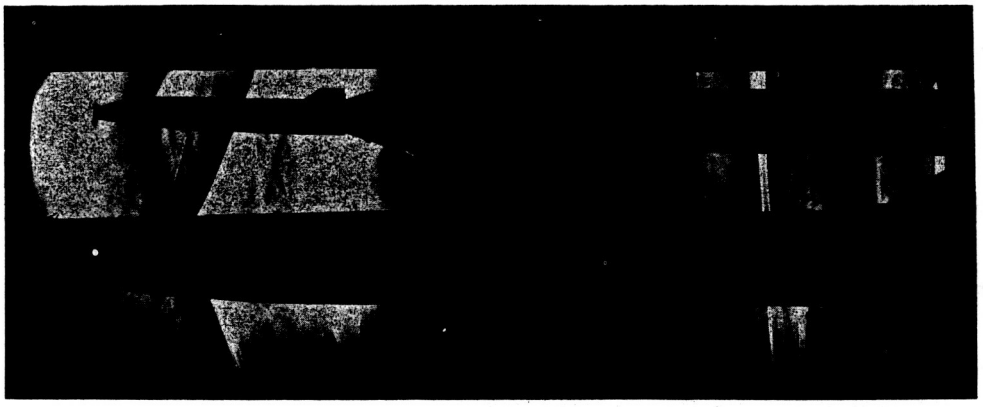

h/d=0.50

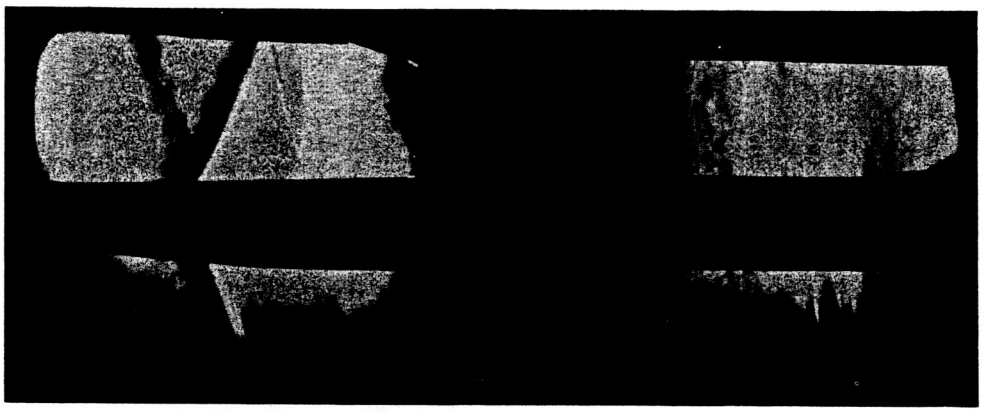

h/d=1.00

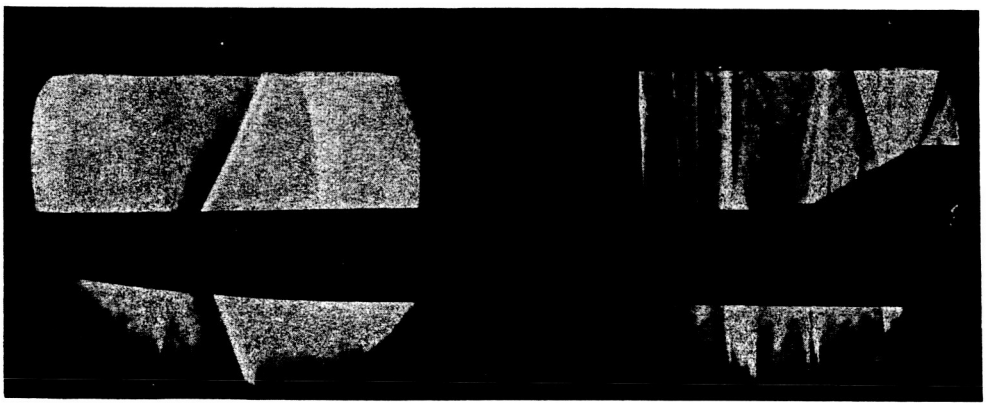

h/d=1.45

(a) M = 1.03.

L-65-195

Figure 23.- Schlieren photographs of the complete first stage in presence of BWFMS. $\alpha = 0^{o}$.

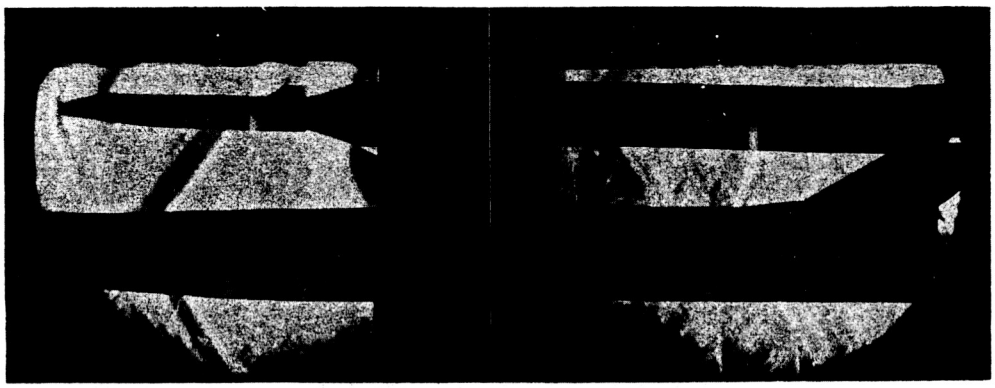

h/d=0.50

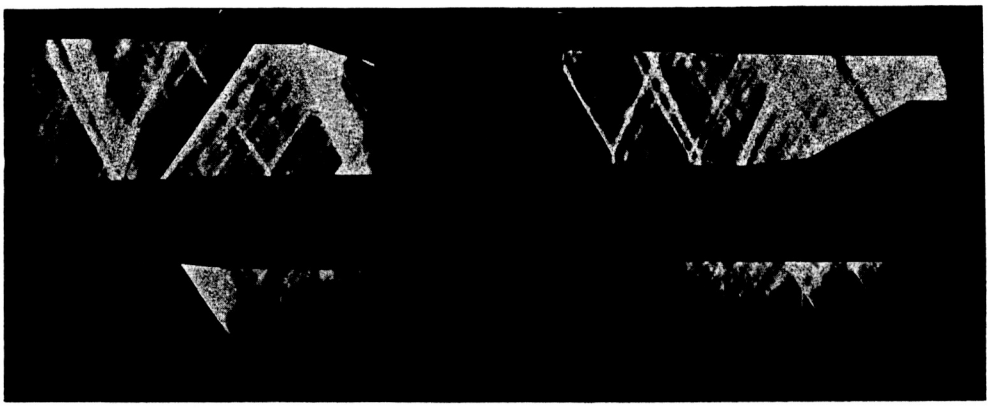

h/d=1.00

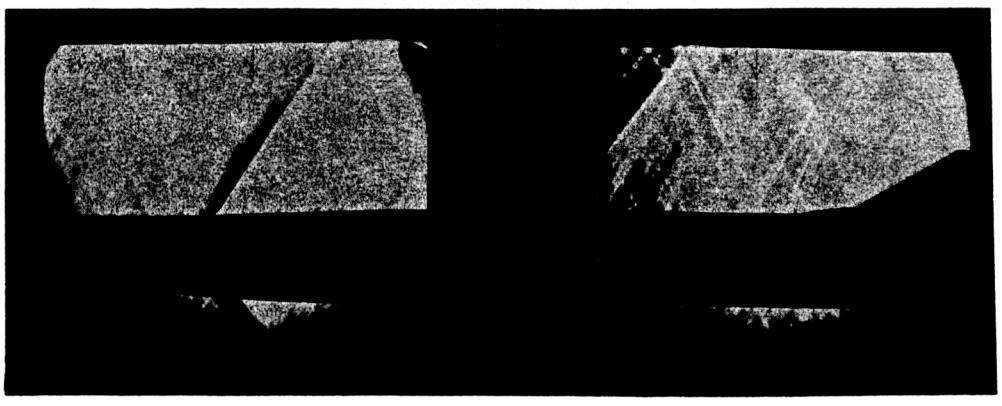

h/d=1.45

(b) M = 1.20. L-65-196

Figure 23.- Concluded.

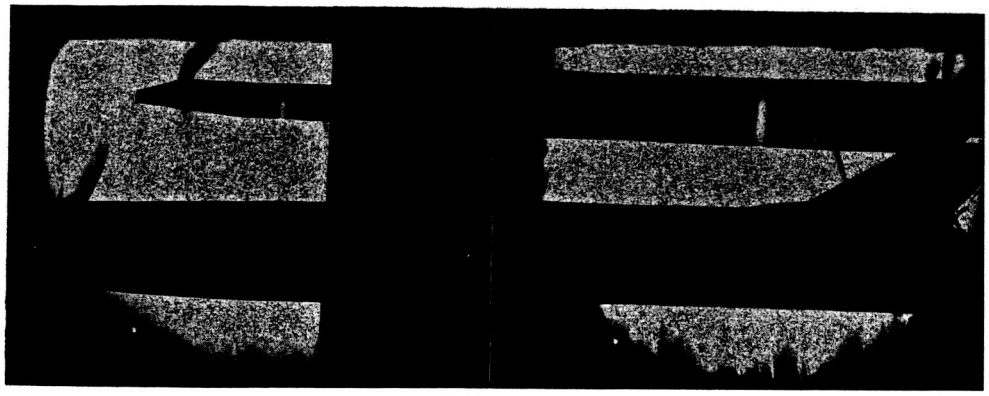

h/d= 0.50

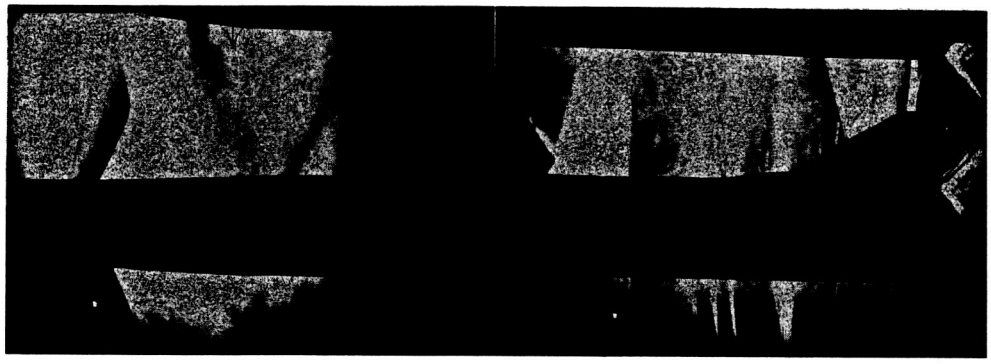

h/d= 1.00

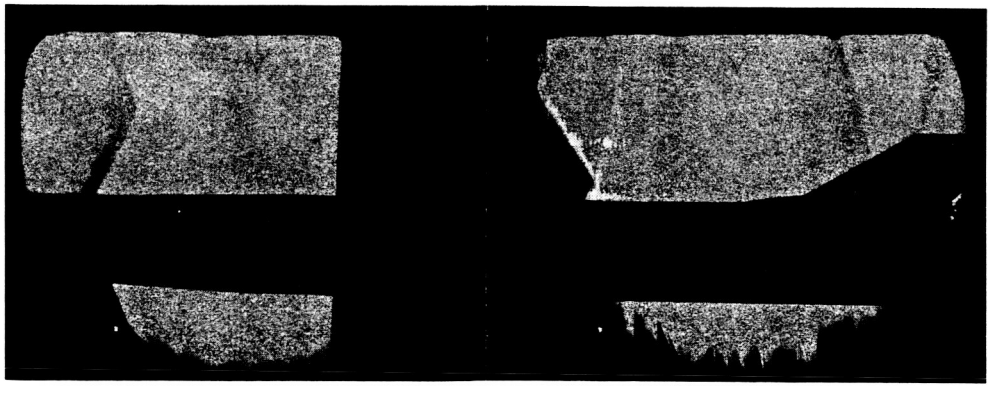

h/d= 1.45

(a) M = 1.03. L-65-197

Figure 24.- Schlieren photographs of the complete first stage in presence of BWFS. $\alpha = 0^{\circ}$.

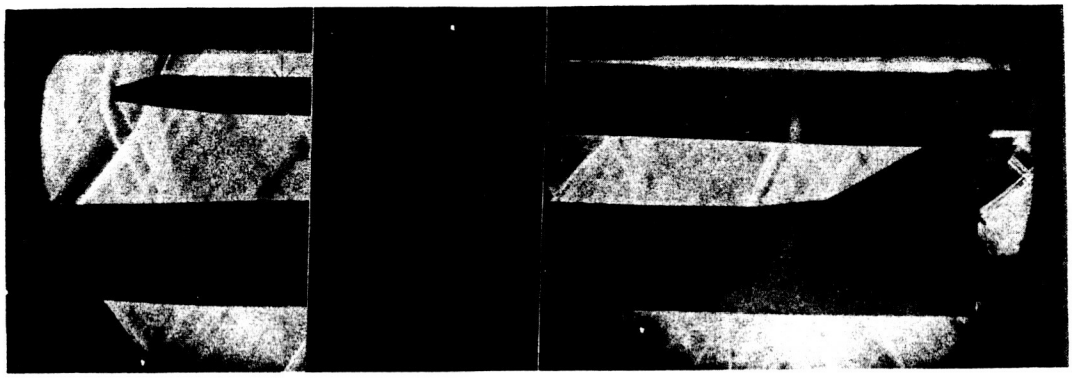

h/d= 0.50

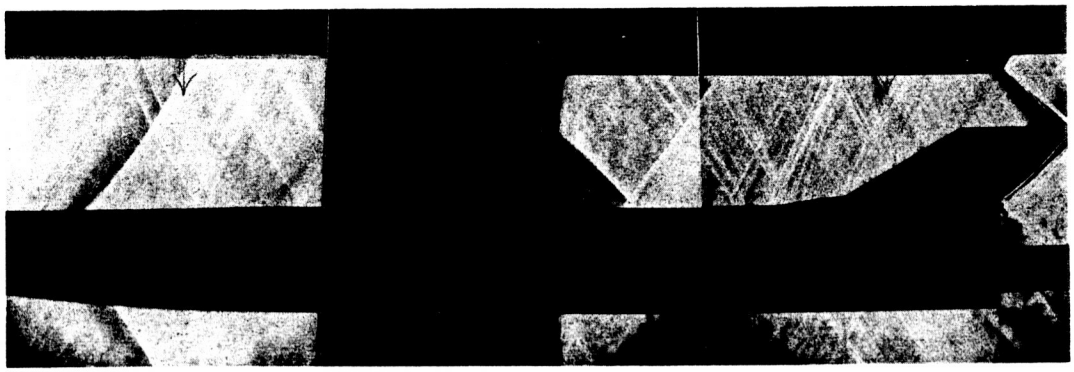

h/d= 1.00

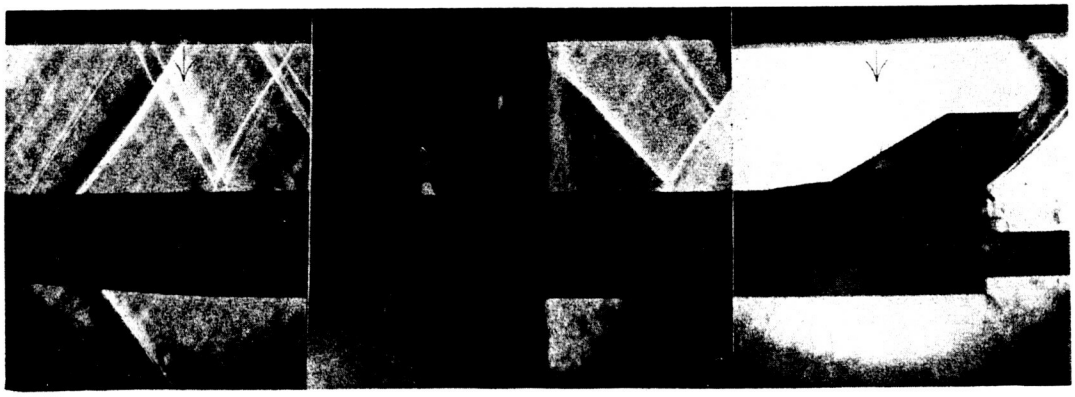

h/d= 1.45

(b) M = 1.20. L-65-198

Figure 24.- Concluded.

NASA-Langley, 1965 L-4519